Terms and Conditions of Use of Digitised Theses from Trinity College Library Dublin

Copyright statement

All material supplied by Trinity College Library is protected by copyright (under the Copyright and Related Rights Act, 2000 as amended) and other relevant Intellectual Property Rights. By accessing and using a Digitised Thesis from Trinity College Library you acknowledge that all Intellectual Property Rights in any Works supplied are the sole and exclusive property of the copyright and/or other IPR holder. Specific copyright holders may not be explicitly identified. Use of materials from other sources within a thesis should not be construed as a claim over them.

A non-exclusive, non-transferable licence is hereby granted to those using or reproducing, in whole or in part, the material for valid purposes, providing the copyright owners are acknowledged using the normal conventions. Where specific permission to use material is required, this is identified and such permission must be sought from the copyright holder or agency cited.

Liability statement

By using a Digitised Thesis, I accept that Trinity College Dublin bears no legal responsibility for the accuracy, legality or comprehensiveness of materials contained within the thesis, and that Trinity College Dublin accepts no liability for indirect, consequential, or incidental, damages or losses arising from use of the thesis for whatever reason. Information located in a thesis may be subject to specific use constraints, details of which may not be explicitly described. It is the responsibility of potential and actual users to be aware of such constraints and to abide by them. By making use of material from a digitised thesis, you accept these copyright and disclaimer provisions. Where it is brought to the attention of Trinity College Library that there may be a breach of copyright or other restraint, it is the policy to withdraw or take down access to a thesis while the issue is being resolved.

Access Agreement

By using a Digitised Thesis from Trinity College Library you are bound by the following Terms & Conditions. Please read them carefully.

I have read and I understand the following statement: All material supplied via a Digitised Thesis from Trinity College Library is protected by copyright and other intellectual property rights, and duplication or sale of all or part of any of a thesis is not permitted, except that material may be duplicated by you for your research use or for educational purposes in electronic or print form providing the copyright owners are acknowledged using the normal conventions. You must obtain permission for any other use. Electronic or print copies may not be offered, whether for sale or otherwise to anyone. This copy has been supplied on the understanding that it is copyright material and that no quotation from the thesis may be published without proper acknowledgement.

Microcracks and the Fatigue Behaviour of Compact Bone

Fergal Joseph O'Brien

BA, BAI

A dissertation submitted to the University of Dublin for the degree of Doctor in Philosophy

October, 2000

Department of Mechanical and Manufacturing Engineering

Trinity College

&

Department of Anatomy

Royal College of Surgeons in Ireland

INDEX of CONTENTS

LIST of TABLES

LIST of FIGURES

Dedicated to my Parents
Pat and Pauline O'Brien

Thanks for everything!

PREFACE

The work presented in this thesis has been published as follows:

Lee, T.C., O'Brien, F.J., Pellegrini, F. and Taylor, D. (1998) Microcrack morphology in fatigued compact bone. *Journal of Rehabilitation Research and Development* **35:** 38-39.

O'Brien, F.J., Pellegrini, F., Dickson, G., Lee, T.C. and Taylor, D. (1998) Morphology of fatigue microcracks in compact bone. *Irish Journal of Medical Science* **167:** 276.

Taylor, D., Prina Mello, A., Ryan, C., O'Brien, F.J., O'Reilly, P. and Lee, T.C. (1999) The fatigue strength of compact bone in compression. *Journal of Bone and Joint Surgery* **81-B (Suppl.1):** 94.

O'Brien, F.J. Grady, T., Diamond, D., Taylor, D. and Lee, T.C. (1999) The use of fluorescent chelating agents in the detection of microdamage in compact bone. *Journal of Bone and Joint Surgery* **81-B (Suppl. III):** 321.

Taylor, D., O'Brien, F.J., Prina Mello, A., Ryan, C., O'Reilly, P. and Lee, T.C. (1999) Compression data on bovine bone confirms that 'stressed volume' principle explains the variability of fatigue strength results. *Journal of Biomechanics* **32:** 1199-1203.

O'Brien, F.J., Taylor, D and Lee, T.C. (1999) Visualisation of microdamage in compact bone. *Irish Journal of Medical Science* **168:** 216.

O'Brien, F.J., Taylor, D, Dickson, G.R. and Lee, T.C. (2000) Microcracks in human bone: the third dimension *Irish Journal of Medical Science.* **167 (Supp 1):** 8.

O'Brien, F.J., Taylor, D, Dickson, G.R. and Lee, T.C. (2000) Three dimensional behaviour of microcracks in compact bone. *Journal of Anatomy* **197:** 319.

O'Brien, F.J., Taylor, D, Dickson, G.R. and Lee, T.C. (2000) Visualisation of three-dimensional microcracks in compact bone. *Journal of Anatomy* **197:** 413-420.

Lee, T.C.; O'Brien, F.J. and Taylor, D. (2000) The nature of fatigue damage in bone. *International Journal of Fatigue* **22:** 847-853.

O'Brien, F.J., Taylor, D and Lee, T.C. (2000) Detection of microdamage in compact bone, In: Prendergast, P.J., Lee, T.C. and Carr, A.J. (Eds.) *Proceedings of the 12th Conference of the European Society of Biomechanics*, Dublin: Royal Academy of Medicine in Ireland: 41.

Taylor, D., O'Brien, F.J., Falsetti, F. and Lee, T.C. (2000) Fatigue properties of the chicken tibia, In: Prendergast, P.J., Lee, T.C. and Carr, A.J. (Eds.) *Proceedings of the 12th Conference of the European Society of Biomechanics*, Dublin: Royal Academy of Medicine in Ireland: 48.

Lee, T.C., O'Brien, F.J., Hardiman, D., Ryan, C., Prina Mello, A and Taylor, D. (1999) Microcrack labelling and fatigue strength of compact bone. *Journal of Rehabilitation Research and Development* (In press) (abstract).

O'Brien, F.J., Taylor, D, Dickson, G.R. and Lee, T.C. (2000) Microdamage in bone: a three-dimensional approach, In: *Computer Methods in Biomechanics and Biomedical Engineering* – 3, Middleton, J., Pande, G. and Williams, K.R. (Eds.) Gordon & Breach: Amsterdam (In press) (book chapter).

Lee, T.C., O'Brien, F.J. and Taylor, D. (2000) Microcrack labelling in three dimensions. *Journal of Rehabilitation Research and Development* (In press) (abstract).

Taylor, D., Lee, T.C. and O'Brien, F.J. (2000) Understanding fatigue in bone. *Journal of Rehabilitation Research and Development* (In press) (abstract).

ACKNOWLEDGEMENTS

It has been my extreme good fortune to have, had the privilege to work for the last three years as a Trinity College postgraduate student based in the Royal College of Surgeons in Ireland. Having spent so much time in two institutions, and having sought advice from so many people in different disciplines, it is very difficult to even begin to acknowledge all the people who have contributed to this project.

First and foremost, to my supervisors, Prof. Clive Lee in whose debt I will always remain, for his unequivocal support and guidance, I am very grateful. His patience in teaching an engineer about the biological aspects of skeletal research was incredible, Perhaps, the greatest tribute I can pay Clive, is that I now consider him a good friend. Prof. David Taylor to whom I owe so much, his encouragement and perseverance over the course of this project have been fantastic. I am honoured to continue working with both men for another year.

My Head of Department in RCSI, Professor Stanley Monkhouse has been supportive both academically and financially throughout the course of this project. My thanks are also due to Mr. Alec Elliot and Peter Stafford in the Biology Division of RCSI and to Margaret McCarthy and the Anatomy Technicians, Terry Byrne, John O'Brien and Peter Kelleghan. My thanks to all the staff who have worked in the Anatomy Dept. at different stages over the past three years, especially Paul Ridgway, Peter and Jonathan McCullough, Alice McGarvey, and Skantha Kandiah.

To everyone in Trinity College, I am especially grateful, Dr. Patrick Prendergast and Mr. Garry Lyons for their advice and support at various stages during my undergraduate and postgraduate years and thanks to my Head of Department, Prof. John Monaghan and to both Joan Gillen and Virginia Coulter for all their help. I am especially grateful to all the postgrads for all their support and friendship, with and without the influence of alcohol.

My thanks are also due to Professor Kevin Nolan in the Dept. of Chemistry and Physics in RCSI for all his help and advice in chemical analysis. Terry Murphy was invaluable win helping prepare chemical solutions for analysis and Dr. Dermot Diamond and Dr. Teresa Grady in the Dept. of Analytical Sciences in Dublin City University helped greatly with the ion chromatography work.

Peter O'Reilly and Colm Ryan in Trinity helped with specimen preparation and mechanical testing and Adriele Prina Mello's help with the first set of fatigue tests and his friendship in general is greatly appreciated. Thanks too, to David Hardiman and Ciaran Connolly who assisted with the tedious process of embedding and serial sectioning of calcified bone.

Special thanks are due to Dr Glenn Dickson in the Queen's University of Belfast for making available a confocal microscope for our use and for his help, support and indeed

provision of accommodation during my time in Belfast. Dr. Stephen McQuaid was magnificant in providing his time and expertise with the confocal microscopy process.

Thanks are also due to Professor Lorna Gibson for her invitation and for her help and guidance in my brief stay in MIT, to her assistant Diego Gonzalez, and to everyone in the Harvard Medical School, Orthopaedic Biomechanics Lab at Beth Israel Hospital in Boston, I am very grateful. Special thanks to Tara Arthur who probably understands more than most, the pitfalls of being an engineer studying microcracks in bone using chelating agents.

To the best group of friends, without whom this project would never have reached fruition, it is too difficult to name everyone, but special thanks to Conor O'Gorman, Joe Jolley, Liam Glennon, Siobhan Kehoe, Declan Gaynor, Sarah Bothwell, Jedd Comiskey, and my colleague, friend and flatmate Maeve Flynn. Claire Fahy and the Murphys, Bruce, Linda and Helen have always been there, and have put up with me through good times and bad over the past seven years.

Finally to my brother Cian and to my parents, to whom everything I have ever achieved is a tribute. They have stood behind me throughout all my endeavours, and to them I am eternally grateful.

Financial support for the Health Research Board, the Research Committee of the Royal College of Surgeons in Ireland, the Trinity Trust and Cappagh Hospital Trust is gratefully acknowledged.

DECLARATION

I declare that the present work has not previously been submitted as an exercise for a degree at this or any other University.

The thesis consists entirely of my own work except where references indicate otherwise.

The library of the University of Dublin, Trinity College, may lend or copy this thesis upon request.

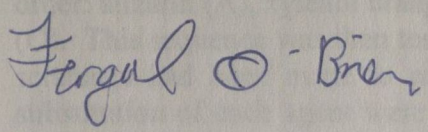

F.J. O'Brien

October, 2000.

SUMMARY

Microcracking in bone acts as a stimulus for bone remodelling, contributes to the loss of bone quality in osteoporosis and is thought to play a major role in both fragility and stress fractures. This study seeks to refine a method of crack detection using fluorescent chelating agents and to label microcrack initiation, growth and coalescence during fatigue testing in compression. The three dimensional shape of microcracks and their interaction with the microstructure of bone will also be investigated.

Five fluorescent stains have been identified which chelate calcium ions lining crack walls. However, when applied in sequence, agents displaced each other by chemical substitution, preventing accurate measurement of crack growth. The calcium affinity of each agent was measured using ion chromatography and the agents ranked in descending order: alizarin (A), xylenol orange (X), calcein blue (CB), calcein (C) and oxytetracycline (O). This sequence was then tested on polished bovine bone specimens on which surface scratches had been made to mimic microcracks. The quality, clarity and degree of substitution of each agent were measured and concentration and tissue penetration time were varied. The optimal sequence was A – X – C– CB, with a penetration time of 30 minutes and the A, X and C at 0.0005M concentration and CB at 0.0001M. The chemical behaviour of O was variable and so it was excluded from the study.

Specimens from fresh bovine tibiae were machined into typical, waisted type of circular cross section and fatigue tested in cyclic compression at 3 Hz. They were initially stained with alizarin, to label pre-existing damage, and the other agents applied in sequence during the test. Specimens were then sectioned and examined using UV epifluorescence microscopy. Microcracks accumulated early in a specimen's life but the rate then levelled off before a second increase in the period prior to failure. Bone microstructure greatly influenced microcrack growth with the 75 – 95% of microcracks found in interstitial bone between Haversian systems. Microcracks grew in length primarily in the longitudinal direction, parallel to Haversian systems and the longitudinal axis of the bone. These results support the concept of a microstructural barrier effect in bone.

Human ribs were stained with basic fuchsin to label *in vivo* microcracks and viewed in the longitudinal direction and in three dimensions using two different computer-based methods of reconstruction: (i) laser scanning confocal microscopy of sections stained in basic fuchsin followed by reconstruction of microcracks into a 3D image and (ii) serial sectioning of methyl-methacrylate embedded sections with identification of microcracks using UV epifluorescence followed by computerised reconstruction individual cracks. Both LSCM and serial sectioning showed similar results regarding the shape and size of microcracks in bone. Microcracks were elliptical in shape with a ratio of longitudinal length: transverse width of 4.6: 1, consistent with theoretical predictions.

ABBREVIATIONS

a	crack length (μm)
Ca	calcium
$CaCl_2$	calcium chloride
CCTV	closed circuit television
CNC	computer numerical control
Cr.Dn	numerical crack density (no. of cracks/ mm^2)
Cr.Le	mean crack length (μm)
CT	computed topography
d	spacing of microstructural barriers
da/dN	crack growth rate
DPX	mounting medium for histological slides
$\Delta\sigma$	stress range
$\Delta\sigma_o$	fatigue strength of a material
$\Delta\sigma_{th}$	fatigue threshold value
E	Young's modulus, a measure of the stiffness of a material
ETOH	ethanol
ε	strain, percentage change in length
$\mu\varepsilon$	microstrain (strain 10^{-3})
g	gram
mg	gram x 10^{-3}
G	strain energy release rate
HCl	hydrochloric acid
Hz	hertz (unit of frequency, 1/s)
K	stress intensity
Kc	critical stress intensity
l	litre
ml	litre x 10^{-3}
μl	litre x 10^{-6}
LSCM	laser scanning confocal microscopy
λ	wavelength
mV	millivolt (volt x 10^{-3})
m	metre
cm	metre x 10^{-2}
mm	metre x 10^{-3}
μm	metre x 10^{-6}
nm	metre x 10^{-9}
mm Hg	mm of mercury (measure of pressure)
M	molarity (one mole=actual weight/ molecular weight of substance)
mM	mole x 10^{-3}
Mag	magnification
Mg	magnesium
Min	minutes
MMA	methylmethacrylate

n	sample size
N	newtons (measure of force)
Na	sodium
N_f	Number of cycles to failure
^{o}	degrees
^oC	degrees celcius
Pa	pascals (measure of stress: 1Pa= $1N/m^2$)
MPa	pascals x 10^6
GPa	pascals x 10^9
P_f	probability of failure
rpm	revolutions per minute
s	seconds
σ	stress, force per unit area
S.D.	standard deviation
V	volume

Chapter 1

INTRODUCTION

Bone is the primary structural element of the human body. It serves to protect vital internal organs and it forms a series of levers that multiply the forces generated during skeletal muscle contraction, transforming them into bodily movements (Martin et al, 1998). It is self-repairing and can alter its properties in response to the stresses placed upon it (Hayes and Bouxsein, 1997). It also serves as a reservoir of calcium, phosphate, and other ions that can be stored or released in a controlled fashion to maintain homeostasis in body fluids.

The major difference between bone and most engineering materials is that bone is a living material. Following formation of the skeleton, continual adaptation of the bone tissue maintains structural integrity. The process by which bone is shaped or customised in known as modeling while the process by which is bone is repaired and 'fine tuned' is known as remodelling. Bone adaptation is controlled by mechanical as well as metabolic factors (Martin, 2000), i.e. Wolff's Law, which states that "the law of bone remodelling is the law according to which alterations of the internal architecture clearly observed and following mathematical rules, as well as secondary alterations of the external form of the bones following the same mathematical rules, occur as a consequence of primary changes in the shape and stressing of the bones" (Wolff, 1892): i.e. the phenomenon of bone adaptation under altered load. For example, increased loading as in the dominant arm of baseball pitchers or tennis players leads to an increase in cortical bone. Bone adaptation however, can also lead to a decrease in bone mass, prolonged bed rest or weightlessness causes loss of bone: disuse osteoporosis (Lee and Taylor, 1999). Another major function of bone remodelling is to replace damaged tissue such as microcracks formed from repetitive loading (Martin and Burr, 1989).

Fatigue may be defined as the progressive loss of strength and stiffness that occurs prior to failure in materials subjected to repeated loads. Bone fatigues as a result of the cyclic fluctuating loads imposed during normal daily activities (Carter and Hayes, 1977a,b; Piekarski, 1980). Changes in the strength and stiffness of bone have been attributed to the formation of microscopic cracks within the material during each load cycle (Martin and Burr, 1989). The fatigue life of bone is a function of crack accumulation and crack growth (Agarwal and Broutman, 1980, Mori and Burr, 1993). These microcracks can, under continued loading, grow into macrocracks eventually resulting in complete failure or fracture.

Fatigue damage in bone acts as a stimulus for bone remodelling (Martin and Burr, 1982; Burr et al, 1985; Burr and Martin, 1993; Mori and Burr, 1993; Prendergast and Taylor, 1994; Lee et al, 1999; Martin, 2000). Bones, therefore, have an advantage over most engineering structures in that they have an inherent ability to repair damage. However if this damage accumulates at such a rate that the capacity for bone repair is exceeded, stress fractures result. These fractures occur commonly in athletes and soldiers engaged in high intensity, repetitive activities such as marching or running. If, on the other hand, damage accumulates at 'normal' rates but the bone's repair mechanism is deficient, fragility fractures result. This occurs in ageing bone (Schaffler et al, 1994a, 1995). It is also thought that fatigue damage accumulation in bone plays a role in prosthesis loosening (Goldring et al, 1993). Microdamage is, therefore, of great clinical importance yet our understanding of microcrack initiation and growth is incomplete. A greater understanding of the fatigue behaviour of bone is required for predicting and preventing fractures.

1.1 Bone

Bone consists of cells embedded in a fibrous organic matrix (osteoid) which is composed of collagen and other proteins. The osteoid matrix makes up approximately half of the bone volume. Bone's characteristic rigidity and strength are derived from the mineral phase which makes up the remaining volume. The principal constituents of bone mineral are hydroxyapatite [$Ca_{10}(PO_4)_6(OH)_2$], calcium phosphate and calcium carbonate with lesser quantities of sodium, magnesium, potassium and fluoride. Microscopically, bone is made up of a number of different bone cell types (10% by weight) (Schiller, 1994).

There are four types of cells in bone tissue, each of which has a specific role in the formation, resorption and remodelling of bone.

(a) Osteoprogenitor cells which line the walls of the bones. In response to an appropriate stimulus, these stem cells may differentiate into osteoblasts.
(b) Osteoblasts are large cells which are arranged in lines along the bone surface. They are responsible for the formation of new bone tissue.
(c) Osteocytes are osteoblasts trapped by the secretion of the extracellular matrix and are found in lacunae throughout this matrix. They have numerous processes that extend through bony canals called canaliculi and communicate with each other. These canaliculi are thought to play a role in sensing changes in the bone matrix (Cowin et al, 1995).
(d) Osteoclasts are large multinucleated cells which are involved in the resorption of damaged or old bone. On the surface of bone, they are found in small depressions known as Howship's lacunae.

Bone changes with age. Microscopic examination shows that two varieties exist: immature, or woven bone, and mature, or lamellar bone.

Woven Bone: woven bone is the first bone to appear during growth. It is characterised by a random structure of fine collagen fibres. It is temporary and is replaced in adults by secondary bone.

Lamellar Bone: this is the type of bone found in adults. Characteristically it is composed of a layer of collagen fibres arranged in lamellae parallel to each other or concentrically arranged around a vascular canal (Fig. 1.1a). The whole network of concentric lamellae surrounding a canal, containing blood vessels nerves and loose connective tissue is called a Haversian system or osteon (Fig. 1.1b). These concentric lamellae around the central canal run parallel to the long axis of the cortex (Schiller, 1994).

Haversian systems are bounded by cement lines formed where osteoclastic behaviour ceases and osteoblastic bone behaviour begins. As they mark the limit of bone resorption prior to the formation of an osteon, they are sometimes known as reversal lines. Canaliculi may sometimes pass through cement lines, providing a route for exchange between interstitial bone and vascular canals within osteons (Atkinson and Hallsworth, 1982). Burr et al (1988) found that the cement line contained 85-90% of the calcium and phosphorous found in the adjacent bone lamellae, they suggested that the cement line may be more compliant and viscoelastic than other components of the bone matrix. The irregular areas of bone between adjacent Haversian systems are referred to as interstitial bone and consist of the remnants of woven fibred bone, circumfrential lamellar bone, and osteons that previously occupied the area (Martin et al, 1998) and are now wedged between osteons (Schiller, 1994).

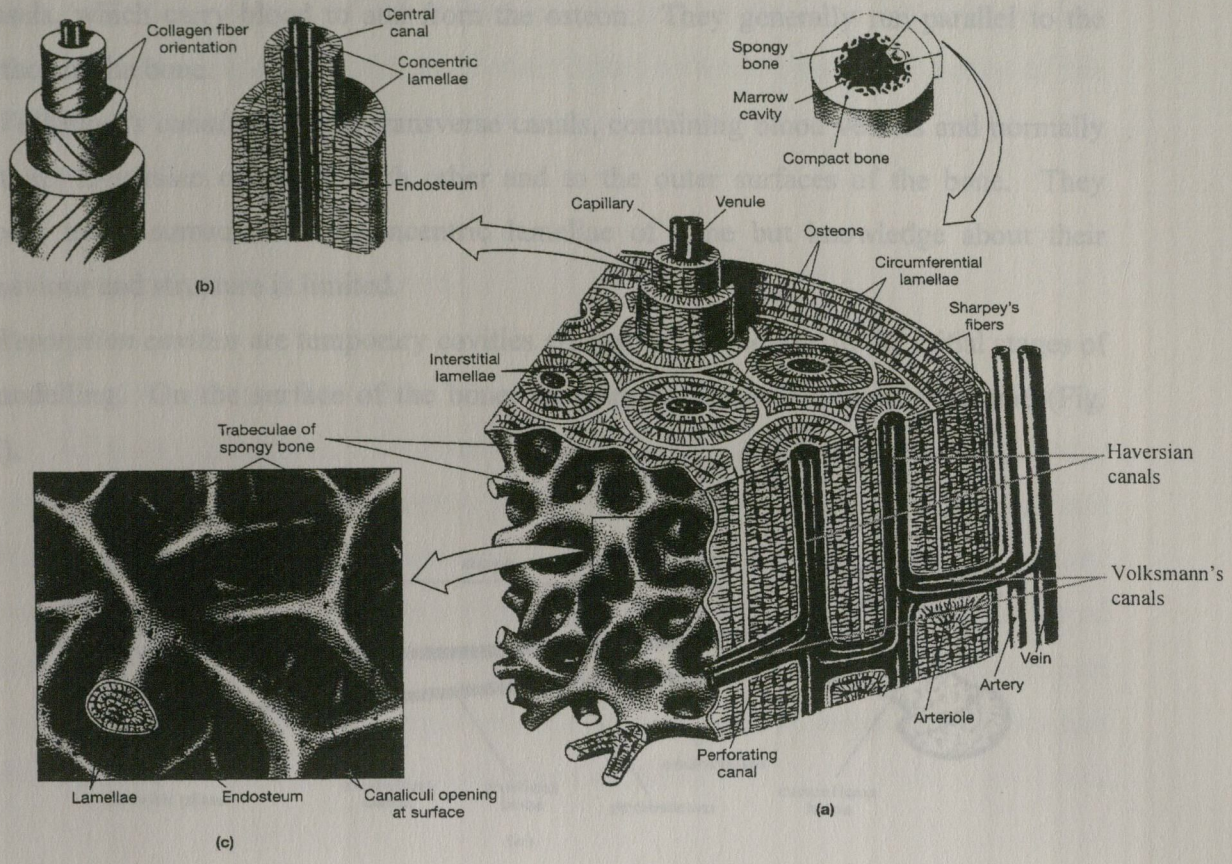

Fig 1.1 Structure of bone (a) the relationships between compact bone, trabecular boneand the marrow cavity (b) the orientation of collagen fibres in adjacent lamellae and (c) details of the organisation of trabecular bone (Martini, 1998)

Mature bone can be classified into two types of tissue, compact bone and trabecular bone (Figs. 1.1, 1.2). Compact bone is the bone found in the shafts of long bones and forming a cortex or shell around vertebral bodies and other spongy bone. Hence it is also called cortical bone. It has a porosity of 5-30%, the pores and cavities within it can be assigned to the following three categories:

1. *Haversian canals* run parallel to the long axis of the bone and contain capillaries and nerves. The Haversian canal is surrounded by cyclindrical lamellae of bone and the entire structure is known as a Haversian system. The canal contains one or more blood

vessels, which carry blood to and from the osteon. They generally run parallel to the surface of the bone.

2. *Volkmann's canals* are short transverse canals, containing blood vessels and normally connect Haversian canals to each other and to the outer surfaces of the bone. They appear to be surrounded by concentric lamellae of bone but knowledge about their behaviour and structure is limited.

3. *Resorption cavities* are temporary cavities created by osteoclasts in the initial stages of remodelling. On the surface of the bone, they are known as Howship's lacunae (Fig. 1.2).

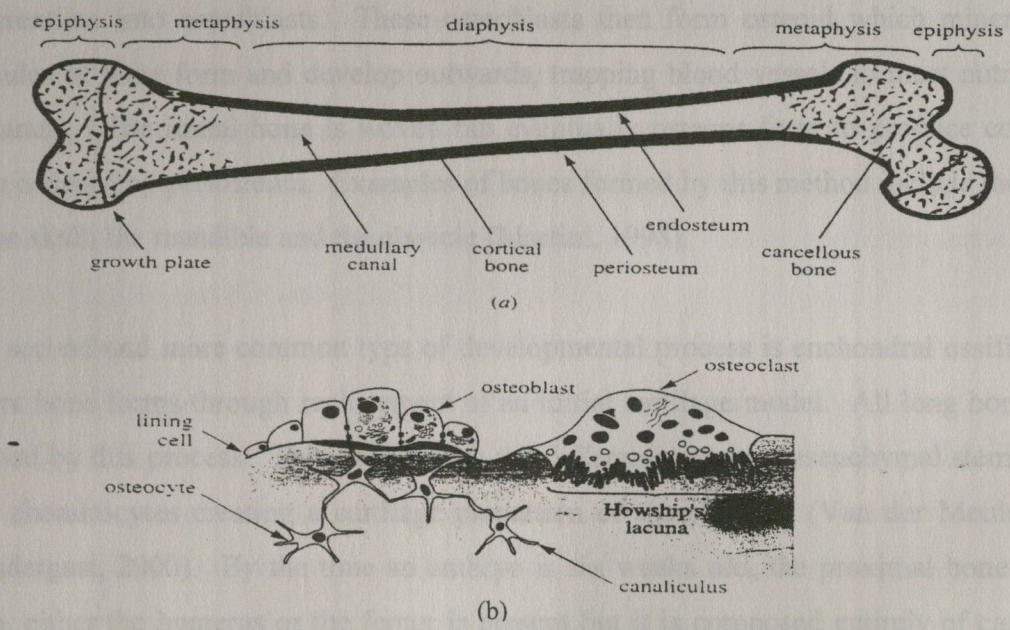

Fig. 1.2 (a) The distribution of compact and trabecular bone in an adult long bone (b) bone cells (Van der Meulen and Prendergast, 2000)

Trabecular bone (also called cancellous or spongy bone) is an orthotropic material, with a porous architecture formed by individual struts or trabeculae (Gibson, 1985). In long bones, the bulbous ends (epiphyses) are composed of trabecular bone covered by a thin layer of compact bone. The cylindrical central sections of the long bones (diaphyses) are comprised almost entirely of a thick shell of compact bone surrounding the bone marrow, or medullary cavity (Fig. 1.2). Trabecular bone has a relative density varying from 0.05

to 0.7. The arrangement of the trabeculae is variable, they can be arranged into orthogonal arrays (e.g. distal end of human tibiae) with the shape and density of the trabeculae depending on the loads to which they are subjected (Gibson and Ashby, 1988, 1997).

1.1.1 Bone Formation and Growth

Skeletal formation begins in humans when the embryo is six weeks old. Bone forms by two different processes, intramembranous and endochondral ossification. Intramembranous ossification begins when mesenchymal stem cells cluster and differentiate into osteoblasts. These osteoblasts then form osteoid which mineralises. Spicules of bone form and develop outwards, trapping blood vessels to meet nutritional demands. The initial bone is woven but eventually osteons form to produce compact bone covered by periosteum. Examples of bones formed by this method include the vault of the skull, the mandible and the clavicle (Martini, 1998).

The second and more common type of developmental process is enchondral ossification where bone forms through replacement of an initial cartilage model. All long bones are formed by this process. This begins with the differentation of mesenchymal stems cells into chondrocytes creating a cartilage prepattern of the skeleton (Van der Meulen and Prendergast, 2000). By the time an embryo is six weeks old, the proximal bone of the limb, either the humerus or the femur is present but it is composed entirely of cartilage. As the cartilage expands, chondrocytes begin to enlarge and the matrix is reduced to struts of cartilage that begin to calcify. With lack of nutrition, the chondrocytes die. Blood vessels then enter the cellular layer surrounding the cartilage (perichondrium), bringing with them osteoclasts, which resorb the calcified cartilage. The inner layer of cells in the perichondrium, differentiate to osteoblasts and a periosteum is formed. Osteoblasts and blood vessels go towards the centre of the matrix and osteoid is laid down from the centre outwards, increasing the length and diameter of the newly formed bone (Martini, 1998). Bones are then further shaped by a process known as modelling.

Once the skeleton is formed, continual remodelling of individual bones maintain structural integrity (Van der Meulen and Prendergast, 2000).

1.1.2 Modelling and remodelling

Bones are shaped by a process called modelling, where activation is followed by osteoblast activity (bone formation) at some sites and osteoclast activity (bone resorption) at others. In contrast, bone remodelling is the bone replacement mechanism of the skeleton and mediates the effects of all agents - hormonal, nutritional or mechanical - that act on it. Bone remodelling is carried out by temporary anatomic structures termed *basic multicellular units* (BMUs). During remodelling, each BMU comprises a cutting cone of osteoclasts in front, which removes old bone thereby digging a tunnel, which is then filled in by a closing cone of osteoblasts. In both trabecular and cortical bone, remodelling comprises an activation phase followed by resorption, followed by formation (Frost, 1973). In the adult, remodelling serves to repair, renew and adapt bone tissue (Van der Meulen and Prendergast, 2000).

Activation operates by the recruitment and differentiation of osteoclasts from stem cell populations. Resorption of bone is carried out by osteoclasts moving longitudinally at a rate of 40-50 microns per day. These osteoclasts are arranged in a cutting cone which is about 100 microns in diameter and 300 microns in length. During formation, osteoblasts appear around the periphery of the tunnel dug by the osteoblasts and start to form osteoid which will be mineralised to form bone. The osteoblasts lay down concentric lamellae. These move from the periphery towards the centre and, when finished, leave a central Haversian canal for blood vessels and nerves (Martin and Burr, 1989).

1.1.3 The role of microcracks role in remodelling

Various theories exist as to the mechanism by which bone remodelling is initiated (Cowin, 1995; Lanyon, 1991). However, a consistent finding has been that the activating stimulus must be repetitive, i.e. cyclic, hence bone remodelling can be viewed as a

fatigue phenomenon. Tschantz and Rutishauser (1967) provided the first experimental evidence that the damage caused by repetitive stresses can stimulate bone adaptation. Subsequent theoretical arguments (Carter and Hayes, 1977b; Martin and Burr, 1982; Currey, 1984; Burr and Martin, 1993; Prendergast and Taylor, 1994; Prendergast and Huiskes, 1996; Martin, 2000) and experimental data (Burr et al, 1985; Mori and Burr, 1993; Bentolila, 1998; Lee et al, 1999; Muir et al, 1999; Verborgt et al, 2000) have supported this link between fatigue microdamage and remodelling.

The process by which microcracks initiate bone remodelling remains poorly understood. Frost (1960, 1986) suggested that the disruption of canalicular connections that occurred when cracks crossed them, could provide the stimulus to initiate remodelling. Bentolila et al (1998) showed that intracortical remodelling could be induced in rats, which normally do not have intracortical remodelling by creating microdamage in the cortex. His study also showed regions of altered osteocyte morphology in the vicinity of the microcracks. Recently, evidence has emerged that controlled death or cell suicide (apoptosis) of osteocytes is an important factor in initiating new remodelling sites (Burr, 2000). Vashishth et al (2000) showed that decline in osteocyte density in human cortical bone is associated with accumulation of microcracks. Verborgt et al (2000) suggested that microdamage induces osteocyte death, which signals for a repair response. This study showed strong associations between bone microdamage and osteocyte apoptosis and also between osteocyte apoptosis and subsequent activation of bone remodelling in regions of microdamage (Burr, 2000). Computational modeling too, supports the concept that microdamage can stimulate remodelling. Prendergast and Huiskes (1996) showed that one of the effects of the high local strain around osteocytic lacunae is that stress concentration centres are formed between lacunae. This provides sites for crack nucleation and paths for crack growth effectively unloading the lacunae adjacent to the damaged region.

1.2 Mechanical properties of bone

1.2.1 Static Properties

The mechanical properties of any structure depend upon both the properties of the material and its geometry. The fracture behaviour of individual bones is strongly dependent on the material behaviour of bone tissue. Bone is an anisotropic material, hence its elastic and strength properties are dependent on the direction of applied loading (Hayes and Bouxsein, 1997).

Table 1.1 shows the ultimate strengths of adult femoral cortical bone under various modes of loading in both the longitudinal and transverse directions. The age span of the subjects varied from 19-80 years.

Table 1.1 Strength of wet human femoral cortical bone (Hayes and Gerhart, 1985)

Loading Mode	Ultimate Strength (MPa)
Longitudinal	
Tension	133
Compression	193
Shear	68
Transverse	
Tension	51
Compression	133

These results indicate that the material strength of bone tissue depends on the type of loading as well as the loading direction. The compressive strength is greater than the tensile strength in both longitudinal and transverse directions. Transverse specimens are weaker than longitudinal specimens in both tension and compression.

The modulus values for adult femoral cortical bone are shown in Table 1.2. For loading in tension or compression, the elastic modulus or Young's Modulus gives an indication of the relationship betweeen stress and strain in a material. For shear loading, the material modulus is known as shear modulus. The longitudinal elastic modulus is about 50% greater than the transverse modulus. The shear modulus for torsion about the longitudinal axis is about 20% of the longitudinal modulus.

Table 1.2 Moduli of wet femoral cortical bone (Hayes and Gerhart, 1985)*

Longitudinal	17.0 GPa
Transverse	11.5 GPa
Shear	3.3 GPa

* Age span of population 19-80 years

The material properties of cortical bone also decrease with age as can be seen from Fig. 1.3. Human bone reaches maturity by the age of 30-35 years and then deteriorates. Its mechanical soundness is reduced and its response to mechanical stimuli for new bone formation is impaired. This reduction in modulus and in strength makes it easier for microcracks to initiate in the material. Tests carried out by Zioupos and Currey (1994) on bones of varying ages, showed that a 2.3% reduction in stiffness between the ages of 35-92 years is accompanied by 3.7% reduction in flexural strength and a 4.1% reduction in the critical stress intensity, K_C required to initiate a macrocrack. In ageing bone, it was found that macrocracks were preceded by less damage and once formed, needed less energy to drive through the tissue, thus requiring fewer cycles to ultimately cause failure.

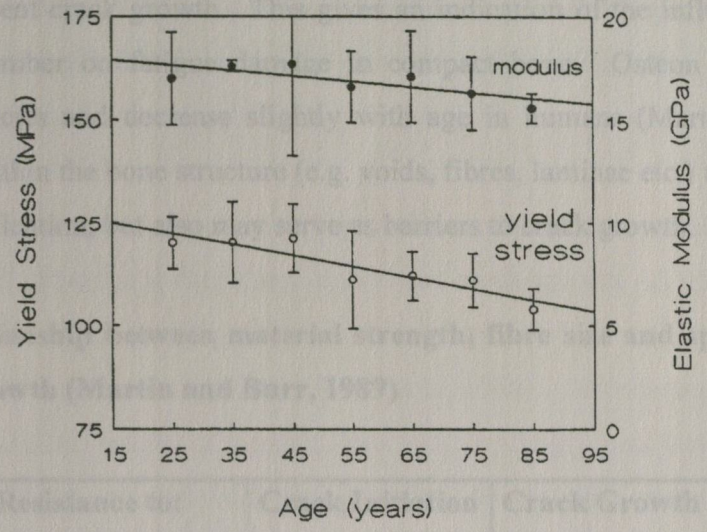

Fig. 1.3 Ultimate strength and modulus versus age for human femoral cortical bone (Burstein et al, 1975).

1.2.2 Fatigue properties

The resistance of any material to fatigue fracture is a function of its resistance to microcrack initiation, microcrack propagation and macrocrack growth. These factors are in turn, highly dependent on the microstructural characteristics of the material (Martin and Burr, 1989). Secondary compact bone may be considered as a fibre reinforced composite material in which the Haversian systems act as the reinforcements (Burr et al, 1988; Piekarski, 1973).

In any composite material, several microstructural features can affect crack initiation and crack growth. These factors include material strength, fibre diameter and fibre spacing and they affect crack initiation and growth in different ways. In general, a reduction in the strength of a material increases the potential for crack initiation but it also increases the resistance to crack growth. The initiation energy for new cracks appears to be directly related to shear strength. Because most of the lifetime of a crack is spent in the growth stage, mechanisms that reduce shear strength such as poor fibre-matrix bonding,

may slow or prevent crack growth. This gives an indication of the influence of osteon diameters and number on fatigue damage in compact bone. Osteon diameters vary somewhat by species and decrease slightly with age in humans (Martin et al, 1982). Discontinuities within the bone structure (e.g. voids, fibres, laminae etc.) too may provide sites for crack nucleation, but also may serve as barriers to crack growth.

Table 1.3 Relationship between material strength, fibre size and spacing to crack initiation and growth (Martin and Burr, 1989)

Resistance to:	Crack Initiation	Crack Growth
Material Strength		
Increased	Increased	Decreased
Decreased	Decreased	Increased
Fibre Diameter		
Increased	Decreased	Increased
Decreased	Increased	Decreased
Fibre Spacing		
Increased	Decreased	Increased
Decreased	Increased	Decreased

The fact that Haversian bone is similar in its osteonal arrangement to a very tough fibrous composite laminate material, provides a clear indication that osteonal bone is tough even though it is not very strong. Toughness, is a measure of a material's ability to resist fracture, i.e. the greater a materials toughness the more difficult it is for cracks to propagate and coalesce (Piekarski, 1973). The fact that osteonal bone is laminated also provides evidence of the difficulty for crack propagation, lamellar interfaces cause stress enhancement at the tip of a propagating crack to be inhibited as the crack enters the interface. The crack first meets a ductile interface and then meets a stiffer one, this causes the crack to be first accelerated and then decelerated by the interface. This then requires an increased threshold stress for the crack to continue propagating into the stiffer

layer (Burr et al, 1988). This prevents catastrophic brittle failures propagating through the Haversian system, and so increasing the size of the largest crack that can be tolerated at a particular stress level.

Similarly, the morphology of the cement line in Haversian bone permits relatively easy crack initiation but prevents or slows any significant crack growth. A cement line, lying adjacent to the stiffer more heavily mineralised bone matrix, is thought to be responsible for significant stiffness variations in bone (Burr et al, 1988). As with bone lamellae, this means that cracks in the region of cement lines will inevitably pass between regions of varying ductility which as explained above, slows down crack growth or eventually arrests it completely.

In summary then, the morphology of osteonal bone appears to provide an abundance of crack initiation sites but its structure prevents or slows any significant crack growth. Consequently, although osteonal bone is a relatively weak material, it has good fatigue and impact properties when loads are applied at physiological strain and strain rates. Furthermore, since large numbers of cracks initiated at relatively low stresses are repaired by bone remodelling, crack initiation may not be as detrimental to the fatigue life of bone as it would be in a non-living material.

1.3 Clinical relevance of microdamage in bone

1.3.1 Stress fractures

Stress fractures occur due to the accumulation of stress induced microcracks, which eventually result in a true fracture through the bone cortex (Schiller, 1994). They are caused by repetitive stresses, rather than by a specific traumatic episode, and occur in normal healthy bone. Such fractures are usually the result of repetitive, prolonged stresses on a bone that has not accomodated itself to that action. In most cases, they occur in individuals who are engaged in rigorous activity that is either totally new or to which they are not yet conditioned.

This is, in part due to a mechanical imbalance. Muscles tend to adapt more quickly than bones to a new activity and the increased muscle force acting on the relatively weaker bone causes deformation, microdamage accumulation and fracture. They occur commonly in military recruits. Pester and Smith (1992) carried out a study on army recruits and found that 0.91 % of male recruits and 1.09 % of females suffered from stress fractures. Stress fractures of the metatarsals and calcaneus are common in runners, Johnson et al reported an incidence of 3.7 % in varsity athletes (1994). Fatigue fractures within trabecular bone have been found clinically in the proximal femur, in the calcaneus and in the proximal tibia (Pais and Wang, 1989). In horses, humeral stress fractures usually require the animal to be destroyed. Stover et al (1992) reported 21 such fractures during an 18 month period at one California racetrack.

Clinically, stress fractures present as pain associated with a particular activity. The pain is relieved by rest and becomes worse when the activity is resumed. Diagnosis of stress fracture is important as continued activity may result in a complete fracture or in splinters of bone breaking off. The normal treatment for stress fractures is usually cessation the activity to allow the bone to heal. As the majority of people who suffer from stress fractures are young, bone repair usually takes place quite quickly.

1.3.2 Fragility fractures

Fragility fractures occur in response to minor traumas which in healthy adult bone would not lead to fracture (Heaney, 1993). The causes of bone failure may be intraosseous, extraosseous or a combination of the two. Extraosseous factors include the tendency to fall, manner of falling, amount of soft tissue at the point of impact to dissipate the force of falling, and environmental hazards. Intraosseous factors include both the quantity and quality of bone present.

Previous studies have found that the force of a fall from standing height, properly applied, is sufficient to break virtually any adult bone (Robinovitch et al, 1993). They conclude that older people are more inclined to break bones such as the hip because, in falling, they fail to adequately protect the hip in the way a younger person would (Heaney, 1993). Hip fracture alone is associated with a mortality of 10-20% within six months and overall morbidity is estimated to cost $10 billion per year (Riggs and Melton, 1995). Demographic trends predict a three-fold increase in the number of hip-fractures in the US by the year 2040 and world-wide, the number is predicted to increase from an estimated 1.7 million in 1990 to 6.3 million in 2050 (Melton 1996). The estimated world wide annual cost of hip fracture alone will reach US$ 131.5bn in the year 2050 (Johnell, 1997). In ageing bone there is clear evidence that the repair process is inefficient, leading to accumulation of microdamage within the bone. Schaffler et al (1994a, 1995) found that microcrack density in compact bone specimens taken from the femoral shaft and neck increased with age as a strong power-law relationship. Such damage accumulation in bone makes it a weaker material and so contributes to fragility fractures.

1.3.3 Osteoporosis

Osteoporosis is characterised by decreased bone mass and increased susceptibility to fracture (Lane et al, 1996). It effects 20 million individuals in the US. These individuals sustain more than 20 million fractures annually.

The World Health Organisation defines osteoporosis as levels of bone density more than two standard deviations below the young adult mean (Kanis, 1993). This description fails to take account of the role of bone quality in osteoporosis. Recent investigations have uncovered significant shortcomings in the use of bone mass as a predictor of bone fractures, particularly in older individuals (Sherman and Hadley, 1993). Bone mass increases during childhood, and peak bone mass is obtained by the middle of the third decade. Adequate calcium intake during childhood and the teenage years is essential to achieve peak bone mass and the greater the peak bone achieved, the greater the chance of avoiding osteoporosis in later life (Lane et al, 1996).

The primary goal in the treatment of osteoporosis is to prevent bone loss beyond the fracture threshold (Lane et al, 1996). Calcium supplementation is one of the most widely used treatments in osteoporosis, however as Heaney (1992) has pointed out, the administration of calcium supplements during growth may only accelerate the attainment of peak bone mass and there is no direct evidence to show that it increases the actual peak bone mass ultimately attained. Vitamin-D is also used commonly with calcium supplements in the treatment of osteoporosis. It has been found that individuals suffering from vitamin-D deficiency often have poor calcium absorption as well. A marked decrease in the rate of fractures of the hip was demonstrated in a study of elderly patients from France who had received dietary supplements of calcium and vitamin-D (Lamberg-Allardt et al, 1993).

Oestrogen deficiency plays a prominent role in the pathogenesis of osteoporosis. Oestrogen inhibits bone resorption and positively effects calcium balance. The administration of oestrogen to post-menopausal women not only prevents bone loss but also protects against vertebral and femoral fractures (Lane et al, 1996). However oestrogen has some severe side effects which prevent its prolonged use, primarily endometrial bleeding, and concern about the risks of cardiovascular disease due to evidence that it can lead to excess blood clotting, as well as endometrial and breast cancer.

1.3.4 The role of bone quality in osteoporosis

The strength of bone is derived from the same basic features that determine the strength of all structures. These are, the strength of the structural material itself, its three dimensional arrangement and its mass density. The first two are commonly categorised together under the term 'bone quality' in contrast to the mass density of bone which is a reflection of bone quantity.

Tests conducted on trabecular bone samples from various sites (including femoral neck and vertebral body) have found that 60-70% of the variance in bone strength can be explained by both linear and power functions of density (Goldstein, 1987, Rice et al, 1988). From this, it is evident that bone mass alone is insufficient to predict bone failure. This would suggest an important role for bone quality (Lee, 1997), the 30-40% unaccounted for, can be explained by the fact that although bone density is a scalar quantity, bone tissue is anisotropic and of varying quality depending on age, degree of mineralisation and porosity (Goldstein et al, 1993).

Prospective clinical studies have confirmed that bone mass (or density) is not the sole risk factor for predicting vertebral fracture (Ross et al, 1993), nor is it entirely specific or sensitive to predicting fracture (Ott, 1993). Virtually every study that has contrasted bone mass density in patients with and without fragility fractures have found an overlap between both groups (Melton et al, 1989; Kimmel et al, 1990). Individuals with fractures commonly have normal bone mass values and sometimes have been found to have above average bone mass. In contrast, other studies have found that individuals with well below average bone mass density often fail to sustain fractures.

The idea of bone quality having wide-scale importance in osteoporosis and fragility fractures is still a relatively new one. Ross et al (1991) showed that individuals with one or more spinal fractures were much more likely to suffer a subsequent fracture, than those without a prior fracture. His study, showed that individuals in the *highest tertile* of bone

mass were more likely to develop another fracture than individuals in the lowest tertile of bone mass who had not previously sustained fracture. This illustrates the importance of fragility arising from non-mass related factors (Heaney, 1992) and requires us to look beyond the bone mass density hypothesis with regard to fragility fractures.

The bisphosphonate range of drugs have recently been introduced as a treatment for osteoporosis (Liberman et al, 1995), but their exact mode of action remains unknown (Lin, 1996). They are characterised pharmacologically by their ability to inhibit bone resorption, so increasing the quantity of bone present (Lee, 1997). Alendronate was the first of the bisphosphonate drugs to be widely used in clinical practice. Initial tests carried out on women with post menopausal osteoporosis showed that those treated with alendronate had significant increases in bone mineral density. Tests carried out on animals in which osteoporosis had been induced showed a similar increase in bone density when treated with alendronate. Mechanical testing of the lumbar vertebrae of the animals treated with alendronate also showed a 100% increase in strength (Balena et al, 1993).

These data on alendronate activity may not be quite as impressive as they seem. Some reports suggest that bisphosphonates are absorbed into the crystal structure of the exposed hydroxyapatite. During bone resorption, osteoclast activity releases bisphosphonate from the bone matrix, which then inhibits the osteoclasts (Sato et al, 1991). Sahni et al (1993) suggests that bisphosphonates operate by having at least a partial effect on osteoblasts which then results in activity of the osteoclasts being inhibited.

Whatever the specific mode of action of the bisphosphonates, it is generally accepted that the drugs do inhibit osteoclast activity and suppress the resorption phase of remodelling. In the medium term it is clear that suppression of this resorptive phase prevents bone loss and should therefore reduce fracture risk. However microdamage stimulates remodelling which in turn repairs damage in bone. Therefore the possibility exists, that, by administering bisphosphonates to inhibit remodelling, microdamage is accumulating in the bone, leading to a reduction in bone quality. This could, in the long term prove

harmful. Hirano et al (2000) applied high doses of etidronate to skeletally mature beagles and found that the drug did suppress bone turnover. However, this study also showed an increase in fractures in ribs and in the thoracic spinous process. They hypothesised that this increase in fracture numbers was due to the high doses of the drug causing formation of excess unmineralised bone but the exact cause was uncertain. Mashiba et al (2000) have shown the first real evidence that treatment with bisphosphonates can lead to an increase in microdamage accumulation. They treated two groups of healthy dogs with high doses of risedronate and alendronate respectively over the course of one year. They found that the treatment suppressed intracortical remodelling in both groups and significantly increased microdamage accumulation.

1.4 Objectives of this research

This study seeks to learn more about the process by which microcracks initiate, propagate and accumulate, ultimately bringing about bone failure, or fracture.

Principal Objectives

(1) To develop a repeatable technique to carry out mechanical fatigue tests on samples of bone. This would allow for experimental evidence on the fatigue behaviour of compact bone to be obtained, in particular, a logarithmic stress/life curve (S/N curve), which would permit analysis of the degree of scatter in the fatigue life of different specimens of bone which had been tested in identical conditions. By carrying out these experiments, it is hoped to test the predictive capacity of a mathematical model which had been developed by our research group (Taylor, 1998a). This is described in Chapter 2.

(2) To refine a technique for labelling microcrack growth. Previous work in this laboratory (Lee, 1997; Lee et al, 2000a) developed fluorescent chelating agents to label microcracks in trabecular bone. This work showed, that when applied in sequence, chelating agents could be used to monitor microcrack growth in trabecular bone. However, substitution of one agent from another sometimes occurred, making differentiation of one agent for another difficult and preventing crack growth being accurately measured (Lee, 1997; O'Brien et al, 1997, 1998; Lee et al, 2000a). Using chemical analysis, it is hoped to rank the chelating agents in order of affinity for calcium. By applying the agents in decreasing order of affinity, substitution should be minimised. It is also proposed to determine the optimal concentration regime for the five agents which will allow them to fluoresce equally clearly when viewed using UV epifluorescence microscopy. This is described in Chapter 3.

(3) To apply the chelating agents in the determined sequence to label microcracks formed before, and at different intervals during a mechanical test. This work aims to

provide new information on the process by which microcracks initiate, propagate and accumulate leading to failure. By sectioning fatigued specimens both transversely, and longitudinally (in which direction little research has been carried out), it is hoped to develop information on the three dimensional shape of microcracks, and to look at the direction of microcrack growth, and the extent to which bone microstructure influences the ability of individual microcracks to initiate and grow. This work is described in Chapter 4.

(4) To study the three dimensional shape of *in vivo* microcracks. Having hypothesised as to the three dimensional shape of microcracks in Chapter 4, the theory is now tested. Two different computer-based methods of reconstruction were used to study microcracks in three dimensions: (i) serial sectioning of methylmethacrylate embedded sections using a sledge macrotome, followed by microcrack identification by means of UV epifluorescence microscopy, and subsequent reconstruction using computer software and (ii) laser scanning confocal microscopy followed by reconstruction of microcracks into a 3D image. By using two techniques, it was proposed to develop an accurate description of the true three dimensional shape of microcracks in bone. Epifluorescence microscopy is also used to study microcracks in the longitudinal rather than the more commonly looked at transverse direction. This work is described in Chapter 5.

Chapter 2

THE FATIGUE BEHAVIOUR OF BONE

2.1 Introduction

The process of fatigue can be described as the gradual deterioration and eventual failure of a material when subjected to a periodic or cyclic stress. Fatigue damage occurs with the initiation and growth of microscopic cracks which, develop within the material during each load cycle (Martin and Burr, 1989). The fatigue life of any material is thus a function of crack accumulation and growth (Agarwal and Broutman, 1980; Mori and Burr, 1993). In bone, fatigue failures occuring *in vivo*, due to excessive use of a limb are known as stress fractures. Microdamage also accumulates in the elderly reducing bone quality and contributes to fragility fractures. Fatigue damage has been shown to play a major role in bone remodelling and adaption (Martin and Burr, 1982; Burr et al, 1985; Burr and Martin, 1993; Mori and Burr, 1993; Prendergast and Taylor, 1994; Lee et al, 1999; Martin, 2000). Therefore, it is clearly important to have precise information on the tendency of bone to fail by fatigue, so that the above phenomena can be analysed and predicted.

2.1.1 Fatigue in bone

In order to begin to understand the nature of microdamage in living bone, the *in vitro* behaviour of compact bone must be understood. One of the problems is that there is a relatively large amount of experimental data available on the fatigue of compact bone from numerous studies, but variations in the test protocol used by different authors (Table 2.1) have made it difficult to compare results in any systematic way.

Taylor (1998a) found 12 separate studies which recorded the number of cycles to failure (N_f) as a function of applied stress range ($\Delta\sigma$) or strain range ($\Delta\varepsilon$), for the relatively high N_f values of 10^5 - 10^6 cycles (Table 2.1). He carried out a Weibull analysis in order to show that the measured fatigue strength of a material is affected by specimen size i.e. tests using a large stressed volume result in lower fatigue strength due to the increased probability of weak regions in a specimen. This analysis revealed an important size effect in bone and predicted this effect with an accuracy of 12 %.

The model grouped together all the fatigue strength results in the literature (Table 2.1). Differences in measured fatigue properties arose due to a number of testing parameters, including temperature, frequency, and loading type. Loading type included zero-tension, zero-compression, tension-compression and tension-tension. Data were compared in terms of the fatigue strength at 10^5 cycles. At this level, the applied stress is sufficiently low to eliminate any effects of creep, so results could also be related to physiological conditions. 10^5 cycles also represents about one month of normal activity in living bone

Table 2.1 Experimental data on fatigue of compact bone Taylor, 1998a)

Reference	Material	Specimen	Loading	Freq. (Hz)	Temp. (°C)
Carter and Hayes (4)	Bovine	Rotating bend	TC	125	21-45
Evans and Riolo (8)	Human	Flexural	TC	High	Room
Gray and Korbacher (10)	Bovine	Uniaxial	OC	30	22
Lafferty and Raju (12)	Bovine	Rotating bend	TC	30	21
King and Evans (11)	Human	Flexural	TC	30	Room
Carter and Caler (6)	Human	Uniaxial	TC and OT	2	37
Carter et al. (5)	Human	Uniaxial	TC	0.5-1	37
Choi and Goldstein (7)	Human	Flexural	OT	2	Room
Caler and Carter (3)	Human	Uniaxial	OT and OC	2	37
Martin et al. (15)	Equine	Flexural	OT	2	37
Shaffler et al. (23)	Bovine	Uniaxial	OT	10-12.5	21
Zioupos et al. (27)	Bovine	Uniaxial	OT	2	21
Nunamaker et al. (20)	Equine	*In vivo*		*In vivo*	*In vivo*

TC = tension-compression, OC = zero compression, OT = zero tension (including tension-tension with ratios of minimum stress to naximum stress as high as 0.18).

2.1.2 Theoretical Model

Fatigue failures occur in response to cyclic loading. Tests are usually conducted at a constant cyclic amplitude and it is found that the number of cycles to failure, N_f is a function of the stress range $\Delta\sigma$, which is the difference between the maximum and minimum stress in a cycle. This relationship can be expressed as an inverse power law with two constants, A and α, where α defines the slope of the logarithmic stress life curve.

Equation 2.1

$$N_f = A/(\Delta\sigma)^{\alpha}$$

The values for these constants vary depending on the differences in measured fatigue properties. In some tests, strain range can be substituted for stress range and a similar relationship exists. For example, when comparing human, bovine and equine bone, it is clear that they have distinctly different properties. This would be expected since microscopically they are very different. Bovine bone also has higher values of ultimate strength, toughness and stiffness (E). In this case, the use of strain range instead of stress range would probably eliminate the difference between bovine and human bone.

Weibull analysis is commonly used in the treatment of scatter in fatigue fracture and fracture of brittle materials. It is assumed that the measured fatigue strength (maximum stress to which a specimen can be subjected without failure occurring) of a series of identical specimens which have been mechanically tested will vary according to:

Equation 2.2

$$P_f = 1 - \exp[-(\Delta\sigma_0/\ \Delta\sigma_0^*)^m]$$

P_f is the probability of failure of a given specimen where m and $\Delta\sigma_0^*$ are constants and $\Delta\sigma_0$ is the fatigue strength of the material which is defined as the value of $\Delta\sigma$ corresponding to a given N_f. Taylor (1998a) analysed the degree of scatter in properties

measured from two large data sets, Carter et al (1981) tested 74 specimens at various levels of stress, their data fell within a scatter band in which N_f varied by about one order of magnitude. Evans and Riolo (1970) tested 30 specimens at the same $\Delta\sigma$ and also found a large degree of scatter. By relating these studies and normalising the fatigue strength by dividing by its mean value $\Delta\sigma_{mean}$, Taylor obtained values for the constants with m = 8 and $\Delta\sigma_0^*/\Delta\sigma_{mean} = 1.067$. Equation 2.3 can then be used to calculate the fatigue strength, $\Delta\sigma_0$ for any specimen volume, Vs if the fatigue life $\Delta\sigma_0'$ for a particular specimen volume Vs' is known and where P_f defines the probability that a specimen will fail before a given number of cycles has elapsed. P_f varies from 0, no chance of failing to 1.0, certain to fail. So setting P_f=0.5 gives the average of the distribution for a given N_f and specimen size (Taylor, 1998a).

Equation 2.3

$$\Delta\sigma_0=1.067\Delta\sigma_0'[-(Vs'/Vs)\ln(1-P_f)]^{1/8}$$

By analysing all the experimental data (Table 2.1) using equation 2.3, it was possible to plot the experimental data as shown in Fig. 2.2 which summarised all the studies at physiological frequencies. This graph shows experimental data at physiological frequencies for human and bovine bone in 0T (zero-tension) loading, for human bone in 0C (zero-compression) loading and TC (tension-compression loading) and for equine bone *in vivo*. It also shows predictions for human bone in zero-tension loading using Eqn. 2.3 with failure probabilities of 0.5, 0.1 and 0.01 (Taylor, 1998a).

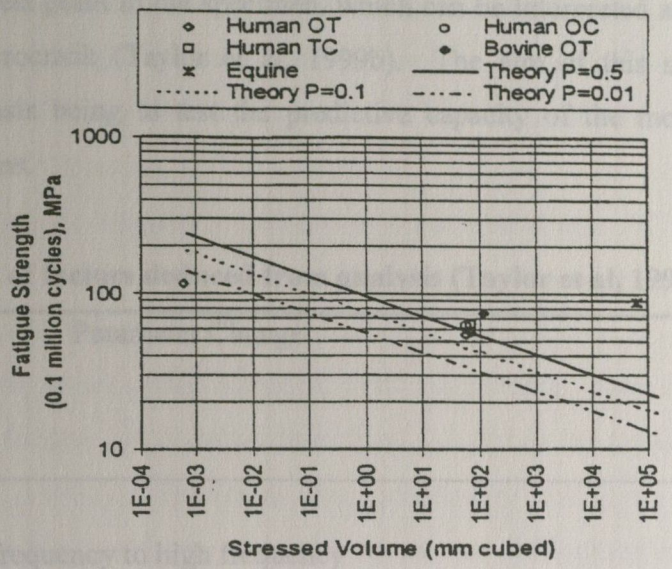

Fig. 2.1 Fatigue strength (10^5 cycles) as a function of stressed volume, (Taylor, 1998a).

By showing that all the existing data on bone fatigue conformed to this Weibull analysis, Taylor showed that fatigue limits at 10^5 cycles could be successfully predicted when stressed volume was accounted for. When considered in the this way, the data revealed consistent and seperable effects of frequency, bone type and loading type. By comparing the different values of predicted fatigue life for the different frequencies, bone type and loading type it was possible to devise multiplication factors in order to relate the data. The effect of temperature had already been established by Carter and Hayes (1976). The magnitude of the different effects is shown in Table 2.2 which shows the multiplying factors to be applied to the fatigue strength in each case. The error in this model was predicted to be a maximum of 12% in fatigue life, which is comparable with the error inherent in the experimental data.

This predictive model is not essentially a mechanistically based theory. It was formulated from a statistical analysis of previous data, the intention being to show that data from various sources, tested in a variety of ways, are telling the same story and from this this new predictions can be made. There is however a certain mechanistic approach to the model in that it is based on the 'weakest link' approach and assumes failure will

occur from the weakest point in the specimen, which can be interpreted as the largest or most dangerous microcrack (Taylor et al, 1999b). The aim of this study is purely experimental, the basis being to test the predictive capacity of the model by fatigue testing bone specimens.

Table 2.2 Summary of factors deduced from analysis (Taylor et al, 1999b).

Parameter Change	(Effect on fatigue strength) Multiplying Factor
Frequency	
From physiological frequency to high frequency	1.33
Bone Type	
From old human bone to bovine bone	1.44
Temperature	
From physiological temperature to room temperature	1.16
Loading Type	
From zero tension to zero compression (human bone)	1.08
From zero tension to tension-compression (human bone)	1.12
From zero compression to tension-compression (human bone)	1.04

Low frequency refers to physiological frequencies (0.5-3 Hz.), and high frequency refers to frequencies of 30-125 Hz. The multiplying factor is that needed to make the given change at 37^0C.

2.1.3 Objectives

The aims of this study are:

(1) To establish a mechanical testing protocol so as to obtain experimental evidence on the fatigue life of compact bone, and in particular to obtain a logarithmic stress/life curve (S-N curve) to show the degree of scatter in the fatigue life of different specimens of bone which had been tested in identical conditions.

(2) To test the predictive capacity of the mathematical model (Taylor, 1998a) using this experimental data by applying it to data which had not been considered when formulating the theory i.e. fatigue testing of bovine specimens in zero-compression at physiological frequency. Gray and Korbacher (1974) carried out tests on bovine bone samples in compression but they used a frequency well above physiological rates (30 Hz). Caler and Crater (1989) tested in zero-compression cycling at physiological frequency but they used human rather than bovine bone. Using these experimental data, it was proposed to determine whether the actual value obtained from experimental data agreed with the theoretical value for fatigue life obtained from Eqn. 2.2 within the predicted 12% error proposed by Taylor (1998a). Specimens for compressive testing are also easier to manufacture than tensile specimens since there are no difficulties in gripping the specimen and, unlike bending specimens where a smaller area is stressed, results from compression tests are easier to interpret.

(3) Lee et al (2000a) were the first to use a series of chelating agents to look at microcrack growth during mechanical testing. This study showed that individual chelating agents were as effective as the standard stain (basic fuchsin) in labelling microcracks, although some problems were identified with the application of the agents in series. By applying a series of flourescent chelating agents before and during testing (Lee et al, 2000a), it was proposed to carry out a preliminary study into the process by which microcracks initiate and grow in compact bone and to test the efficiency of this detection method.

2.2 Materials and Methods

2.2.1 Fatigue testing protocol

In order to provide accurate data, a repeatable, standardised test technique was required. A standard specimen should be designed such as to minimise potential areas of stress concentration whilst being able to withstand buckling under load. It should also be designed such that the region of failure can be predicted to a certain extent. These factors should all be considered while the amount of machining should be minimised to reduce build-up of artefactual damage which give inaccurate results regarding the process of fatigue damage accumulation during testing. Keaveny et al (1994a) proposed such a technique for fatigue tests on cancellous bone. They designed a test specimen which could be used in both tension and compression and reduced experimental artefacts associated with conventional bone test specimens.

In many previous studies, specimens exhibited weaknesses which could have been eliminated with better design. To prevent the problem of stress concentrations within a specimen, it was decided to use a cyclindrical specimen which could be machined using computer controlled conditions, so as to produce a similar specimen each time. By waisting the centre of the specimen (Fig. 2.2), a weaker region was designed where we would expect crack accumulation to be dominant compared with the rest of the specimen.

2.2.2 Manufacture of specimen

Samples of cortical bone were removed from the mid-diaphysis of bovine tibiae using a band saw. Care was then taken to ensure that the samples were cored with the axis aligned parallel to the longitudinal axis of the bone. Initially these sections were cored using a diamond tipped coring tool (Starlite Industries, PA, USA) using the technique developed by Keaveny et al (1994a) for cancellous bone. However, because of the localised excessive heat build-up in the tool during coring of the denser material, it was

found that this technique was unsuitable for coring compact bone. The problem was solved by obtaining a special coring tool (Peranko Ltd., Dublin) which could withstand heat by distributing it up the length of the tool. This tool was heavier and bulkier than the diamond tipped tool and was made from high speed steel. Using this tool, it was possible to core cyclindrical specimens, diameter 7 mm of consistently high quality.

The original irregular shaped bone samples which had been cut with the band saw were placed in a small steel box (50x25x25 mm) and plaster ('Handi Mix Plaster', GM Handipack Products Ltd., Armagh, N. Ireland) was poured over them, and allowed to set overnight in order to fix them in position. Coring was carried out at 350 rpm. The coring tool was located over a region of bone in the steel box, which was gripped in a vice. The tool was slowly moved downwards into the bone to a depth of 35mm. Coolant (Century Lubricant, UK) was applied to both the specimen and the tool throughout the machining process to ensure that dehydration did not occur.

This process resulted in cyclindrical specimens of length 35mm and diameter 7mm. The centre sections of these specimens were then waisted using a VS 450 CNC lathe (Harrison, UK). Specimens were placed in the lathe and a computer numerical control (CNC) program (Appendix 2.1) was fitted which transferred the original drawing (Fig. 2.2) to a digital array of numbers which could be identified by the CNC machine. The CNC program turned the centre region of the specimen to a gauge diameter of 5.25mm and a gauge length of 7mm. Again, all machining was carried out under wet conditions and the specimens were not allowed to dry out. The main advantage of using the CNC lathe was the attention to minute detail, a very good surface finish and the gauge diameter remained constant from specimen to specimen. Visual inspection of the final specimens showed good surface finish in the gauge length with no obvious machining defects. After machining, the specimens were frozen to -20^{0}C prior to mechanical testing.

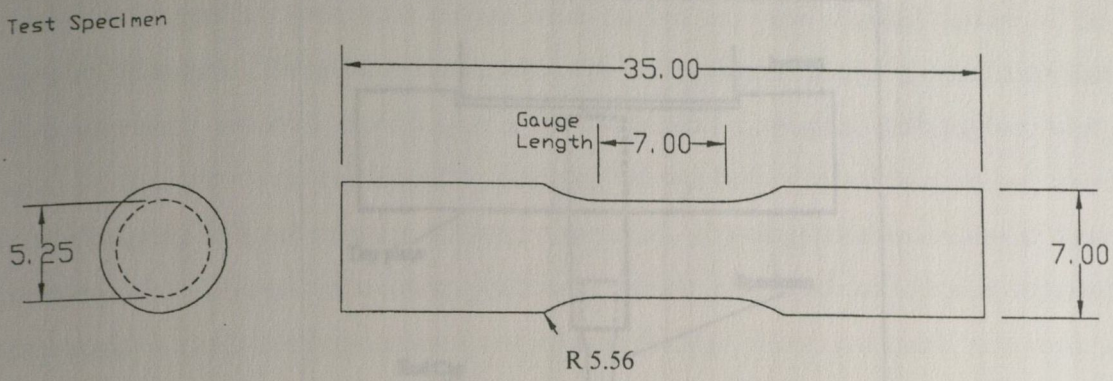

Fig. 2.2 Dimensions of final specimen obtained (mm)

2.2.3 Mechanical testing

An INSTRON 8501 servo-hydraulic testing machine was used in load control to apply an axial compressive force to the specimens. Testing was carried out in the rig shown in Fig. 2.3. Brass end caps were attached to the specimens before testing to facilitate loading without contact damage (Keaveny, 1994a). The machine was fitted with parallel aluminium plates into which depressions had been machined to accommodate the specimens' end caps. This method helped to avoid errors in the axial alignment of the specimens, which is a potential problem leading to the creation of bending stresses. All specimens were tested at a frequency of 3 Hz, cycling between 11 and a 111 MPa to give a stress range value of 100 MPa and a stress ratio of 0.1. A constant stress range was used in order to study the number of cycles to failure (N_f) and to correlate the results for all the specimens (Taylor et al, 1999b).

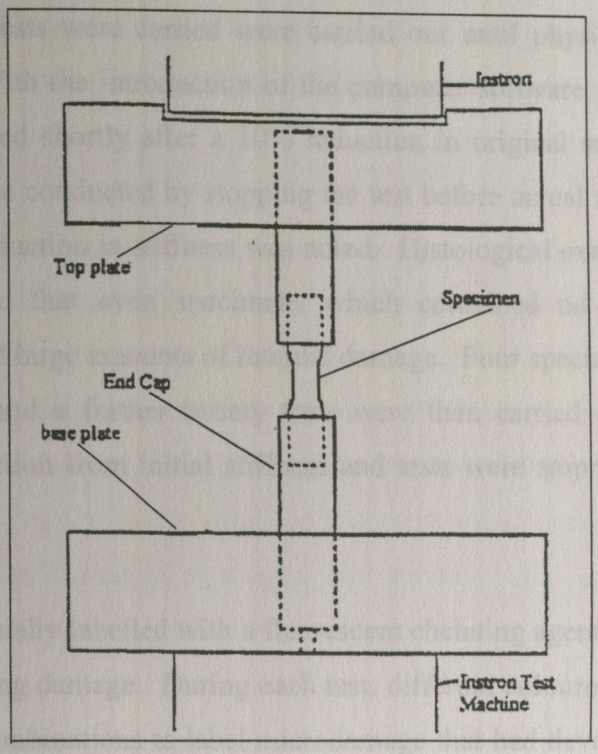

Fig. 2.3 Schematic of rig used in experiments

Initially a chart recorder was used to analyse the deformation that occurred in the specimen during the course of a fatigue test. However problems were encountered with the accuracy of this method, especially regarding calibration of the machine and conversion of the machine output (mV) to actual deformation (mm).

This problem was resolved by the use of an input/ output acquisition card (Amplicon PC30AT, Liveline Ltd.) whereby a computer was linked to the Instron machine and the machine output was calibrated to the card output in order to convert voltage output to deformation in millimetres. Then, by the use of a Microsoft Turbo C program (Appendix 2.1), it was possible to read the machine output, convert it to millimetres and store it in a file. By sampling, at various intervals during the test, it was possible to look at the deformation that occurred during the progression of a test and relate it to the loss in stiffness. This ability to read the reduction in stiffness during the course of a test allowed failure to be defined at a given loss of elastic stiffness.

Initially, a number of tests were carried were carried out until physical failure of the specimen occurred. With the introduction of the computer software, it was found that failure generally occurred shortly after a 10% reduction in original stiffness had taken place. Further tests were conducted by stopping the test before actual fracture had taken place when this 10% reduction in stiffness was noted. Histological examination of these specimens then showed that even specimens which contained no obvious external microcracking contained large amounts of internal damage. Four specimens were used to establish the protocol and a further twenty tests were then carried out. Failure was defined as a 10% reduction from initial stiffness and tests were stopped when this had been reached.

The specimens were initially labelled with a fluorescent chelating agent prior to testing in order to label pre-existing damage. During each test, different coloured chelating agents were used in various combinations to label microdamage that had developed at different intervals (determined by a certain loss of stiffness) during the course of testing.

2.2.4 Labelling of microcracks

The standard and accepted method for labelling microdamage in bone is the use of basic fuchsin as a labelling agent. Lee et al (2000a) introduced the principle of using chelating agents to label microdamage accumulation during testing of trabecular bone specimens (more detail on the use of chelating agents in microdamage detection in bone can be found in Chapter 3). Chelating agents have a basic advantage over fuchsin in that they are site specific and bind to the exposed calcium that line crack walls. Rahn (1977) identified a series of 5 agents which could be used in labelling bone: alizarin, calcein, calcein blue, xylenol orange and oxytetracycline. It has been shown that by applying a number of these labels in sequence at different intervals during testing of trabecular bone specimens, crack propagation can be monitored (Lee et al, 2000a). The problem of differentiating damage incurred during the test from *in vivo* damage and machining-induced damage was approached with the idea of using a pair of fluorescent chelating

agents. By applying one chelating before testing and another during the test, it was possible to distinguish between the two types of damage by the presence of the different coloured labels.

In this study, each specimen was initially placed overnight in a vial of a chelating agent, in a vacuum desiccator (50 mm Hg), to label pre-existing damage. During testing, data were displayed on the computer screen and so it was possible to stop the test at intervals (determined by a certain reduction in stiffness) to apply different chelating agents to label microdamage initiation and accumulation during the test. Lee (1997) had identified some problems with the use of applying the agents in sequence whereby certain combinations tended to a lead to substitution of one agent for another. For this reason various combinations of the agents were applied during testing.

2.2.5 Preparation of ground sections

After testing, the specimens were washed in de-ionised water and returned to the freezer prior to sectioning and mounting. The following protocol was used to obtain sections of the suitable thickness and quality for histological examination (Frost, 1958).

1. Specimen was placed in a small clamp and approximately 250μm was cut using a diamond saw (Struers Miniton, Copenhagen, Denmark).

2. A sheet of No. 400 silicon carbide paper was placed on a flat surface under running water and the section was placed upon it. Another piece of paper was wrapped around a glass slide and the section was manually ground down between the two pieces of paper in a circular fashion using light pressure.

3. This grinding was continued and periodically the thickness was checked using a micrometer screw until the required thickness (100-150μm) had been obtained (Frost, 1960).

4. Specimens were agitated in 0.01% wash up liquid in a beaker, placed in a Coors porcelain funnel with fixed perforated plate and washed in distilled water.

5. Specimens were then air dried and mounted using a mounting medium (Eukitt's mounting medium, Germany) under a glass coverslip.

2.2.6 Histological examination of ground sections

The ground sections were examined using epifluorescence microscopy and microcracks were identified using established criteria (Table. 2.3). The microcrack images were captured and transferred to a HP PIII Brio personal computer (Hewlett Packard, Grenoble, France) using an CCD colour video camera (Optronics Engineering, Goleta, Ca) and stored for analysis.

Table 2.3. Criteria for identifying microcracks in bone (Lee et al, 1998)

Step 1: Fluorescence microscopy - green incident light (G – 2A filter block, λ=546 nm), x125 magnification: Candidate crack should be intermediate in size, being larger than canaliculi but smaller than vascular canals.

Step 2: Fluorescence microscopy - green incident light (G – 2A filter block, λ=546 nm), x125 magnification: Candidate crack should have a sharp border, with fluorescence of chelating agent within crack borders evident.

Step 3: Fluorescence microscopy - UV incident light (λ=365 nm), x125 magnification: Candidate crack should be stained through the depth of the section.

Step 4: Light microscopy, x250 magnification: When the depth of focus is changed, the edges of the crack can be observed to be more deeply stained than the intervening space.

2.3 Results

2.3.1 Mechanical data

Of the twenty one specimens analysed, five failed before the predicted 10% reduction in stiffness had taken place. The failure pattern was similar with all specimens, with the main fracture crack occurring in the gauge length of the specimen at an approximate angle of 45^0 to the specimen axis.

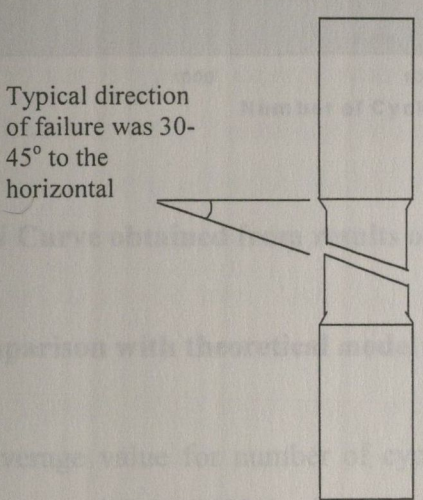

Fig. 2.4 Direction of failure of specimen

Fig. 2.5 shows the logarithmic stress/life curve (S-N curve) obtained from the data. The average number of cycles to failure (N_f) was 36265 cycles and, as expected, scatter over several orders of magnitude was found.

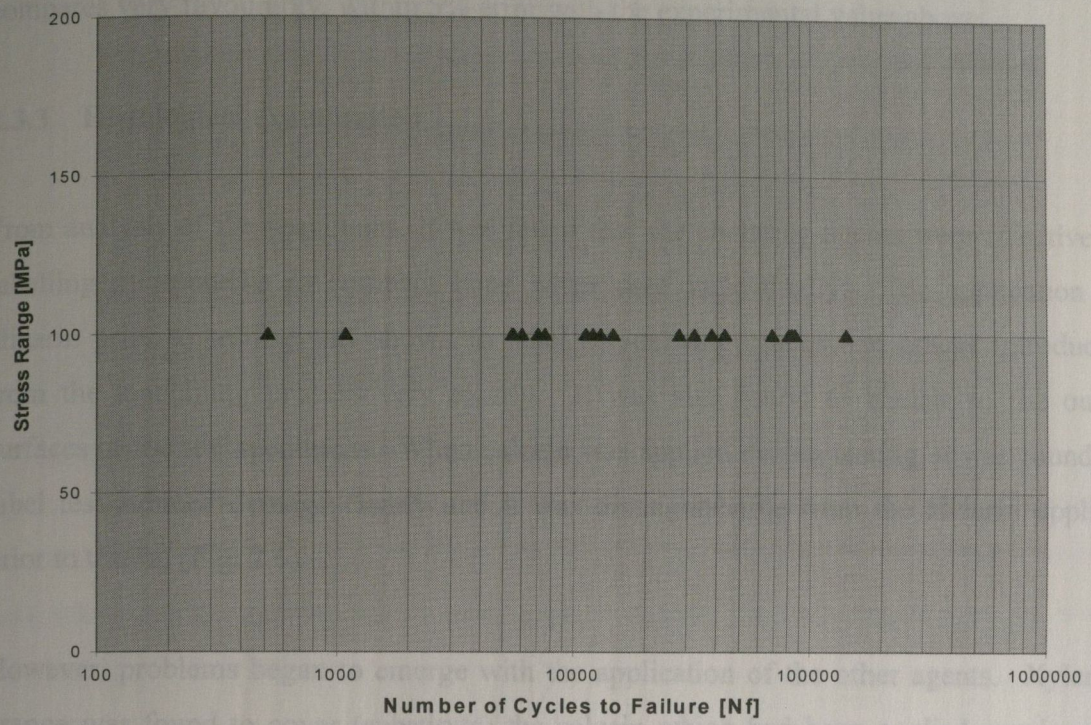

Fig. 2.5 S/N Curve obtained from results of compressive fatigue tests

2.3.2 Comparison with theoretical model

When the average value for number of cycles is entered into equation 2.1, using the results of Carter and Caler (1981) who carried out zero-compression, cyclic loading tests on specimens with a similar volume to those used in this study with α=11.78 and finding the value for fatigue strength at 100,000 cycles, we obtain a value for $\Delta\sigma$ = 91.84 MPa.

The stressed volume for the specimen used (gauge length x cross sectional area) was found to be 151.53 mm^3. When this value is added to the theoretical line with P=0.5 (Fig. 2.1) a value for the fatigue strength is obtained of 53 MPa. This line is predicted at physiological temperature (37 ^oC) for human bone specimens in zero tension loading. If the multiplication factors are used (Table 2.2) to convert the value by relating human to

bovine bone, physiogical temperature to room temperature and zero tension loading to zero compression loading, a value of 95.61 MPa is obtained for the fatigue strength. This compares very favourably, within 5% error with the experimental value above.

2.3.3 Histological examination

From analysis of the specimens, it was found that the chelating agents were effective at labelling microcracks in compact bone when used individually. The application of alizarin prior to testing was shown to label pre-existing cracks and cracks introduced from the machining process very clearly. It was also found to chelate to the outer surfaces of the test specimens. When calcein was applied during testing, it was found to label test-induced damage clearly and it was distinguishable from the alizarin applied prior to testing (Fig. 2.6).

However, problems began to emerge with the application of the other agents. Xylenol orange was found to cover (substitute) the calcein which had been applied previously. Calcein blue, when applied as an individual agent was found to label microdamage extremely well. However, when applied sequentially, it was found to substitute some of the other agents as can be seen clearly in Fig. 2.7. Problems were also found with the application of oxytetracycline whereby it appeared to substitute all the agents with the exception of alizarin, while surprisingly, alizarin, xylenol orange and calcein blue also appeared to substitute it when applied after oxytetracycline.

Fig. 2.6 Section through fatigue- tested specimen viewed using UV epifluorescence. Alizarin (red), which was applied prior to testing can be seen on the surface of the bone while calcein (green) which was applied during the test can be seen to label microdamage. Bar=100 μm.

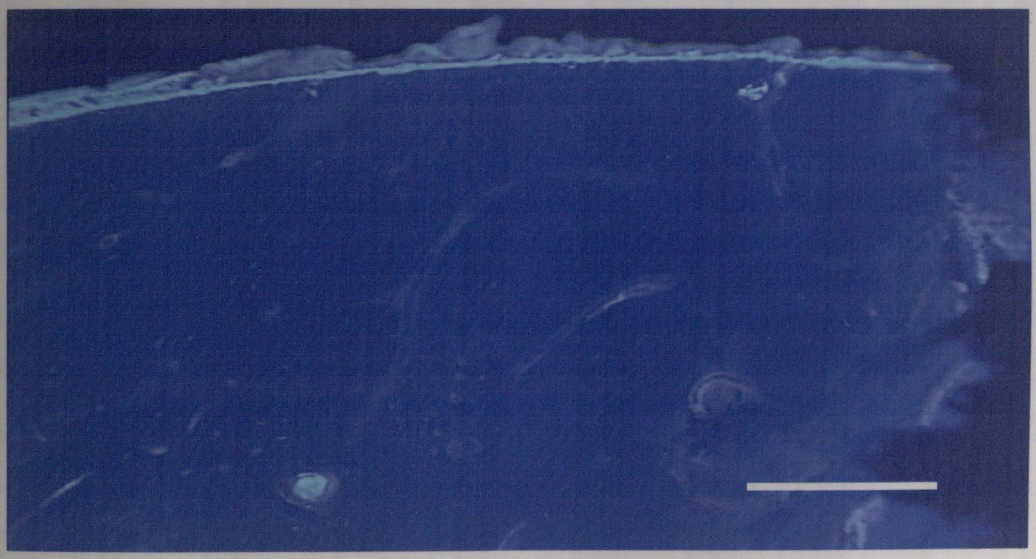

Fig. 2.7 Specimen viewed using UV epifluorescence. Initially, alizarin (red) had been applied prior to testing followed by calcein (green) and then calcein blue (sky blue) during the test. It can be seen that there is great difficulty distinguishing any of the agents as the entire section appears bright blue. Bar=100 μm.

2.4 Discussion

The results obtained and the methods used, provide a new insight into the fatigue behaviour of cortical bone. Fig. 2.5 shows the S-N curve obtained from the fatigue tests carries out. Scatter to the extent of several orders of magnitude can be seen. However the degree of scatter was found to be very similar to that found by other authors (Evans et al, 1970; Carter et al, 1981). This suggests that the scatter is not due to inadequacies in the testing technique but is due to the bone material itself. Although the specimens tested were of exactly the same dimensions and all came from the mid diaphysis of bovine tibiae, other factors such as orientation of the bone lamellae, porosity and degree of mineralisation may explain the large variation in fatigue life from specimen to specimen.

The average life for the specimens in this study was 36,000 cycles to failure, which corresponds to a fatigue strength at 100,000 cycles of 91.84 MPa. This compares favourably with the value of 95.61 MPa predicted by Taylor's model (1998a). These initial experimental results appear to have validated the accuracy of the mathematical model as it appears to be able to predict the strength of bovine bone in compression by combining the effects of specimen size, temperature and loading frequency.

The chelating agents were found to be effectively label fatigue cracks in compact bone. Previous work had shown them to label microdamage effectively in cancellous bone (Lee et al, 2000a) but this was the first attempt to label microdamage in dense cortical bone using fluorescent chelating agents. From the histological examinations carried out on the fatigued specimens, it was clear that the chelating agents had penetrated the bone specimens. The agents were found to penetrate Haversian canal systems and lodge in them and were also found in the canalicular network.

The application of alizarin before testing and then, calcein or xylenol orange during the fatigue tests, showed that it was possible to differentiate between pre-existing and test induced damage. The sequence was then extended with the application of two or more agents during the test with the aim of labelling crack propagation at intervals during

testing. With some sequences e.g. alizarin-calcein-xylenol orange, this appeared to work. However, in some cases, when three or more agents were applied in sequence, substitution of one dye for another took place. This is consistent with the observations made by Lee et al (2000a) in trabecular bone. It was proposed that this substitution was due to the different binding strengths of each agent for calcium ions. One of the initial aims of this study, was to refine the detection method by carrying out tests on the chelating agents in order to determine the optimal concentrations of each of the agents, and to determine the optimal application sequence required to minimise the substitution problem when two or more agents were used. More details on the methods used, the results obtained and on microdamage labelling in bone in general can be found in Chapter 3.

All specimens were found to contain varying amounts of microcracks and from analysis, it was clear that the waisted centre sections of the specimen had acted as the stress concentration region as microdamage was very prominent here. Pre-existing damage was found in all specimens, but from these initial examinations it appeared that the presence of machining artefacts did not generally lead to damage accumulation and any cracks formed from these artefacts were minute and did not propagate or cause extensive damage.

As might be expected in an anisotropic material such as bone, microcracking was greatly influenced by the bone's microstructure. Often, the direction of crack growth appeared to be influenced by the presence of lamellar interfaces and Haversian canal systems. From this study, it appeared that although the Haversian canals did not act as stress concentrators, they did influence the orientation of cracks, for example, cracks were commonly found in the areas of interstitial bone, and often midway between adjacent Haversian canals (Fig. 2.8). From the specimens examined, it was obvious that this area of microcrack interaction with the bone's microstructure was worthy of further investigation. This was studied in detail in Chapter 4.

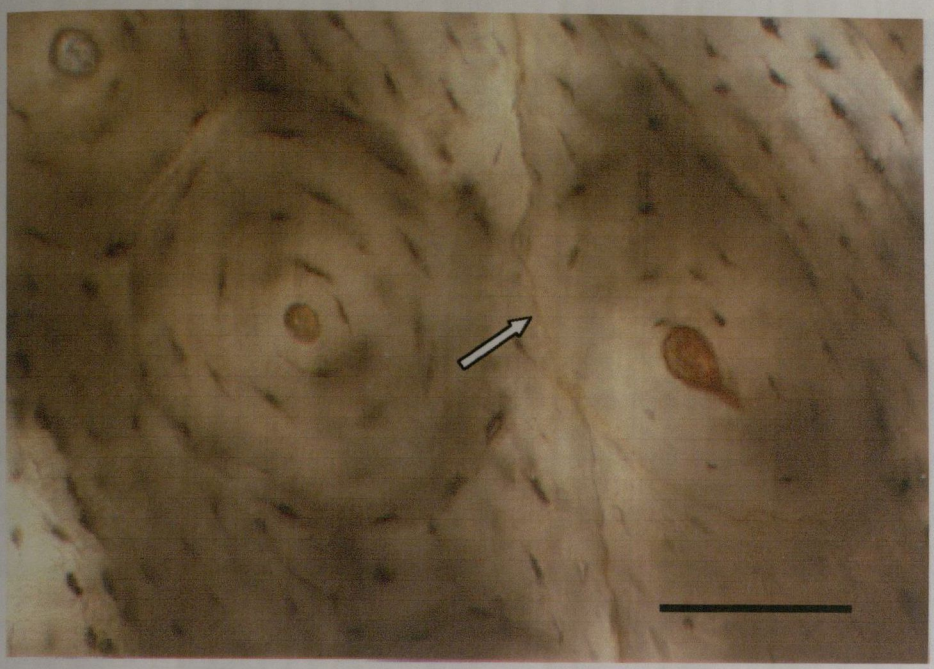

Fig. 2.8 Example of crack growth between adjacent Haversian systems. Bar=100 μm.

2.5 Conclusions

(1) A mechanical testing protocol has been established which allows changes in material stiffness to be monitored during the course of a fatigue test and initial tests have shown a degree of scatter regarding number of cycles to failure similar to that observed by other authors.

(2) The experimental work has validated the accuracy of the mathematical model (Taylor, 1998a) as it was able to predict the fatigue strength of bovine bone in compression within an accuracy of 4%.

(3) The chelating agents were found to be effective markers of microcracks in bone when applied individually, however problems emerged when two or more of the agents were applied in sequence.

(4) Microcracks were found to interact with the bone's microstructure and were found to occur predominantly in the waisted centre sections of the specimens and outright failure always occurred in this region.

Chapter 3

MICROCRACK DETECTION

3.1 Introduction

A variety of techniques have been used to detect microcracks in bone. Chamay and Tschantz (1972) examined overloaded ulnae using scanning electron microscopy. Carter and Hayes (1977) used reflected light photomicrography in order to show the difference in damage patterns on compressive and tensile surfaces. Zioupos (1994) used acoustic-emission in order to detect microcracks. Zioupos and Currey (1994) used laser scanning confocal microscopy (LSCM) to study the morphology of *in vitro* microcracks in fatigue-tested compact bone, while LSCM has also been used to study microdamage in trabecular bone (Fazzalari et al, 1998) and dense arrays of ultra-microcracks in human tibiae (Boyce et al, 1998). However the most common method of microcrack detection has been the use of transmitted light microscopy, either alone or often using a penetrant dye in order to allow differentiation of microdamage from the surrounding bone matrix.

3.1.1 Agents used in microcrack detection

Frost (1960) introduced the technique of bulk staining sections of bone in basic fuchsin dye in order to label *in vivo* microcracks in bone. This technique has been used in many studies in order to label microdamage in bone and remains the most commonly used technique. Fuchsin is an ethanol-soluble dye, but is relatively insoluble in water (Rost, 1992). This property of the dye allows processing of bone specimens to be carried out in an aqueous medium after staining, thus minimising the fuchsin leaching out and staining artifacts introduced during processing. Forwood and Parker (1990) used bulk-staining with basic fuchsin to label *in vitro* damage, Burr and Stafford (1990) modified Frost's criteria (1960) for identifying microcracks (Table 3.1). This process has been

successfully used to detect microcracks both *in vitro* (Akhter et al, 1993) and *in vivo* (Mori and Burr, 1993). Huja et al (1999) looked at tensile microcracks easily visible under brightfield light microscopy.

Table 3.1 Criteria for identifying microcracks (Burr and Stafford, 1990)

1. They are intermediate in size, being larger than canaliculi but smaller than vascular canals.
2. They have sharp borders with a halo of basic fuchsin staining around them.
3. They are stained through the depth of the section.
4. When the depth of focus is changed, the edges of the crack can be observed to be more deeply stained than the intervening space.

Zioupos and Currey (1994) used a fluorescent dye, fluorescein to detect cracks, using laser scanning confocal microscopy. Reilly (2000) used this technique to study tensile microdamage in bovine, equine, human and rat long bones. Fluorescent dyes or fluorochromes work by absorbing energy in the form of light, which causes electrons to move into higher energy levels away from the nucleus. When these electrons return to more stable, lower energy shells, the energy is dissipated as both heat and light. The wavelength of the emitted photon is longer than the excitation photon as it has less energy (Stokes' Law) and the difference between the wavelengths of the excitation and emission spectra is known as Stokes' Shift. Epifluorescence microscopy takes advantage of this property by selectively transmitting light at the excitation maximum to strike the fluorochrome using an excitation filter and then, en route to the eyepiece, a barrier filter blocks this wavelength while transmitting as much as possible of the fluorescence emission (Rost, 1992, 1995).

Basic fuchsin, is both a fluorochrome and a diachrome, as it also appears coloured under transmitted light. Maximal absorption of light occurs at a wavelength of 545nm (Rahn,

1977; Rost, 1995), which is in the green area of the spectrum. When fuchsin is excited by an incident light of this wavelength, it emits a light of longer wavelength, which appears orange, when a red barrier filter is used. Lee et al (1998) utilised the fluorescent properties of basic fuchsin in addition to bulk-staining in order to detect microdamage.

Table 3.2 Refined criteria for identifying microcracks (Lee et al, 1998)

1. They are intermediate in size, being larger than canaliculi but smaller than vascular canals. Method: fluorescence, green incident light (546 nm), x125 magnification.
2. They have sharp borders with a halo of basic fuchsin staining around them. Method: fluorescence, green incident light (546 nm), x125 magnification.
3. They are stained through the depth of the section. Method: fluorescence, UV incident light (365 nm), x125 magnification.
4. When the depth of focus is changed, the edges of the crack can be observed to be more deeply stained then the intervening space. Method: transmitted light microscopy, x250 magnification.

This study improved the technique of crack detection using basic fuchsin, by varying the magnification and light type when sections were examined under a fluorescent microscope and the refined protocol (Table 3.2) was used. His study (Lee, 1998) however identified some of the problems with the use of basic fuchsin in the detection of microdamage. The cutting and grinding processes used in preparation of sections tend to produce large amounts of scratches and cracks which appear black in colour under transmitted light. Variation of the light intensity reveals that some of these are true microcracks, but others are preparation artefacts, either cracks unstained by fuchsin or containing some dye and debris from the grinding process. By varying light intensity, depth of focus and magnification, pre-existing microcracks that had been generated *in vivo* can be differentiated from artefactual damage, but the procedure is both difficult and time-consuming.

The two main problems as shown by Lee et al (1998) with the use of basic fuchsin in detection of microdamage, relate to its site specificity and also the fact that it is a single agent. In order to differentiate artefactual damage from either *in vivo* damage or *in vitro* damage formed during mechanical testing, a second agent would be required. Vashishth et al (1994) combined basic fuchsin and toluidine blue stains. Machined specimens of cortical bone were immersed in toluidine blue for 16 hours prior to testing. The specimens were then tested in tension, following which, were placed in basic fuchsin for 16 hours. Under the microscope, pre-existing cracks were stained with both toluidine blue and basic fuchsin whereas cracks newly-created by tensile testing, were stained with basic fuchsin alone. This study distinguished between pre-existing and test induced microcracks but neither of the agents used were site specific and they were difficult to distinguish. For microcrack growth to be monitored, a series of agents would be required.

Bone is made up of collagen and hydroxyapatite crystals. In a structure such as bone; a microcrack may be described as a break or fissure in the hydroxyapatite matrix, which exposes new surfaces (Lee et al, 2000b). It is estimated that in $1\mu m^3$ of bone, 55% of the ions present are calcium (Landis, 1995). Therefore, the breaking up of the hydroxyapatite matrix ($Ca_{10}(PO_4)_6(OH)_2$) with the formation of microcracks would lead to calcium ions becoming exposed on the walls of these cracks. However, the two major constituents of basic fuchsin, rosanilin and parasanolin are not capable of binding strongly and selectively with ions lining the walls of microcracks. Their molecular structures are shown in Fig. 3.1. The absence of NH_2 groups close together prevents the formation of a chelate ring in both constituents, which would be required to allow such binding to occur.

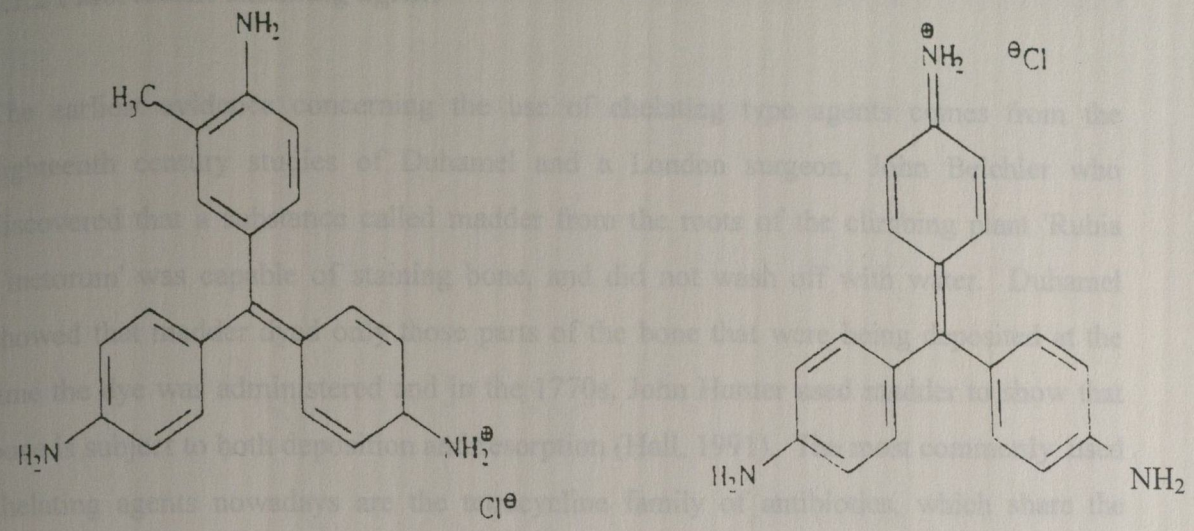

Fig. 3.1 Molecular structures of rosanilin and pararosanilin (Rost, 1995)

The majority of ions present in bone, Ca^{2+}, Na^{+} and Mg^{2+} are considered to be "hard" metal ions and have little affinity for nitrogen donor atoms (Huuhey, 1983). Basic fuchsin does however have the capability to bind with proteins such as elastin and collagen. Collagen comprises approximately 30% of bone by weight compared with 60% for hydroxyapatite. The formation of microcracks which break up the bone matrix might therefore, be expected to have some collagen exposed along their walls. Thus it is possible that fuchsin labels microcracks partially by binding to exposed collagen but for the most part it can be accepted that fuchsin labels microdamage as a space occupying agent, i.e. by diffusing through the bone matrix into microcracks and lodging there. From this it can be hypothesised that the ideal marker for labeling microdamage in bone would be both site specific and easily detected. Lee (1997) showed that a chelating fluorochrome fulfills both requirements, it is site specific in that it chelates to calcium ions which line the walls of microcracks and its fluorescent properties make it ideal for crack detection.

3.1.2 Fluorescent chelating agents

The earliest evidence concerning the use of chelating type agents comes from the eighteenth century studies of Duhamel and a London surgeon, John Belchier who discovered that a substance called madder from the roots of the climbing plant 'Rubia Tinctorum' was capable of staining bone, and did not wash off with water. Duhamel showed that madder dyed only those parts of the bone that were being deposited at the time the dye was administered and in the 1770s, John Hunter used madder to show that bone is subject to both deposition and resorption (Hall, 1991). The most commonly used chelating agents nowadays are the tetracycline family of antibiotics, which share the calcium chelation ability of the earliest madder dyes and also their fluorescence properties.

The tetracyclines have strong chelation properties. They are able to sequester a calcium ion and bind it into a ring. It is only more recently that the tetracyclines have been used to label bone. Frost (1963, 1966, 1969 and 1973) developed a method for *in vivo* labeling of bone formation using sequential tetracycline labels. By administering the dyes in sequence, a series of bands in the mineralised bone was formed, thus enabling the rate of new bone deposition to be measured. The main problems that arose with administering tetracycline labels to bone were due to the similarities in colour between the various dyes in the tetracycline family. As the colours range mainly from yellow to green, it is difficult to distinguish between the labelled bands.

Harris (1960) combined tetracycline with alizarin red, which could be easily distinguished under both transmitted white light and epifluorescence. Rahn and Perren (1970) developed calcein blue and they also introduced xylenol orange (1971) and then alizarin complexone (1972). All of these dyes are fluorochromes and all possess adjacent donor sites for calcium chelation and thus are site specific. The molecular structures for the chelating fluorochromes are shown in Fig. 3.2. Each of these five agents' structures,

gives them the ability to sequester metallic ions such as calcium and bind it firmly into a ring.

Fig. 3.2 Molecular structures of chelating fluorochromes (Rost, 1995)

Calcein Blue

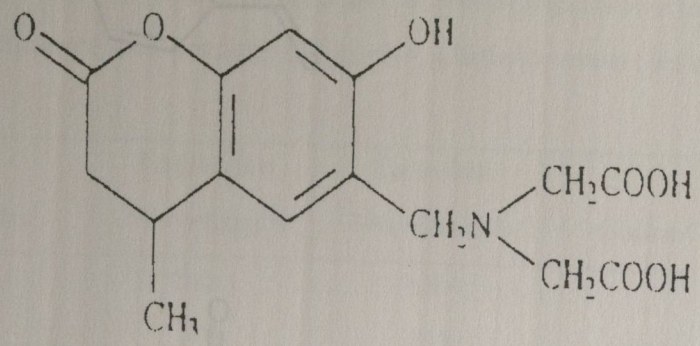

Xylenol orange

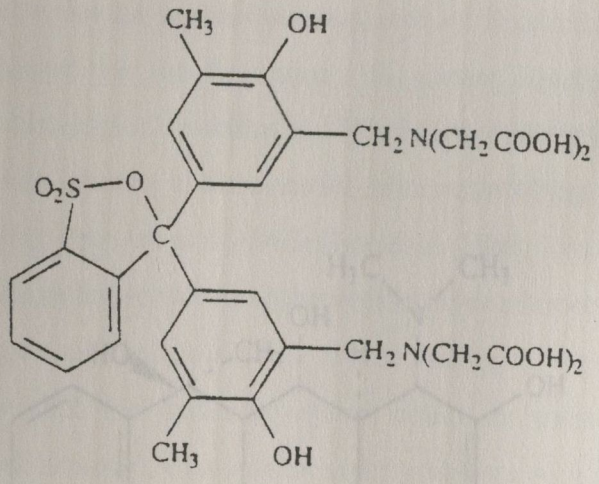

Calcein

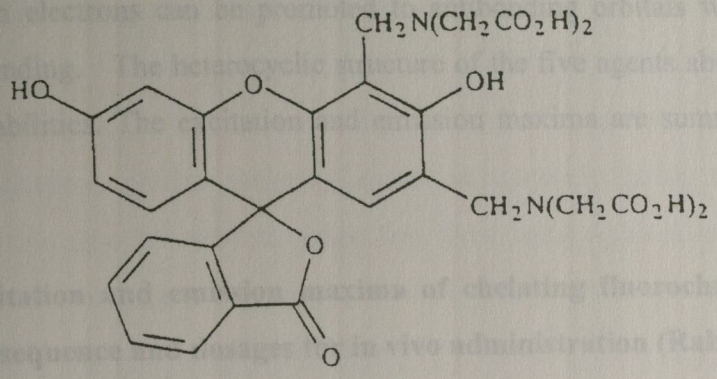

Alizarin

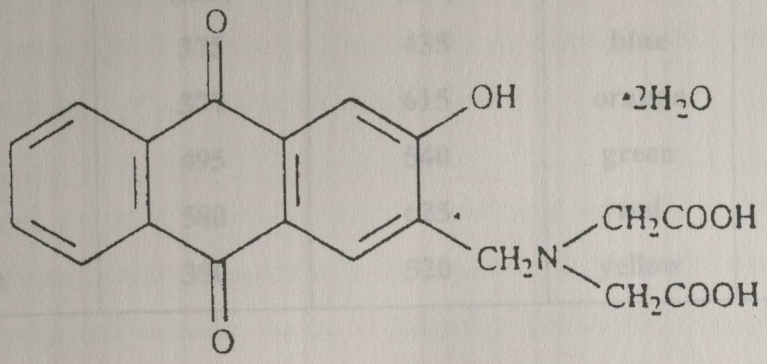

Oxytetracycline

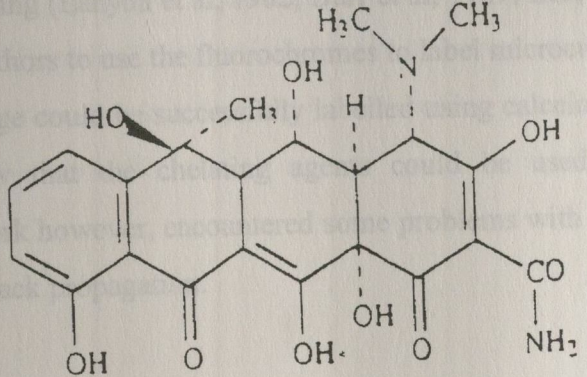

Fluorescence in organic compounds is restricted to those possessing a large conjugated system in which electrons can be promoted to antibonding orbitals without excessive disruption of bonding. The heterocyclic structure of the five agents above enables their fluorescent capabilities. The excitation and emission maxima are summarised in Table 3.3.

Table 3.3 Excitation and emission maxima of chelating fluorochromes and their recommended sequence and dosages for in vivo administration (Rahn, 1977)

Fluorochrome	Excitation Wavelength (nm)	Emission Wavelength (nm)	Colour	Dosage (mg/ kg)
Calcein blue	**375**	**435**	**blue**	**30**
Xylenol orange	**377**	**615**	**orange**	**90**
Calcein	**495**	**540**	**green**	**10**
Alizarin	**580**	**625**	**red**	**30**
Oxytetracycline	**390**	**520**	**yellow**	**30**

Rahn (1977) developed a dosage regime and sequence of fluorochrome administration (Table 3.3) which allowed for the five agents to appear equally bright under the microscope facilitating histological examination. This regime has been used in a number of previous *in vivo* studies in order to demonstrate bone remodelling under conditions of altered mechanical loading (Lanyon et al, 1982; Burr et al, 1989; Lee, 1995). Stover et al (1993) were the first authors to use the fluorochromes to label microcracks. They showed that *in vivo* microdamage could be successfully labelled using calcein. Lee et al (2000a) was the first to show that the chelating agents could be used to label *in vitro* microdamage. This work however, encountered some problems with the use of chelating agents in monitoring crack propagation.

3.1.3 Sequential labelling of microcracks

Lee et al (2000a) carried out fatigue tests on specimens of cancellous bone and applied a series of 1% solutions of the chelating agents at intervals during testing. However substitution of one dye for another when the dyes were applied in sequence made distinguishing individual agents difficult. Initial results from this study (Chapter 2; O'Brien et al, 1998) showed a similar problem.

3.1.4 Objectives

Lee (1997), Lee et al (2000a) and O'Brien et al (1998) had identified problems with the application of chelating agents in sequence and it was proposed that this was due to the different binding strengths of each agent for calcium ions.

(1) It was proposed, by using various methods of chemical analysis, to determine the optimal agent sequence, from the agent with the greatest affinity to the agent with the least affinity for exposed calcium, so as to minimise the substitution problem that occurred when the agents were applied in sequence.

(2) The second aim of this study was to refine the detection method by carrying out tests on the chelating agents in order to determine the optimal concentrations of each of the five agents. Rahn (1977) developed a dosage regime for application of the chelating agents *in vivo* (Table 3.3) while Lee (1997) used 1% solutions of the chelating agents. This study aimed to determine whether the concentration results obtained were as effective as Rahn's *in vivo* method.

3.2 Materials and Methods

3.2.1 Refinement of detection method

From the initial study (O'Brien et al, 1998), it was observed that the problem of substitution occurred with some sequences of chelating agents. For example, when xylenol orange was applied to a bone sample and followed by calcein, no substitution took place and both agents were clearly distinct from each other. However, when calcein blue was followed by alizarin, substitution did occur and distinguishing the individual agents was difficult.

It was proposed that the problem of substitution was due to the variation in binding constants of the chelating agents for calcium ions. Some agents bound to calcium better than others and if they were applied in sequence *after* the weaker agent, they tended to displace it. To test this hypothesis, it was decided to measure the binding strengths of the agents so that they could be applied in order, from the agent with the greatest affinity for calcium, down to the agent with the least affinity.

Three different methods of analysis were considered to establish the affinity of each of the five agents for calcium (i) potentiometric titrations (ii) x-ray crystallography and (iii) ion chromatography. However, after consultation with the Department of Physics and Chemistry in RCSI, it was concluded that the former two methods would be time-consuming and would not provide the type of data required. Instead, it was decided to carry out ion chromatography tests on each of the five chelating agents.

3.2.2 Ion Chromatography

Ion chromatography (IC) is a form of high performance liquid chromatography. It encompasses both ion exchange and size exclusion chromatography, and is routinely used in the determination of organic and inorganic cations and anions. Modern IC was first

described by Small et al (1975) when they reported a novel ion-exchange chromatographic method using conductiometric detection. They used a low-capacity ion-exchange column, called a "stripper", which served to reduce the background conductance of the eluent in order to enhance the signal from the eluted ions. The term 'ion chromatography' was then introduced by the Dionex Corporation who licensed the technology for commercial development.

Ion exchange chromatography is based on the separation of ions on columns that have charge-bearing functional groups attached to a polymer matrix (Haddad and Jackson, 1990). The functional groups are permanently bonded ionic groups associated with counter ions of the opposite charge. The retention mechanism is the simple exchange of sample ions and mobile phase ions with the charged group of the stationary phase. Cation exchange resins bear negatively charged groups, which can be either strong or weak acid cation exchangers. The most commonly used functional groups are the sulphonate type, which are strong acid exchangers.

In this study, IC was carried out in order to determine the affinity of each of the five chelating agents for free calcium ions. The solutions were analysed by measuring the electrical conductivity of the calcium chloride solution (ability of the solution to conduct electricity between 2 electrodes across which an electric field has been applied) and then the conductivity of the solution after a chelating agent has been added. Using this technique, the free calcium and calcium bound to the chelating agent appear as separate peaks in a chromatogram i.e., the amount of free calcium in a calcium chloride solution was measured and shown as the first peak, and the amount of calcium left, after application of each chelating agent, was illustrated by the second peak.. A decrease in peak height gives an indication that a proportion of the free calcium has been bound to the chelating agent, and the greater the decrease observed, the stronger the binding between the agent and the calcium ions. The samples were separated on a Dionex system which incorporated a pump, cation-trap pre-column and a cation micro membrane suppressor (Dionex, Sunnyvale, Ca). The five fluorescent chelating agents were injected

separately in duplicate at a concentration of 5 x 10^{-4}M and a calcium chloride concentration of 1 x 10^{-3}M. The chromatograms were recorded and imported into Microsoft Excel.

3.2.3 Validation of results

The results from the IC experiments provided us with information on the affinities of each of the five agents for calcium ions in a calcium chloride solution (1 x 10^{-3}M). However, in order to relate the above results to bone, more tests were required. The chromatograms gave a staining sequence from greatest to least affinity for calcium ions. It was proposed to apply this sequence to specimens of bone to establish whether the chromatography results were providing the optimal sequence required to minimise the effects of substitution. Three types of data were required on the abilities of each of the agents to chelate exposed calcium ions in bone:

(1) Time required for maximum chelation to occur between each of the agents and calcium.
(2) Effects of applying the chelating agents in a pre-determined sequence and degree of substitution that occured.
(3) Determination of the most efficient concentration which allowed chelating agents fluoresce under UV light.

Rather than carrying out time consuming fatigue tests and applying agents at intervals during a test, a simplified technique was required which would provide consistent exposure of calcium ions for chelation and immediate results. The process of scratching the surface of the bone specimen would break the hydroxyapatite matrix and expose calcium ions which permitted chelation to occur.

Bovine tibiae were obtained from a meat wholesalers (KEPAK Ltd., Clonee, Co. Dublin) from animals slaughtered 2-3 days previously. Flesh was removed from all bones and

they were stored at -20°C until required. Samples of cortical bone were removed from the mid-diaphysis of these tibiae and machined into beam-shaped specimens using a band saw. These were then finely polished using emery paper. All machining was carried out in wet conditions and the bones were not allowed to dry at any time. After machining the specimens were stored at -20°C prior to staining.

3.2.4 Chelation times

It has already been shown that the time it takes for maximum bonding to occur between the chelating agents and calcium ions in bone varies for each individual agent (O'Brien et al, 1998). This study set out to determine the optimal staining time which permitted each individual agent to penetrate and label a scratch whilst preventing overstaining occuring i.e. the agent penetrating the bone matrix beyond the boundaries of the surface scratch. The following protocol was used to scratch and stain each specimen.

Table 3.4 Protocol for generating scratches

1. 5mm straight line scratched on the surface of 25 bone samples using a compass (Faber-Castell, Germany).
2. 5 bone samples placed in a bath of each of the 5 chelating agents.
3. Specimens removed and scratch viewed under UV light at times of 2, 4, 12, 30mins, 1hour, 1.5 hours and 4hours.
4. Specimens were examined using UV epifluorescence microscopy (λ=365 nm, Nikon Optiphot, Japan).

The stained specimens were examined and results presented according to three different modalities; (i) degree of penetration (ii) fluorescence quality of each agent (brightness) (iii) clarity (ease at which scratch could be distinguished from surrounding matrix). These modalities were given marks out of 10 where 1 implied extremely poor and 10 implied excellence.

3.2.5 Labelling of scratches using chelating agents

In order to test the validity of the ion chromatography results, the agents were applied in sequence to small surface scratches on bone samples. Initially paired tests were carried out using two agents applied in the sequence proposed above and then this sequence was reversed. Three agents were then applied in sequence, followed by four agents and finally all five agents were applied using the following protocol to generate scratches (Table 3.5).

Table 3.5 Protocol used to generate scratches to determine optimal chelating agent sequence and test the validity of the ion chromatography results

1. 5mm straight line scratched on the surface of 25 bone samples using a compass (Faber-Castell, Germany).
2. Specimen immersed in 5 x 10^{-4}M aqueous solution of chelating agents for a specific time (using results determined from chelation time tests) in an individual vial and placed under vacuum (50 mm Hg).
3. Specimen washed in de-ionised water and original line extended by a further 5mm.
4. Specimen immersed in 5 x 10^{-4}M aqueous solution of a second chelating agent in an individual vial and placed in the dessicator.
5. Steps 3 and 4 repeated depending on the number of agents to be applied in sequence.
6. Specimens washed in de-ionised water and examined using UV epifluorescence microscopy.

Three modalities; quality of each agent, clarity and degree of substitution were again used to define the efficacy of each sequence, all were measured on a scale of 0-5. Quality (Q) gives an indication of the strength of each agent (after subsequent agents have been applied), it is a measurement of degree of penetration, brightness of fluorescence and ease at which the agent could be distinguished from the surrounding bone matrix. 0 implies the sequence does not work effectively at all while 5 implies that, the degree of

penetration, fluorescence, and ease at which it be distinguished from the surrounding bone are all excellent. Clarity (C) is an indication of the ease with which the areas scratched can be distinguished from each other in sequence i.e. 1 implies that both areas are very similar in colour and contrast i.e difficult to differentiate (potentially due to substitution) whereas 5 implies that both areas can be perfectly distinguished from each other.

The degree of substitution (S) can be understood by the following

0= no substitution

1= 1-20% (i.e. the second dye applied displaced 1-20% of the initial one)

2= 21-40%

3=41-60%

4= 61-80%

5=81-100%

Finally, a grade percentage is given:

Equation 3.1

$$\text{Grade} = \frac{Q1 + Q2 + C}{15} - \frac{S}{20} \times \frac{100}{1}$$

This gives an indication of how effective the sequence was by taking into account the quality of the first agent (Q1), the quality of the second agent (Q2) and the ease at which the agents can be distinguished from each other and the degree of substitution.

3.2.6 Measurement of most effective concentrations

All the verification tests were conducted at concentrations of 0.0005M. This concentration was used since the electrode used to monitor conduction during the ion chromatography tests required low concentrations of the agents and all the agents needed to be of the same concentration in order for the results between agents to be comparable. This was the lowest concentration, which allowed all agents to fluoresce clearly while still permitting chromatograms to be obtained. Rahn (1977) developed a dosage regime and sequence of fluorochrome administration *in vivo* (Table 3.3) which allowed for the

five agents to appear equally bright under the microscope in order to facilitate histological examination.

Table 3.6 Comparison of in vivo dosage concentrations (Rahn, 1977) and new concentrations used in ion chromatography tests.

	GROUP R (Rahn, 1977)		Group C
AGENT	**DOSAGE (mg/kg)**	**CONCENTRATION**	**Ion Chromatography**
Calcein blue	30	0.0000712 M	0.0005 M
Xylenol orange	90	0.000016 M	0.0005 M
Calcein	10	0.0000933 M	0.0005 M
Alizarin	30	0.00012 M	0.0005 M
Oxytetracycline	30	0.00006 M	0.0005 M

Using the dye sequence established from the ion chromatography results, scratch tests were carried out to compare the two concentration groups, group R and group C. Table 3.7 shows the protocol used.

Table 3.7 Protocol used to generate scratches to determine optimal chelating agent concentrations.

1. 5mm straight line scratched on the surface of 5 bone samples using a compass (Faber-Castell, Germany).
2. Specimen immersed in aqueous solution of first agent for 30 minutes in an individual vial and placed in a vacuum dessicator (50 mm Hg).
3. Specimen washed in de-ionised water and original line extended by a further 5mm.
4. Specimen immersed in aqueous solution of the second agent in an individual vial and replaced into the dessicator.
5. This procedure was continued for the third, fourth and fifth agents.
6. The specimens were washed in de-ionised water and the scratches examined using UV epifluorescence microscopy.

3.3 Results

3.3.1 Ion chromatography results

Figs. 3.3-3.6 illustrate the chromatograms obtained from the analysis of four of the five chelating agents. Conductivity is a measure of the ability of the solution to conduct electricity between 2 electrodes across which an electric field has been applied. Its units are microSiemen (μS).

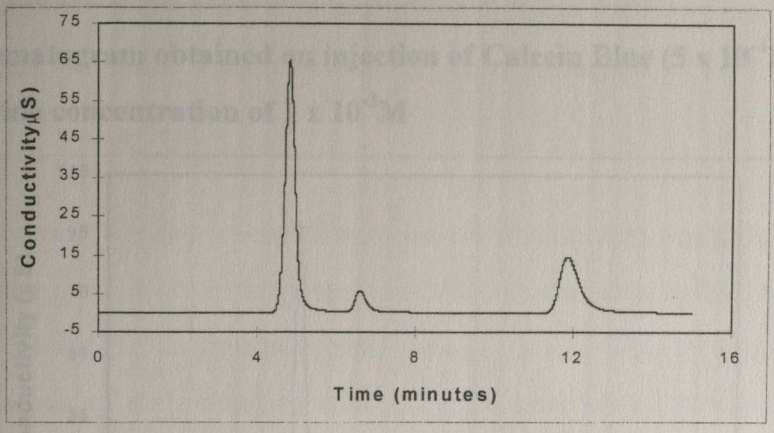

Fig. 3.3 Chromatogram obtained on injection of Alizarin (5×10^{-4}M) with a calcium chloride concentration of 1×10^{-3}M

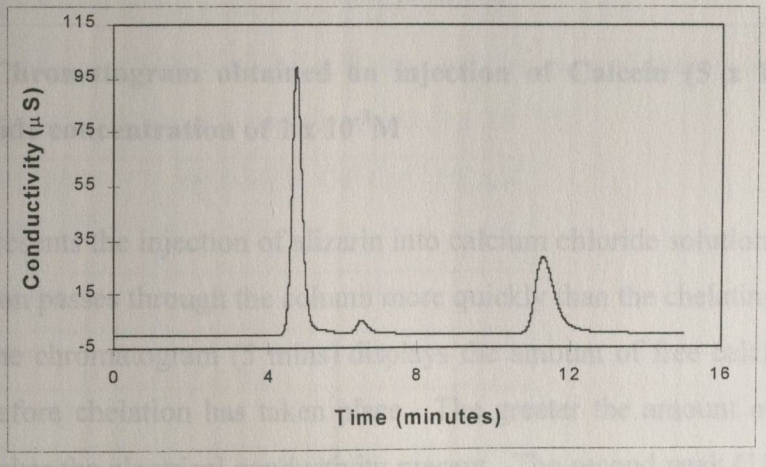

Fig. 3.4 Chromatogram obtained on injection of Xylenol Orange (5×10^{-4}M) with a calcium chloride concentration of 1×10^{-3}M

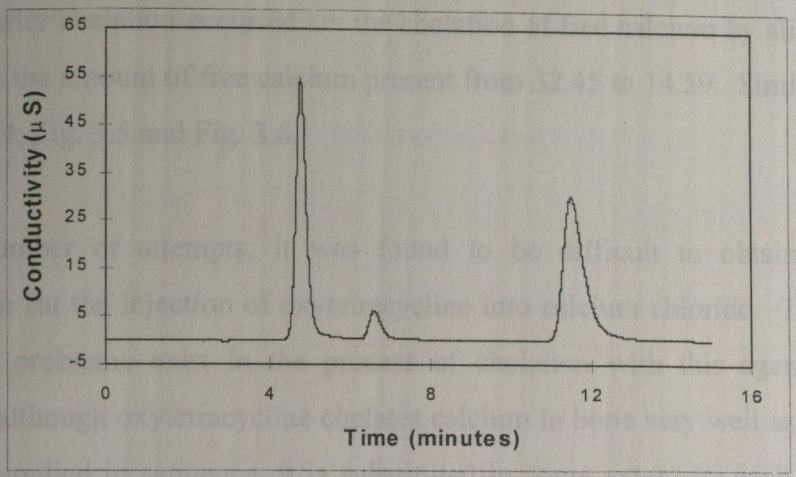

Fig. 3.5 Chromatogram obtained on injection of Calcein Blue (5×10^{-4}M) with a calcium chloride concentration of 1×10^{-3}M

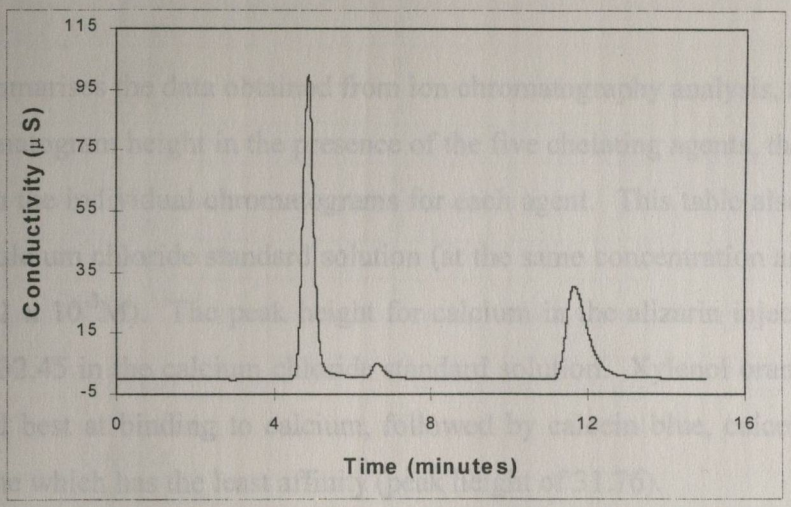

Figure 3.6 Chromatogram obtained on injection of Calcein (5×10^{-4}M) with a calcium chloride concentration of 1×10^{-3}M

Figure 3.3 represents the injection of alizarin into calcium chloride solution. The calcium chloride solution passes through the column more quickly than the chelating agents so the first peak in the chromatogram (5 mins) displays the amount of free calcium present in the solution before chelation has taken place. The greater the amount of free calcium present, the higher the electrical conductivity present. The second peak (11 mins) results when the chelating agent has passed through the column and binds to the free calcium present in the calcium chloride solution and so illustrates the maximum amount of free

calcium left after chelation occurred i.e. the chelation of free calcium by alizarin leads to a reduction in the amount of free calcium present from 32.45 to 14.59. Similar effects are seen in Fig 3.4, Fig. 3.5 and Fig. 3.6.

Despite a number of attempts, it was found to be difficult to obtain an accurate chromatogram for the injection of oxytetracycline into calcium chloride. This suggested that inherent problems exist in the process of chelation with this agent. All results indicate that although oxytetracycline chelates calcium in bone very well as an individual agent, when applied in sequence, it is substituted to some extent by each of the agents while paradoxically it also substitutes all of the other agents with the exception of alizarin.

Table 3.8 summarises the data obtained from ion chromatography analysis, and shows the average chromatogram height in the presence of the five chelating agents, these values are obtained from the individual chromatograms for each agent. This table also includes the data for the calcium chloride standard solution (at the same concentration as is present in the samples, 1 x 10^{-3}M). The peak height for calcium in the alizarin injection is 14.59, compared to 32.45 in the calcium chloride standard solution. Xylenol orange appears to be the second best at binding to calcium, followed by calcein blue, calcein and finally oxytetracycline which has the least affinity (peak height of 31.76).

Table 3.8 The average height of the calcium peak for each of the chelating agents investigated along with the calcium standard (1 x 10^{-3}M)

CHELATING AGENT	HEIGHT. OF Ca^{2+} PEAK
Calcium std.	32.45
Alizarin	14.59
Xylenol orange	28.56
Calcein blue	29.73
Calcein	30.67
Oxytetracycline	31.76

3.3.2 Chelation time results

Table 3.9 Summary of results from penetration time test

TIME	AGENT	PENETRATION	FLUORESCENCE	CLARITY
2 mins	Alizarin	4	5	3
	Xylenol	6	5	5
	Calcein	7	7	7
	Calcein Blue	7	7	7
4 mins	Alizarin	4	5	3
	Xylenol	7	6	5
	Calcein	8	8	7
	Calcein Blue	8	8	8
12 mins	Alizarin	7	5	5
	Xylenol	8	7	7
	Calcein	8	8	8
	Calcein Blue	10	10	10
30 mins	Alizarin	8	6	7
	Xylenol	8	8	8
	Calcein	8	8	8
	Calcein Blue	9	10	9
1 hour	Alizarin	8	7	9
	Xylenol	7	8	9
	Calcein	8	10	9
	Calcein Blue	10	10	7*
1.5 hours	Alizarin	9	7	9
	Xylenol	9	8	9
	Calcein	8	10	9
	Calcein Blue	10	10	7*
4 hours	Alizarin	9	7	9
	Xylenol	9	8	9
	Calcein	8	10	9
	Calcein Blue	10	10	6*

*After 1 hour of staining the calcein blue penetrated the bone surrounding the scratch excessively, making differentiation of scratch from surrounding matrix difficult.

Table 3.9 shows a table for the chelation time results. Alizarin, despite being the agent with strongest apparent affinity for calcium was found to have the poorest penetration of the agents, while calcein blue had the greatest ability to penetrate the bone. However after 30 minutes, excessive bleeding took place into the bone matrix surrounding the scratch making its clarity very poor. At 30 minutes a good balance was reached whereby alizarin had penetrated the scratch to a sufficient extent to label it clearly while calcein blue had not bled excessively into the bone matrix surrounding the scratch. Both xylenol orange and calcein were also found to perform well at this time.

3.3.3 Labelling of scratches using chelating agents

3.3.3a Two stain tests

Table 3.10 shows the results obtained when two agents were used in sequence. From these results a number of points arose. The ion chromatography results showed that calcein had less affinity for calcium ions than calcein blue (30.67 v 29.73 calcium peak after chelation). These tests showed that calcein blue followed by calcein resulted in a lot of substitution (41-60%). Calcein followed by calcein blue resulted in less substitution (0-20%). However, since this sequence did show a slight substitution of calcein by calcein blue, it was proposed to reduce the concentration of calcein blue by 50% in the four agent tests (i.e. 0.00025M). This change was further vindicated by the fact that 0.0005M calcein blue was also found to displace xylenol orange when applied in sequence. Oxytetracycline was found once again to be problematic. It substituted alizarin, xylenol orange and calcein to a small extent and was found to substitute calcein blue to a great degree, 61-80% (Fig. 3.7a). The reversal of this sequence i.e. oxytetracycline followed by calcein blue surprisingly then showed that calcein blue tended to substitute oxytetracyline. Because of these persistent problems, it was decided to eliminate oxytetracycline from further analysis.

Table 3.10 Two stain sequence results

SEQUENCE	QUALITY (Q2) Agent 1	QUALITY (Q2) Agent 2	CLARITY Agent 1 from Agent 2	SUBSTITUTION Agent 2 by Agent 1	GRADE(%)
A-X	4	4	3	0	66.6
X-A	3	3	2	1	55
A-C	4	5	5	0	93.3
C-A	3	2	2	4	26.6
A-CB	4	5	3	1	75
CB-A	3	3	2	4	33.3
A-0	4	3	4	1	68.3
0-A	1	3	1	4	13.3
X-C	4	5	4	1	81.6
C-X	3	4	3	2	56.6
X-CB	3	4	3	1	61.6
CB-X	3	3	2	2	43.3
X-O	4	3	4	1	68.3
O-X	2	4	2	3	38.3
C-CB	4	5	3	1	68.3
CB-C	2	5	2	3	45
C-O	4	3	4	1	61.6
O-C	3	5	3	3	58.3
CB-O	2	3	2	4	26.6
O-CB	2	5	2	4	40

A= alizarin, C= calcein, CB= calcein blue, X= xylenol, O=oxytetracycline

i.e. A-X indicates a sequence of 0.0005M Alizarin followed by 0.0005M xylenol

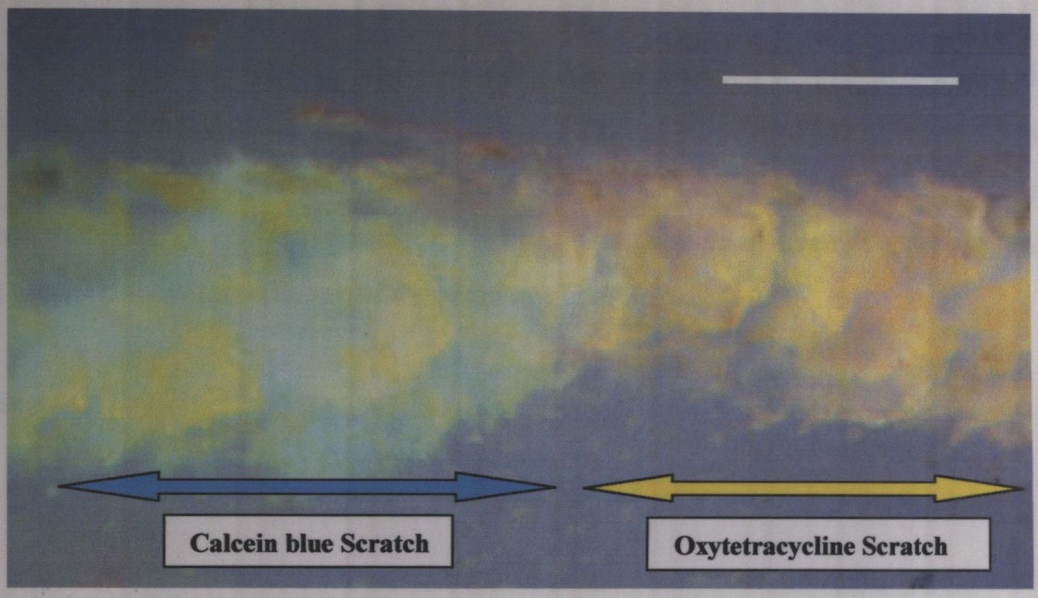

Fig. 3.7a

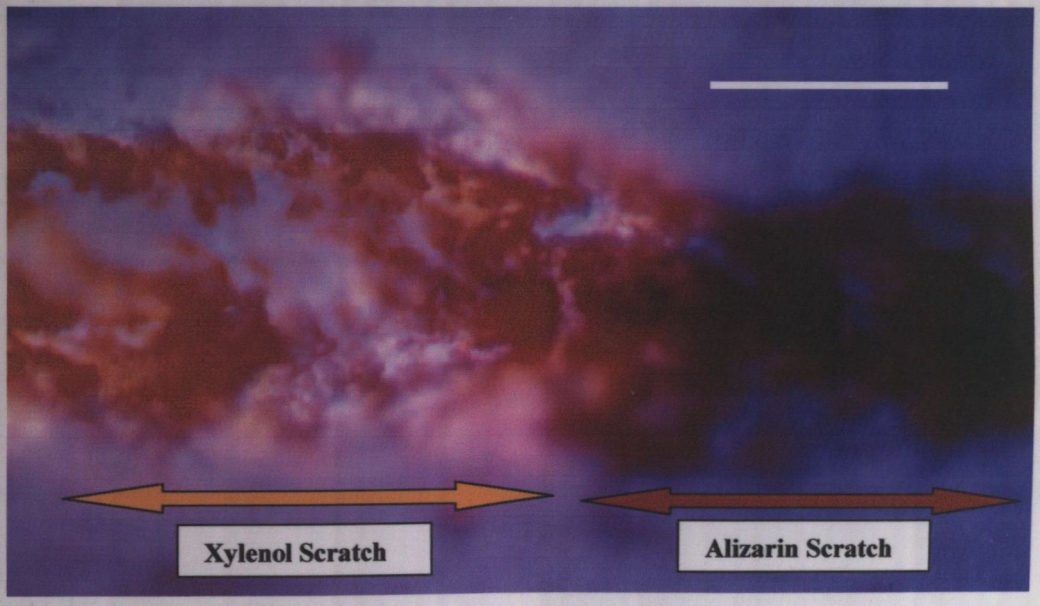

Fig. 3.7b

Fig. 3.7 Examples of substitution occurring (a) Calcein blue followed by oxytetracycline: here the latter agent (yellow) has substituted the former (originally blue) to a large extent and it is not possible to distinguish the two agents separately (b) Xylenol orange followed by alizarin: here the latter agent (dark red) has substituted the former (originally orange). Bar = 200 μm.

3.3.3b Three stain tests

The results from the two agent tests led to a preliminary three stain sequence of alizarin, xylenol orange, calcein being determined. The strength of this sequence was then tested. Table 3.11 shows the results obtained with a grade average again being given for each sequence with Eq. 3.1 revised to include the third agent and an average of these 5 grades is then given to show the efficacy of the sequence (Eq. 3.2).

Equation. 3.2

$$\text{Grade} = \frac{Q1 + Q2 + Q3 + C}{20} - \frac{S}{25} * \frac{100}{1}$$

Table 3.11 Three stain sequence results

0.0005m alizarin - 0.0005M xylenol - 0.0005M calcein

Spec.	SEQUENCE	QUALITY (Q1) Agent 1	QUAL. (Q2) Agent 2	QUAL. (Q3) Agent 3	CLARITY All agents	SUBSTIT.	GRADE (%)
1	A-X-C	4	4	5	5	0	90
2	A-X-C	4	5	5	5	0	95
3	A-X-C	4	5	5	5	0	95
4	A-X-C	3	4	5	4	1	76
5	A-X-C	4	4	5	5	0	90

Mean Grade= 89.2 ±7.8%

The results obtained from the three stain tests again raised a number of points. All five specimens were analysed after each stage of the staining protocol i.e. before the next agent was applied, and it was found that after the second stage of staining, i.e. alizarin and xylenol orange (Fig. 3.8a), clarity between the agents was only moderate as they were similar in colour and difficult to differentiate. However when the third agent, calcein,

was applied, it was not only clearly distinct from the two agents itself, but it also appeared to improve xylenol's fluorescence, making it flouresce a bright orange colour rather than a dull red colout, showing it clearly distinct from alizarin (Fig. 3.8b). This gives an average grade value for the three dye sequence of 89.2 ± 7.8% compared to only 66.6% for the A-X combination and 81.6% for the X-C combination indicating that the three stain sequence is more effective than either of the two stain sequences.

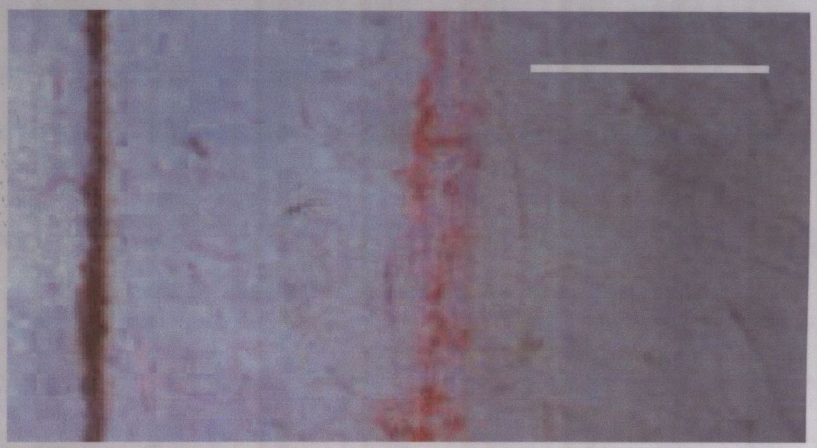

Fig. 3.8a

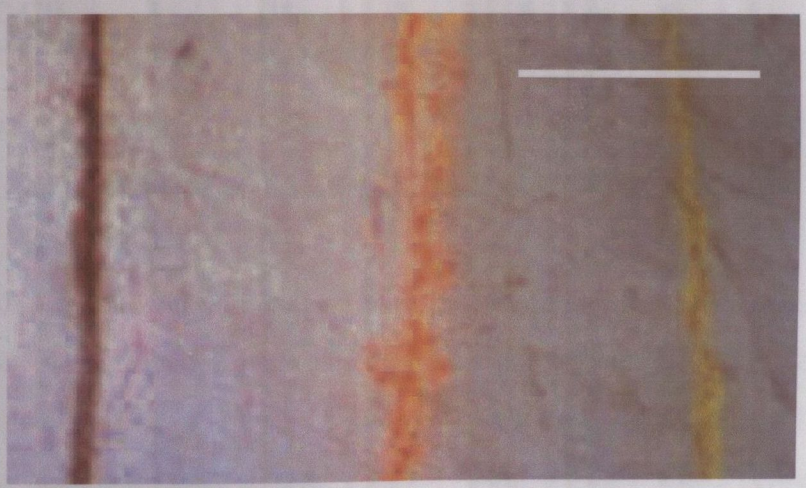

Fig. 3.8b

Fig. 3.8 Examples of scratches labelled with chelating agents (a) two agent sequence 0.0005M Alizarin followed by 0.0005M Xylenol (b) three agent sequence: alizarin (red/ purple) followed by xylenol (orange) followed by calcein (green/ yellow). Bar = 200 µm.

3.3.3c Four stain tests

The verified three stain sequence, was extended to include calcein blue at a concentration of half that of the other three agents (0.00025M v 0.0005M) and the same protocol was used with four agents instead of three. Five specimens were machined from the same five bovine tibiae, that had been used for the three stain tests and stained in the A-X-C-CB sequence using the same staining protocol as above. Table 3.12 shows the results obtained.

Table 3.12 Four stain sequence results

0.0005m alizarin - 0.0005M xylenol - 0.0005M calcein > 0.00025M calcein blue

Spec.	SEQUENCE	QUAL. Agent 1	QUAL. Agent 2	QUAL. Agent 3	QUAL. Agent 4	CLARITY All agents	SUBSTIT.	GRADE (%)
1	A-X-C-CB	3	4	4	5	5	1	80.6
2	A-X-C-CB	3	5	4	5	5	1	84.6
3	A-X-C-CB	3	5	3	5	5	1	76.6
4	A-X-C-CB	2	4	4	5	4	1	72.6
5	A-X-C-CB	3	3*	3	5	5	1	72.6

Mean Grade= 77.4 ± 5.2%

*Calcein blue slightly displaces xylenol orange (<5%)

Even at the reduced concentration calcein blue was found to substitute calcein to a slight extent. The four stain sequence gives a much poorer grade average (77.4± 5.2%) than the three stain sequence (89.2 ± 7.8%). However, since its penetrative and fluorescence abilities are so good and since a clear contrast could be maintained between all four agents, albeit with slight substitution of calcein, it was proposed to further reduce the concentration of calcein blue (0.0001M) and carry out five more tests with the revised concentrations (Table 3.13).

Table 3.13 Revised four stain sequence results

0.0005 M alizarin - 0.0005 M xylenol - 0.0005 M calcein - 0.0001 M calcein blue

Spec.	SEQUENCE	QUAL. Agent 1	QUAL. Agent 2	QUAL. Agent 3	QUAL. Agent 4	CLARITY All agents	SUBSTIT.	GRADE (%)
1	A-X-C-CB	3	4	4	5	5	0	84
2	A-X-C-CB	3	5	5	5	5	0	92
3	A-X-C-CB	3	5	4	5	5	0	84
4	A-X-C-CB	2	4	5	5	5	0	84
5	A-X-C-CB	3	4	4	5	4	1	76

Mean Grade= 84± 5.65%

The results from the revised four stain protocol with 0.0001 M calcein blue showed that all four scratched regions can be clearly distinguished with little or no substitution occurring and all four agents were clearly distinct both from each other and from the surrounding bone matrix (Fig. 3.9). The grade average for the sequence now rises to 84± 5.65% which compares very favourably with the average grade for the three agent sequence (89.2 ± 7.8%).

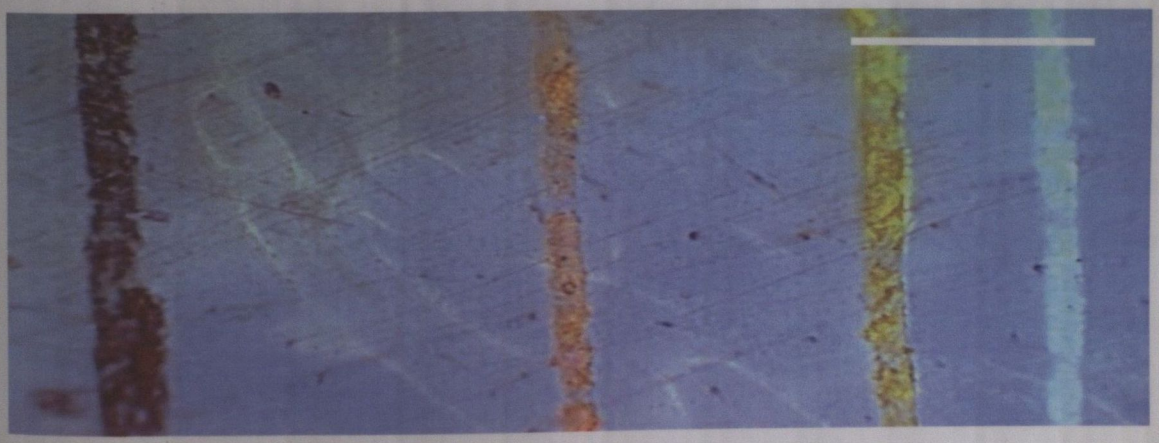

Fig. 3.9 Most efficient 4 agent sequence: alizarin (0.0005M) followed by xylenol orange (0.0005M) followed by calcein (0.0005M) followed by calcein blue (0.0001M). showing all 4 stains clearly distinct from each other and the surrounding bone. Bar = 200 μm

3.3.4 Measurement of most efficient concentrations

Table 3.14 Results of four stain sequence using *in vivo* concentrations (Rahn, 1977)

0.0005m alizarin > 0.0005M xylenol > 0.0005M calcein > 0.0001M calcein blue

Spec.	SEQUENCE	QUAL. Agent 1	QUAL. Agent 2	QUAL. Agent 3	QUAL. Agent 4	CLARITY All agents	SUBSTIT.	GRADE (%)
1	A-X-C-CB	3	3	3	5	3	2	61.3
2	A-X-C-CB	3	4	4	5	4	1	76.6
3	A-X-C-CB	3	3	3	5	3	2	61.3
4	A-X-C-CB	2	4	4	5	4	1	72.6
5	A-X-C-CB	3	3	3	5	3	2	61.3

Mean Grade= 66.7±7.4%

Table 3.14 shows the results obtained from the analysis of the determined four agent sequence using the recommended *in vivo* dosage regime (Rahn, 1977). Using these concentrations, a number of problems arose. Alizarin and xylenol orange were found to be difficult to differentiate from each other. Both agents appeared as a red/ orange colour and there was evidence that xylenol orange displaced alizarin to a certain extent. Similarly, calcein blue was found to displace calcein and calcein blue was also found to displace xylenol orange very slightly. The grade average for the *in vivo* concentrations is 66.7± 7.4% compared to 84± 5.65% for the *in vitro* concentrations. In summary, the concentartaions used in this study were found to be a lot more effective than the *in vivo* regime (Rahn, 1977).

3.4 Discussion

This study has established a sequence of application for the chelating agents which minimises substitution when the agents are applied in sequence. The results obtained from ion chromatography tests provided the basic order of agents, which indicated the affinity of the each agent for exposed calcium in a calcium chloride solution. However, since these tests were carried out in a calcium chloride solution and did not relate to *in vitro* mechanical testing conditions and the formation of microcracks, further work was necessary to validate the sequence using bone and generating artificial cracks in the form of scratches. This determined the optimal chelation times required to give good penetration of all agents while preventing overpenetration (bleeding). It was found that a staining time of 30 minutes was optimal for all of the agents. Oxytetracycline was disregarded from all further work after its chelation properties were found to be unstable. Furthermore, problems were often encountered with differentiating between the agent which had been applied during testing, and tetracycline that existed in the bone prior to testing[1].

The chromatography results established a preliminary sequence of: alizarin, xylenol orange, calcein and calcein blue. Upon application of this sequence, it was found that calcein blue displaced calcein, so the sequence was revised to alizarin, xylenol orange, calcein followed finally by calcein blue. Further tests showed that calcein blue still tended to displace calcein so the latter's concentration was reduced in stages, eventually to 0.0001M until the degree of substitution was negligible. When the *in vivo* concentrations (Rahn, 1977) and the newly established *in vitro* concentrations were compared, the new regime was more effective. These final tests suggest that the optimal sequence and concentrations have been reached and, when applied in sequence before and during mechanical tests, would allow microcrack initaition and growth to be monitored.

[1] Oxytetracycline is regularly administered as an antibiotic to cattle during normal farming practices and remains in bone for a number of years afterwards.

3.5 Conclusions

(1) The technique of sequentially applying chelating agents to specimens of bone has been refined to minimise the problem of substitution occurring. The established sequence is: alizarin - xylenol orange – calcein - calcein blue.

(2) The optimal concentrations which allow each of the agents to fluoresce brightly under UV light have also been determined: alizarin, 0.0005M - xylenol orange, 0.0005M – calcein, 0.0005M - calcein blue, 0.0001M.

(3) This sequence and dosage regime is superior to the one used for *in vivo* bone (Rahn, 1977).

Chapter 4

MICROCRACK GROWTH IN COMPACT BONE

4.1 Introduction

Chapter 2 described the development of a standardised technique to carry out fatigue tests on specimens of bone; the results obtained provided a new insight into the fatigue behaviour of cortical bone. In Chapter 3 a technique has been developed which allows flourescent chelating agents to be applied in a determined sequence to bone specimens without the problem of substitution occurring. The work in this chapter seeks to use the established techniques to label microcracks formed during mechanical testing and in so doing, to learn more about the behaviour of microcrack growth in compact bone.

4.1.1 Bone as a composite material

As discussed in Chapter 1, bone is an anisotropic material, with its strength and elastic properties being dependent on the direction of applied loading. The resistance of any material to fatigue failure is a function of its resistance to both the initiation and propagation of cracks. Osteonal bone is often compared to a composite material and, in composite materials, it has been shown that repetitive loading, which reduces the loads required to initiate microcracks, can actually improve the materials resistance to fatigue crack growth (Agarwal and Broutman, 1980). Discontinuities within the material (e.g. fibres, laminae, voids) may provide stress concentration sites for crack initiation, but they also serve as barriers to crack growth which may slow down or even halt crack propagation completely. In bone therefore, it would be expected that cracks would tend to remain small and follow the fibres instead of propagating across osteons.

4.1.2 Failure in composite materials

The long term fatigue behaviour of fibrous lamellar composites can divided into three regions.

Region I: Crack Initiation

The first stage of fatigue is characterised by a rapid reduction in stiffness which coincides with the inititiation of numerous small microcracks. Cracks develop rapidly, but stabilise quickly without much propagation and they tend to be confined to single lamellae and do not propagate into adjacent lamellae. The reduction in crack growth leads to the loss of stiffness quickly stabilising, generally within the first 25% of the fatigue life (Martin and Burr, 1989) and further loss of stiffness does not occur until just prior to ultimate failure. Cracks in Region I run across lamellae, perpendicular to the load axis.

Region II: Crack Growth and Coalescence

In the second stage of fatigue failure, damage accumulation shifts to interlamellar debonding. The stress field or plastic zone ahead of a propagating microcrack causes debonding at the fibre-matrix interface. When the crack finally reaches the interface , its tip will be blunted by the already present debonding crack. Thus the crack will be diverted and instead of continuing straight across the fibre, it will take the path of least resistance which involves debonding along the weak interface. Cracks tend to grow parallel to weak interfaces between lamellae and although they have been shown to occasionally join other cracks (Reifsneider, 1990) they do not lead to failure of the material, or even change the materials stiffness by a great deal.

Region III: Progression to Failure

The final stage in the life of fibrous composites is relatively brief and results in failure. Further debonding of lamellae occurs, a process combined with the degeneration of the matrix of the composite itself. The lamellae begin to fracture, and, as they break, they increase the stress in the elements remaining intact so creating a 'domino effect' of lamellar fracture. This process occurs quite rapidly in the last 10% of the materials life.

Fig. 4.1 illustrates the process of damage accumulation in comparison to modulus reduction.

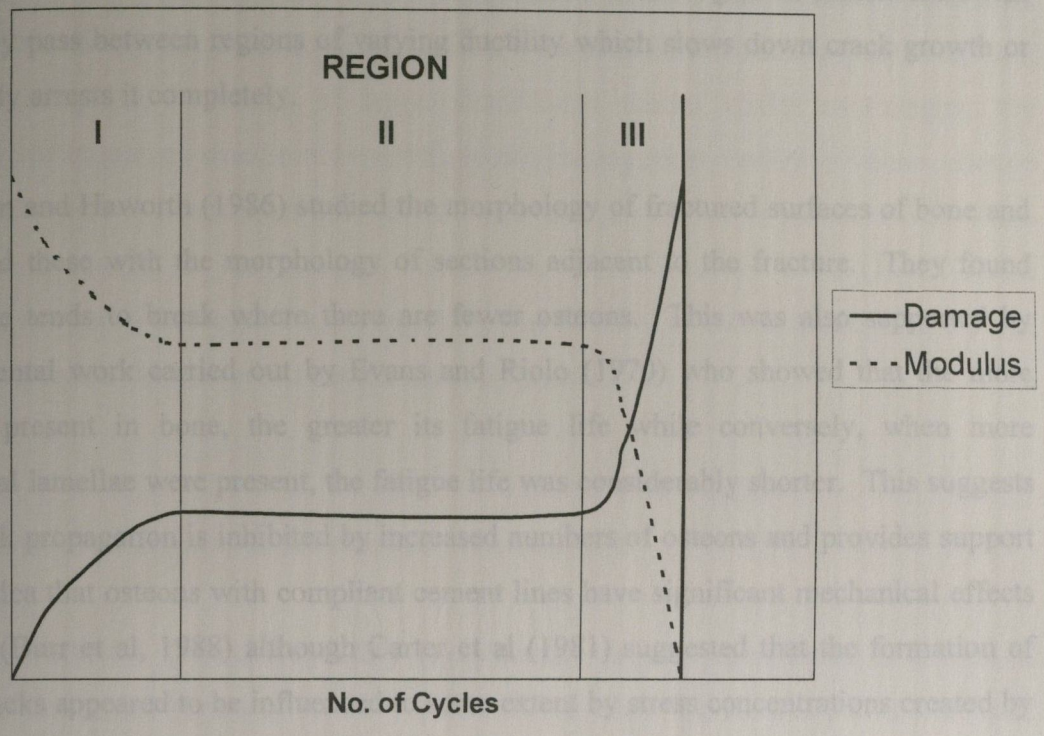

Fig. 4.1 The process of failure in composite materials. In Region I, the initiation of damage leads to an initial reduction in stiffness. Region II, lamellar debonding takes place with no significant increase in damage accumulation occurring. In Region III, the modulus decreases rapidly with the build-up of damage, eventually resulting in failure (Martin et al, 1998).

4.1.3 Effect of bone microstructure on microcrack growth

In Chapter 1, it was shown that the material strength of bone depends on the type of loading, as well as on the loading direction. As Haversian bone is similar in its osteonal arrangement to a tough fibrous composite laminate material, it provides an indication that osteonal bone is a tough material even though it is not very strong. The fact that osteonal bone is laminated also provides evidence of the difficulty of crack propagation. Lamellar interfaces cause stress enhancement at the tip of a propagating crack to be inhibited as the

crack enters the interface. Similarly, the morphology of the cement line in Haversian bone permits relatively easy crack initiation but prevents or slows any significant crack growth. As with bone lamellae, this means that cracks in the region of cement lines will inevitably pass between regions of varying ductility which slows down crack growth or eventually arrests it completely.

Corondan and Haworth (1986) studied the morphology of fractured surfaces of bone and compared these with the morphology of sections adjacent to the fracture. They found that bone tends to break where there are fewer osteons. This was also supported by experimental work carried out by Evans and Riolo (1970) who showed that the more osteons present in bone, the greater its fatigue life while conversely, when more interstitial lamellae were present, the fatigue life was considerably shorter. This suggests that crack propagation is inhibited by increased numbers of osteons and provides support for the idea that osteons with compliant cement lines have significant mechanical effects in bone (Burr et al, 1988) although Carter et al (1981) suggested that the formation of microcracks appeared to be influenced to some extent by stress concentrations created by vascular canals and lacunae.

The fact that the cement line interface between osteons and interstitial bone is relatively weak means that it may reduce the shear strength of osteonal bone (Frasca, 1981). However slipping at this interface may relax shear stresses, reduce strain energy and slow crack propagation. Park and Lakes (1986) studied the viscoelastic creep behaviour of human bone and found experimental evidance which suggested that the osteonal cement line only fails after other damage has accumulated in the bone matrix.

Jepsen et al (1999) showed that the lamellar interface in bone is weak and is the principal site of shear damage formation but the lamellar interface was shown to be highly effective in keeping cracks isolated from each other. Zioupos and Currey (1994) showed that microcracks in bone did interact with the microstructure of the bone and that the grain of the bone did not allow microcracks to travel in straight lines. They hypothesised that the presence of lamellae influenced the process by which microcracks coalesced but

that vascular or other naturally occurring cavities did not initiate microcracking and appeared to deflect microcracks. Schaffler et al (1994b) used back-scattered electron microscopy on fuchsin stained sections of human rib to show that features of the bone matrix ultrastructure, such as the collagen fibre-bone mineral relationship play a key role in minimising the formation of larger detrimental cracks whilst encouraging the formation of numerous small cracks which do not propagate as readily to failure. Boyce et al (1998) showed experimentally that microcracks developed in the interstitial tissue regions and stopped at the osteonal boundaries, while Schaffler et al (1995) added quantitative data to this hypothesis suggesting that 80-90% of all microcracks in cortical bone are found in the interstitial matrix between osteons.

4.1.4 Loss of stiffness with microcrack accumulation

Previous work has demonstrated that microdamage accumulation leads to a loss of stiffness (Carter and Hayes 1976, 1977a; Schaffler et al; 1989; Keaveny et al, 1994a,b; Zioupos et al, 1996; Taylor et al, 1999). Fyhrie and Vashishith (2000) showed that stiffness is a primary predictor for both yield strength and ultimate strength in human trabecular bone in compression.

The work carried in Chapter 2 and reported in Taylor et al (1999) showed that after a 10 % reduction in modulus had taken place, the specimen was close to failure and this reduction from initial modulus always coincided with the presence of at least one large crack, usually oriented at an angle of 45° to the specimen axis. Schaffler (1989) carried out tests in cyclic tension which did not progress to failure and showed that there was a gradual decrease of modulus during the initial loading period (6%) but following this, specimen modulus stabilised and did not change again during the period of loading. This work was carried out at physiological strain range (1500με). It has been shown that the tensile elastic modulus of human femoral bone decreases over its fatigue life (Pattin et al, 1996). There is an early rapid diminishment of stiffness, followed by prolonged gradual loss, until very suddenly the modulus plummets as failure occurs. This is consistent with

observations by Zioupos et al (1994b, 1996) who found that the increase in damage followed a similar pattern to the elastic degradation of the material. Damage increased with the cycle number and was in general non-linear and accelerated rapidly in the last prefailure cycles. This is consistent with the process of failure in composite materials (Fig. 4.1). However these tests were carried out above physiological tensile strain (2500 με). This would appear to indicate that bone has excellent fatigue properties at physiological strains but at strains above physiological, the path to failure is very similar to that of fibrous lamellar composites.

4.1.5 The process of microcrack growth in bone

Little work has been carried out to look at the process of damage accumulation during a bone's life. In attempting to understand the process, previous workers (Burr et al, 1995; Boyce et al, 1996, Forwood and Parker, 1989) have performed fatigue tests, stopping the tests prior to failure to allow histological analysis of damage developed before fracture. Akkus and Rimnac (2000) is the only study to have looked at the process of initiation, propagation and growth of individual microcracks. They investigated microcrack growth of individual surface microcracks in human cortical bone using a video microscopy system. They found that microcracks propagated and generally arrested in less than 10,000 cycles although some accelerated in growth after this stage. Their results support the concept of a microstructural barrier effect for cortical bone tissue. The limitations with their work include the fact that they only looked at surface cracks and also disregarded microcracks that did not run in straight lines and they did not look at the actual mechanisms by which microcrack growth was arrested. The process by which microcracks initiate and grow remains poorly understood and no work has been carried out to show at what periods during a test microcracks initiate, accumulate and ultimately bring about failure.

4.1.6 Microcrack barrier concept

Taylor (1998b) developed a theoretical model to show how information on the fatigue behaviour of microcracks can be obtained by an analysis of stiffness changes measured during cyclic loading. His model showed how, using these stiffness changes and some realistic assumptions, it is possible to derive values of crack length, crack growth rate and stress intensity for the early phase of microcrack development.

The initiation and growth of microcracks in compact bone occurs without difficulty because microcracks tend to initiate in weak regions in the bone matrix. As the crack continues to grow, it encounters barriers within the microstructure which cause growth to slow and in some cases to stop completely. If growth continues, the crack eventually becomes large (macrocracks) and its growth rate is determined by the average resistance of the material. Therefore a plot of fatigue crack growth rate (d*a*/dN, in mm/cycle) as a function of crack length (a), will show a minimum point at $a = d$: the spacing of microstructural barriers (Fig. 4.2). Taylor (1998a) took the spacing of the microstructural barriers to be 100 μm and assumed an elliptical crack shape (Taylor and Lee, 1998). The results showed that the rate of crack growth decreases rapidly as crack length increases in the range 0-100 μm.

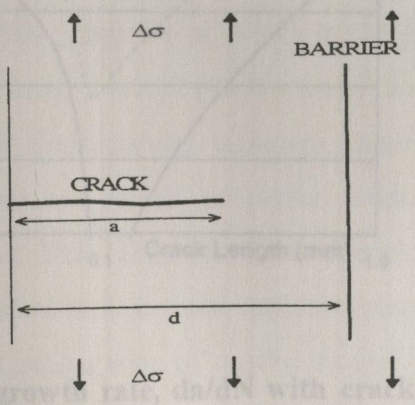

Fig. 4.2 Microstructural barrier, simplified geometry and loading scheme: a crack of length *a* begins a the surface and grows towards a microstructural barrier at a distance *d*, under the influence of a uniform cyclic tensile stress (Taylor, 1997).

Schaffler et al (1989, 1990) predicted that fatigue failure will not occur in bone at strains of 0-1200 με because cracks reach barriers which arrest their growth. However Taylor's model (1998b) predicted that failure will eventually occur but it may take more than 10^{10} cycles. In clinical situations, it is obvious that there will be an increase in this strain level due to rigorous activities (running etc.) or accidents (e.g. stumbling). The model also predicted that if a crack approaching a barrier experienced a sudden overload (e.g. 2000 με) it will break through the barrier. The next barrier will be approximately 100 μm away, the longer crack will now have a higher stress intensity value so even at normal loading (1200 με), it will be able to break through the barrier. This gives an idea of how eventually failure may take place from a single microcrack. Fig 4.3 shows a prediction of how the crack growth rate changes with increasing crack length while Fig. 4.4 shows the decreasing part of the curve as deduced from data by Schaffler et al (1989, 1990) on stiffness reductions during testing.

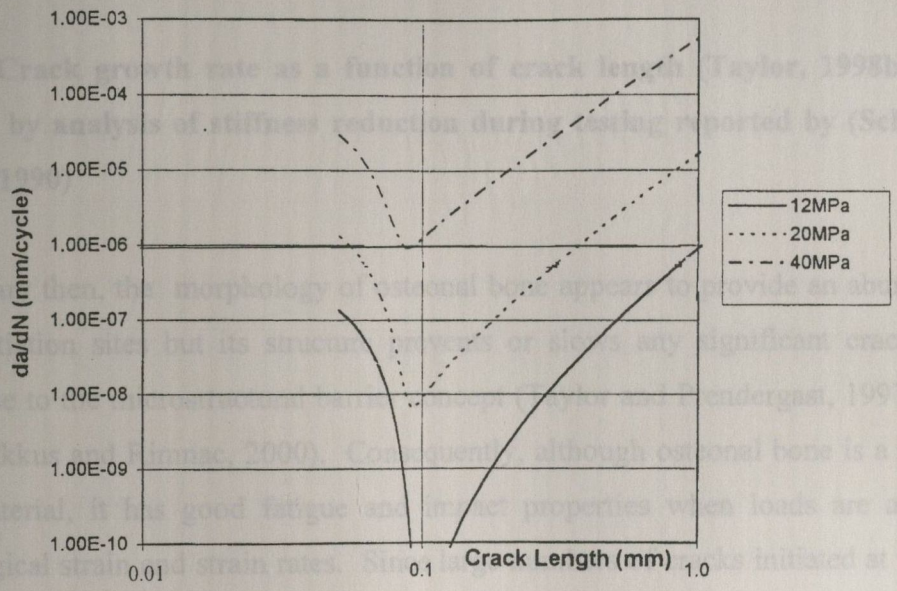

Fig. 4.3 Predicted variation of growth rate, da/dN with crack length for different stress ranges in compact bone. Initially the growth rate decreases as the crack approaches some barrier before increasing again as it develops sufficient energy to overcome the obstacle (Taylor, 1997).

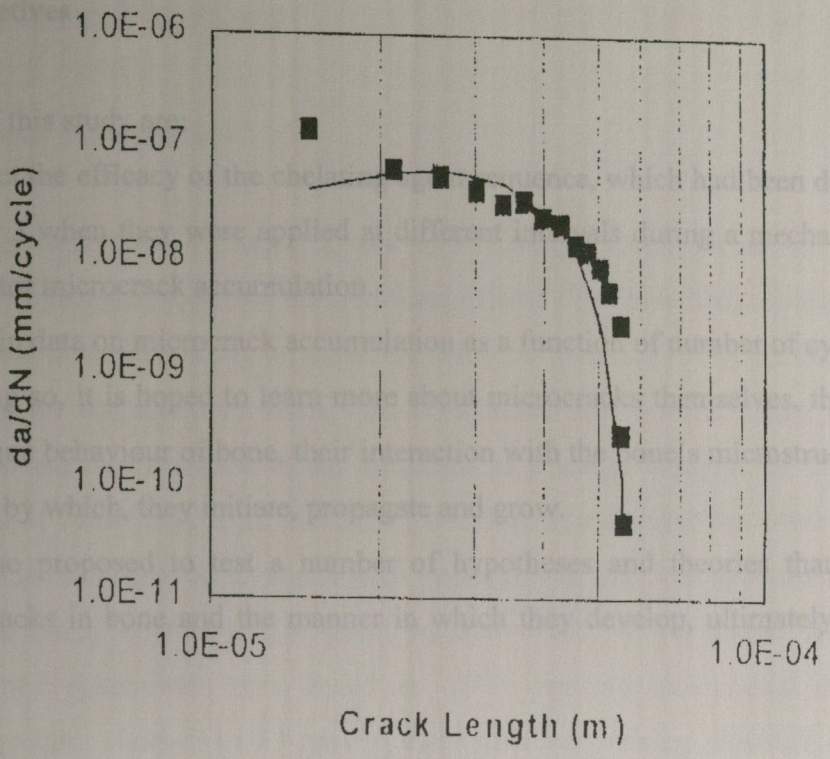

Fig. 4.4 Crack growth rate as a function of crack length (Taylor, 1998b), values obtained by analysis of stiffness reduction during testing reported by (Schaffler et al, 1989, 1990)

In summary then, the morphology of osteonal bone appears to provide an abundance of crack initiation sites but its structure prevents or slows any significant crack growth giving rise to the microstructural barrier concept (Taylor and Prendergast, 1997; Taylor, 1998b; Akkus and Rimnac, 2000). Consequently, although osteonal bone is a relatively weak material, it has good fatigue and impact properties when loads are applied at physiological strain and strain rates. Since large numbers of cracks initiated at relatively low stresses are repaired by bone remodelling, crack initiation may not be as detrimental to the bone's fatigue life as rapid propagation of cracks through a non-living material would be.

4.1.7 Objectives

The aims of this study are:

(1) To detect the efficacy of the chelating agent sequence, which had been determined in Chapter 3 when they were applied at different intervals during a mechanical fatigue to monitor microcrack accumulation.

(2) To obtain data on microcrack accumulation as a function of number of cycles.

(3) By doing so, it is hoped to learn more about microcracks themselves, their effect on the fatigue behaviour of bone, their interaction with the bone's microstructure and the process by which, they initiate, propagate and grow.

(4) It is also proposed to test a number of hypotheses and theories that exist about microcracks in bone and the manner in which they develop, ultimately resulting in failure.

4.2 Materials and Methods

4.2.1 Specimen Manufacture

The technique described in Chapter 2 was used to manufacture specimens. Samples of cortical bone were removed from the mid-diaphysis of 17 bovine tibiae using a band saw. These samples were then cored on a milling machine resulting in cyclindrical specimens of length 35mm and diameter 7mm. These samples then waisted using a CNC lathe which turned the centre region of the specimen to a gauge diameter of 5.25mm and a gauge length of 7mm. Again, all machining was carried out under wet conditions and the specimens were not allowed to dry. Visual inspection of the final specimens showed no obvious machining defects and a good surface finish in the gauge length. After machining, the specimens were stored at -20^0C prior to mechanical testing. The machining process resulted in 15 good quality specimens being obtained, each from a different animal.

4.2.2 Mechanical testing

Specimens were removed from the freezer on the day prior to testing, allowed to thaw and placed in a single vial of 0.0005 M alizarin in a dessicator at 50 mm Hg vacuum for 16 hours to label microdamage which existed prior to testing. An INSTRON 8501 servo-hydraulic testing machine was used in load control to apply an axial compressive force to the specimens. Testing was carried out in the rig shown in Fig. 2.3 with the specimens enclosed in small plastic bath into which the dyes could be added. All tests were carried out at a frequency of 3 Hz, with a stress range of 80 MPa and a stress ratio of 0.1, for which the expected average life was about 100,000 cycles.

For the first stage of the test, the specimens were tested in a bath of 0.0005M xylenol orange. Testing was carried out until 50,000 cycles had elapsed, the xylenol was removed from the bath, and the bath and the specimens were rinsed with distilled water to

wash out any remaining dye. 0.0005 M calcein was then added to the bath and tests were continued until failure occurred. Failure was defined using the established criteria as an increase of more than 10% in the cyclic deflection range (Taylor et al, 1999).

Three final tests were carried out using a four dye sequence, alizarin prior to testing, xylenol orange applied for the first 10,000 cycles which was then replaced with calcein until 50,000 cyles had elapsed followed by the fourth agent, calcein blue until failure occurred. This allowed us to distinguish cracks, and their lengths at approximately 10% and 50% of life, as well as the time of failure.

4.2.3 Histological examination

After testing the specimens were washed in de-ionised water and returned to the freezer prior to sectioning and mounting. Fig. 4.5 show a schematic diagram of how the specimens were analysed.

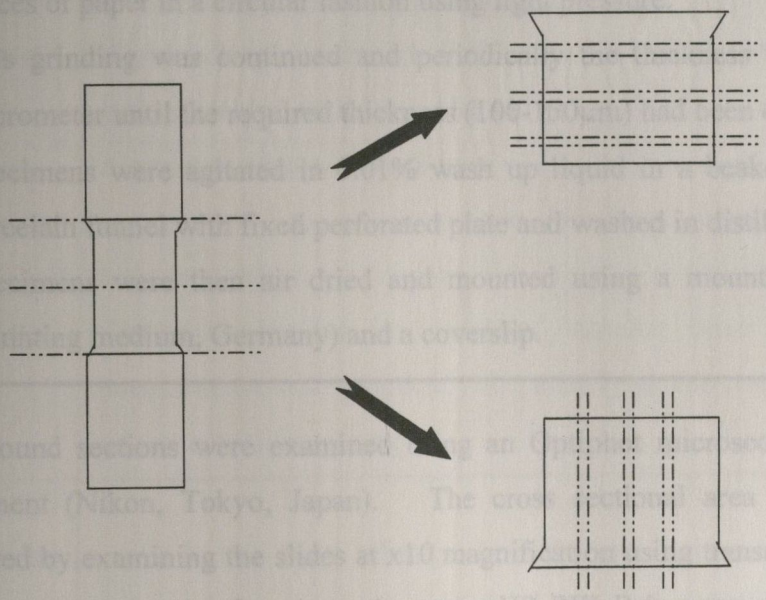

Fig. 4.5 Schematic diagram of specimen analysis

The gauge length of the specimens was removed using a diamond saw (Streuers Miniton) and this was then divided into two sections, and at random, one block was assigned for analysis of longitudinal sections and the other was assigned to analysis of transverse sections.

Ground sections were prepared by handgrinding (Table 4.1). Both sets of sections were then put in sequence and odd numbered slides were analysed. 3 longitudinal slides and 3 transverse slides were examined using epifluorescence microscopy.

Table 4.1 Preparation of ground sections of compact bone (Frost, 1958)

1. Specimen was placed in a small clamp and approximately 250μm was cut using a diamond saw (Streuers Miniton).
2. A sheet of No. 400 silicon carbide paper was placed on a flat surface under running water and the section was placed upon it. Another piece of paper was wrapped around a glass slide and the section was manually ground down between the two pieces of paper in a circular fashion using light pressure.
3. This grinding was continued and periodically the thickness was checked using a micrometer until the required thickness (100-150μm) had been obtained.
4. Specimens were agitated in 0.01% wash up liquid in a beaker, placed in a Coors porcelain funnel with fixed perforated plate and washed in distilled water.
5. Specimens were then air dried and mounted using a mounting medium (Eukitt's mounting medium, Germany) and a coverslip.

The ground sections were examined using an Optiphot microscope with fluorescence attachment (Nikon, Tokyo, Japan). The cross sectional area of each section was measured by examining the slides at x10 magnification using transmitted white light and transferring the image of each section, to a HP PIII Brio personal computer (Hewlett Packard, Grenoble, France) using a CCD colour video camera (Optronics Engineering, Goleta, Ca). Scion Image™ software (Scion Corporation, Frederick, Maryland, USA) was calibrated by transferring an image of a graticule containing a 1 mm scale bar (at the

same magnification as the ground sections) from the CCD camera to the PC and the cross sectional areas of each transverse and longitudinal section were then measured.

The sections were then examined for microcracks using the technique described by Lee et al (1998) (Table 2.3). Images of microcracks were transferred to an RGB monitor and using the switchbox, the image was enhanced by improving such modalities as exposure, contrast, sharpness and degree of red/ green/ blue colouring so as to allow each chelating agent to show up clearly while also being distinct from each other. Images of the microcracks were transferred to the PC and archived before measurements were carried out. In the case of the transverse sections, the microcrack location were noted in all cases with the location defined using the following criteria (Schiller, 1994).

Table 4.2 Criteria for the classification of microcrack location

Class	Definition
Periosteal	Microcrack in continuity with the periosteal surface or predominantly located in periosteal lamellae
Endosteal	Microcrack in continuity with the endosteal surface or predominantly located in endosteal circumferential lamellae
Osteonal	Microcrack located completely within an osteon or crossing the cement line on concentric lamellae of primary or secondary osteon
Interstitial	Microcrack located in interstitial lamellar bone between osteons or located completely or partially on the cement line, but not actually crossing it

The specimens used in this study all came from the mid-diaphysis of bovine tibiae and were machined from the central cortex of the bone as far away as possible from the periosteal and endosteal surfaces. This was the best way to obtain a specimen of the required dimensions and as such, it was decided to ignore the periosteal and endosteal classes and to categorise microcracks as either osteonal or interstitial. Longitudinal

microcracks were not categorised in terms of location due to the difficulties encountered in identifying cement lines or osteonal boundaries.

Microcrack images were then transferred to the PC, and measured using Scion Image™ and classified according to the chelating agent with which they had been labelled (Table 4.3)

Table 4.3 Microcrack classification with three chelating agents applied

Class	Definition
Stage 2 Microcrack	Stained with xylenol, formed during the first 50,000 cycles of the test
Stage 3 Microcrack	Stained with calcein, formed between 50,000 cycles and failure
Propagating Microcrack	Microcrack stained with 2 or more agents
Preexisting Microcrack	Stained with alizarin, either *in vivo* or artefactual microcrack

For the final three tests in which four chelating agents were used, this classification was refined to include calcein blue (Table 4.4).

Table 4.4 Microcrack classification with four chelating agents applied

Class	Definition
Stage 1 Microcrack	Stained with xylenol, formed during the first 10,000 cycles of the test
Stage 2 Microcrack	Stained with calcein, formed between 10,000 and 50,000 cycles
Stage 3 Microcrack	Stained with calcein blue, formed between 50,000 cycles and failure
Propagating Microcrack	Microcrack stained with 2 or more agents
Preexisting Microcrack	Stained with alizarin, either *in vivo* or artefactual microcrack

In specimens which had failed outright, the main failure crack was ignored as were any smaller microcracks which had been formed in the vicinity of this main crack due to its rapid propagation.

Microcrack analysis results were tabulated in the form of: (i) mean number of cracks occurring per section, (ii) crack numerical density (number of cracks occurring per mm^2) (iii) crack surface density (μm of crack length occurring per mm^2) (iv) mean crack length (v) percentage distribution of microcracks according to the above classification.

4.2.4 *In vivo* microcracks

The classification system defined microcracks labelled with alizarin as either pre-existing or *in vivo* microcracks. Following the fatigue tests it was decided to carry out three further tests in order to establish how many of these cracks existed prior to machining (*in vivo* microcracks) and how many were artefactual microcracks (formed by the machining process). Three samples of bone were removed from the mid diaphysis of three bovine

tibiae using the same technique as had been used for all specimens. However instead of continuing the standard machining process of coring the block and then lathing it to produce a test specimen, the blocks of bone were each placed in a single vial of 0.0005M alizarin in a dessicator at 50 mm Hg vacuum for 16 hours to label microdamage which was formed *in vivo*. These blocks were then sectioned on a diamond saw and ground sections were made (Table 4.1) before being examined for microcracks using fluorescence microscopy. During the analysis process any microcracks found within 500 μm of the bone surface were ignored, so as to prevent any cracks formed by the bandsaw being counted.

4.2.5 Statistical analysis

Unpaired t-tests were used to statistically analyse the microcrack data. These parametric tests are commonly used for comparing two sets of data in order to calculate the ratio of variation between the two sets, so as to determine whether the mean values and standard deviations are significantly different. In this study an unpaired rather than a paired t-test was used because this test allows comparison of two sets of data of a different sample size as was necessary for comparing microcrack numbers for the different stages monitored and also for comparing the data between the three stain test and the four stain test (Cambell, 1974). A probability value of 95% was used ($p<0.05$).

4.3 Results

From the twelve initial fatigue tests carried out, ten successful tests were achieved with six of these specimens failing outright before the 10 % loss of stiffness had occurred. The mean N_f value was 90,190 (S.D. 21,100) cycles to failure (Appendix 4.1). It was initially thought that due to the relatively short testing time (~ 5 hours for each stage of the test), the chelating agent would not have sufficient time to penetrate the bone and label microcracks. The first two tests were carried out with the bone specimens left unloaded in the Instron in a bath of a xylenol orange for 8 hours after the first part of the test had taken place. After the second part of the test (between 50,000 cycles and failure) the specimen was removed from the test rig and placed in a bath of calcein for 8 hours. From analysis of these specimens, it was difficult to distinguish individual agents or even parts of the bone microstructure in certain areas due to overstaining. The remainder of the tests were then carried out with the specimen remaining in the agent during the test only, so as to prevent this overstaining.

As with the earlier study looking at the fatigue life of compact bone (Chapter 2), the failure pattern was similar in all specimens, with the main fracture crack occurring in the gauge length of the specimen at an approximate angle of 45^0 to the specimen axis. When the specimens were sectioned and examined using epifluorescence microscopy, no evidence of substitution of chelating agents was found to occur. In the majority of sections, it was possible to distinguish individual agents with relative ease and in sections where there was some difficulty due to apparent poor penetration, it was possible, by improving the contrast and colour levels on the RGB monitor, to distinguish individual agents. The following four images show examples of microcracks stained with different agents.

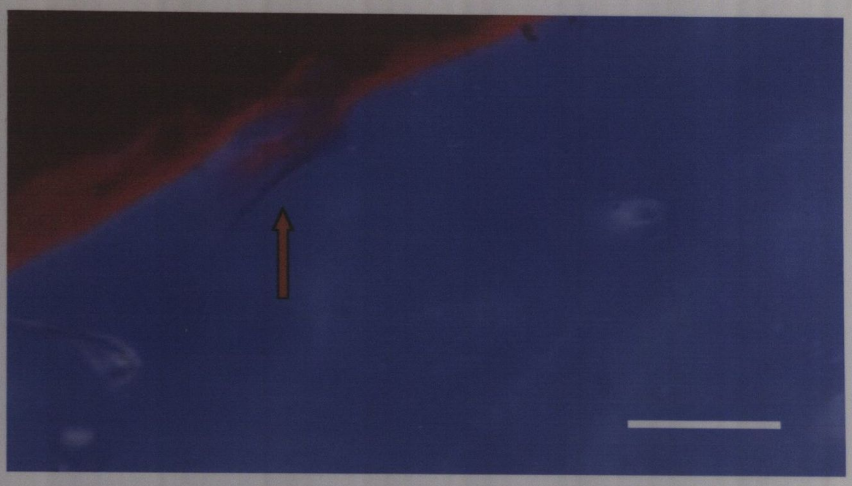

Fig. 4.6 Microcrack from surface labelled with alizarin, showing that it was formed prior to testing. Alizarin can be seen all along the bone surface. Bar= 50 μm.

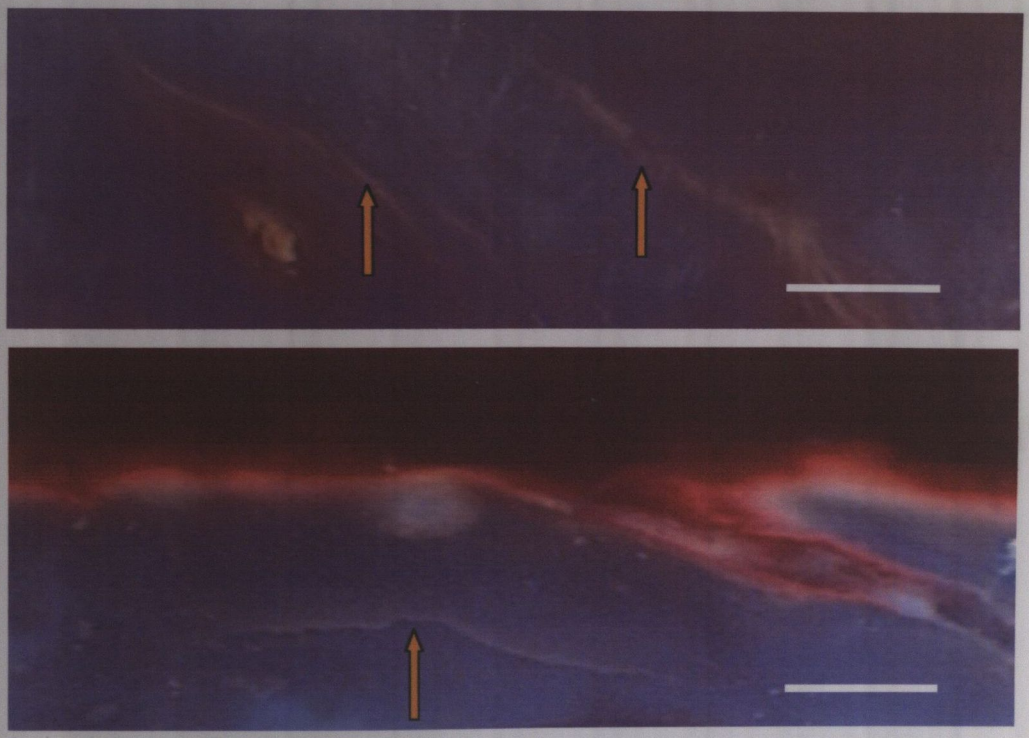

Fig. 4.7 Examples of microcracks labelled with xylenol, showing that they were formed during the first 50,000 cycles of the test. Bar=100 μm.

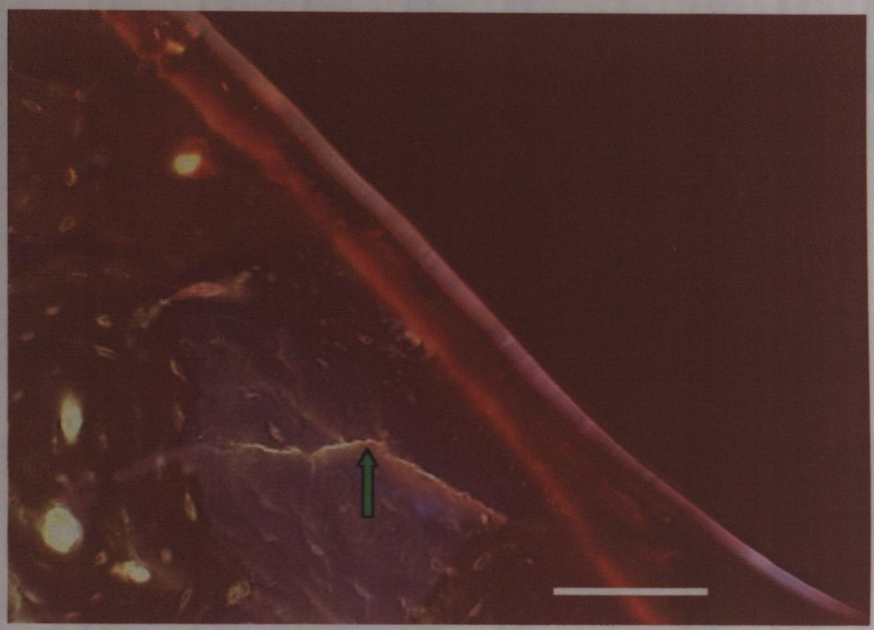

Fig 4.8 Microcrack labelled with calcein showing that it was formed between 50,000 cycles and failure. Alizarin can be seen on the surface of the specimen. Bar=100 μm.

Fig. 4.9a

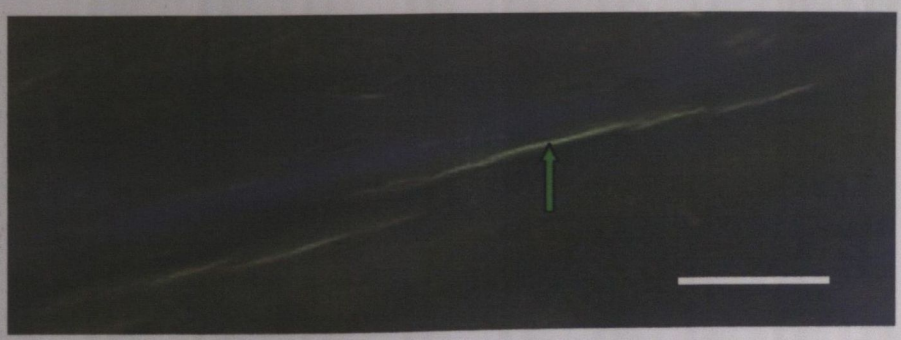

Fig. 4.9b Example of longitudinal microcracks (a) stained with xylenol and viewed using green epifluorescence (b) labelled with calcein and viewed using UV epifluorescence. Bar=100 μm.

4.3.1 Three Agent Tests: Microcrack Densities

Tables 4.5 and 4.6 show the mean data obtained for both transverse sections and longitudinal sections from the fatigue tests in which alizarin was applied before testing, xylenol was applied during the first 50,000 cycles and calcein was applied during the latter part of the test.

Table 4.5 Data obtained from transverse sections

CRACK TYPE	STAGE 2	STAGE 3	PROPAGATING	PREEXIST.
Num. Density (No./mm^2)	0.203	0.386	0.049	0.040
S.D.	0.193	0.287	0.084	0.036
Surface Density (μm /mm^2)	21.5	49.7	9.4	3.4
S.D.	27.6	61.6	17.7	3.1
Percentage of Microcracks	29.81	59.01	6.21	4.97

Table 4.6 Data obtained from longitudinal sections

CRACK TYPE	STAGE 2	STAGE 3	PROPAGATING	PREEXIST.
Num. Density (No./mm$^{2)}$	0.103	0.236	0.032	0.021
S.D.	0.087	0.174	0.023	0.024
Surface Density (μm /mm^2)	19.4	64.8	14.8	1.5
S.D.	21.3	76.4	13.7	1.7
Percentage of Microcracks	25.34	59.59	8.22	6.85

Fig. 4.10 and 4.11 show the graphs obtained from these data

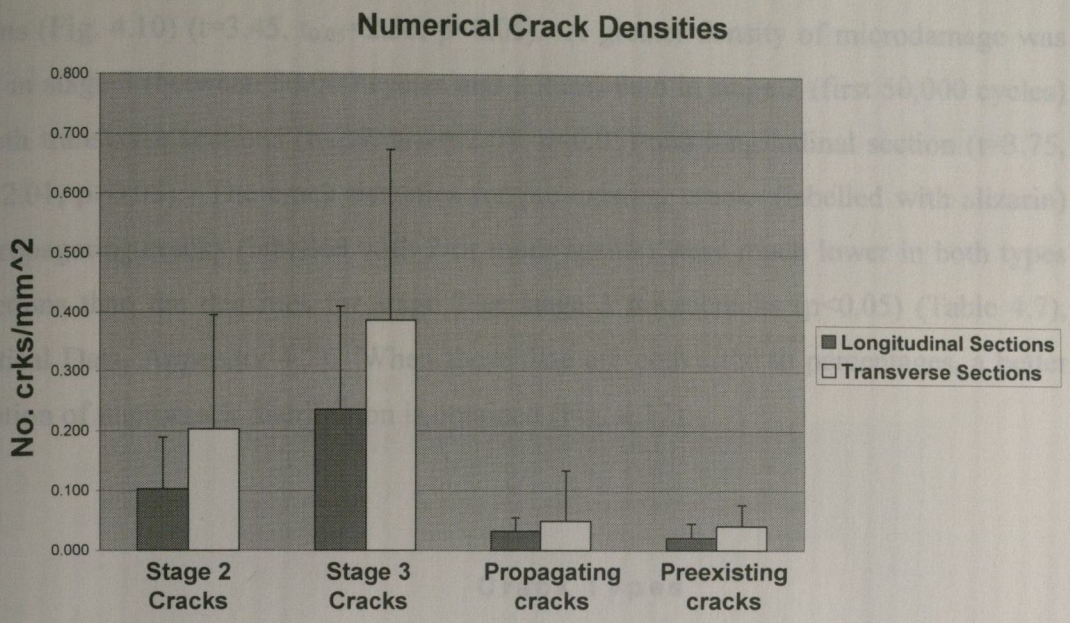

Fig. 4.10 Numerical crack densities for all four crack types

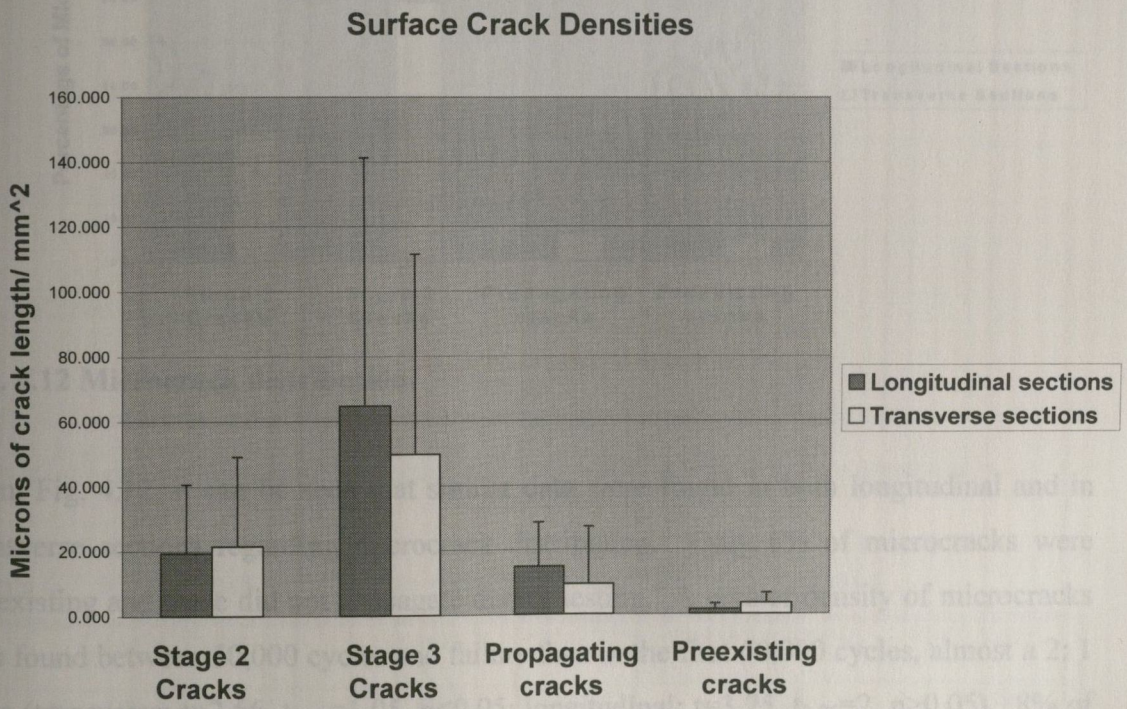

Fig. 4.11 Surface crack densities for all four crack types

A greater proportion of microcracks were found in transverse than in longitudinal sections (Fig. 4.10) ($t=3.45$, $t_{0.05}=2.36$, $p<0.05$). A greater density of microdamage was found in stage 3 (between 50,000 cycles and failure) than in stage 2 (first 50,000 cycles) for both transverse sections ($t=2.9$, $t_{0.05}= 2.01$, $p<0.05$) and longitudinal section ($t=3.75$, $t_{0.05}= 2.01$, $p>0.05$). The crack densities for pre-existing cracks (labelled with alizarin) and propagating cracks (labelled with 2 or more agents) were much lower in both types of sections than the densities for stage 2 or stage 3 microcracks ($p<0.05$) (Table 4.7), Statistical Data, Appendix 4.2). When these data are converted to percentages, a better indication of microcrack distribution is obtained (Fig. 4.12).

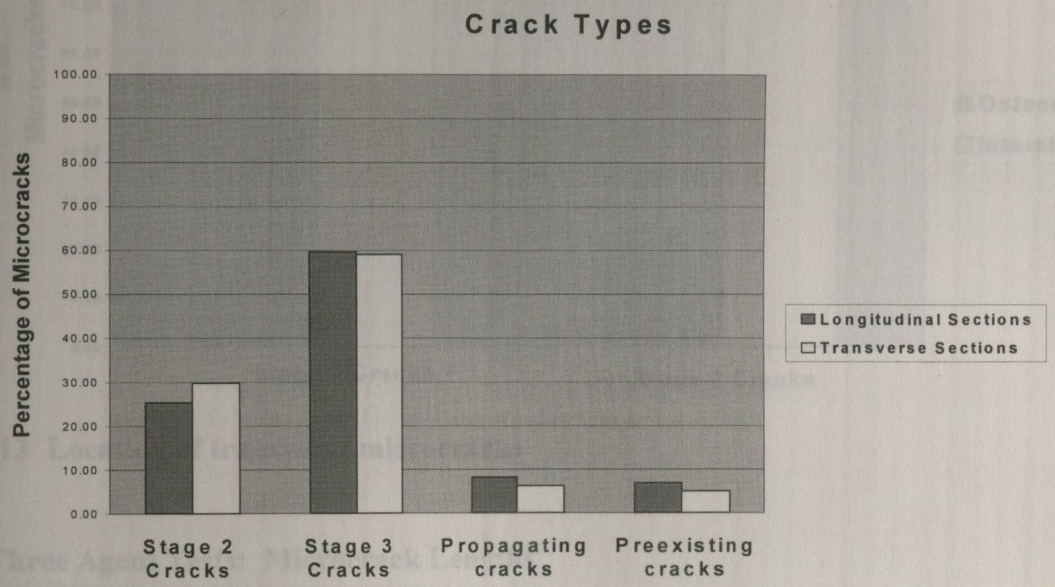

Fig. 4.12 Microcrack distribution

From Fig. 4.12, it can be seen that similar data were found in both longitudinal and in transverse sections regarding microcrack distribution. Only 6% of microcracks were preexisting and these did not propagate during testing. A greater density of microcracks was found between 50,000 cycles and failure than in the first 50,000 cycles, almost a 2: 1 ratio (transverse: $t=2.66$, $t_{0.05}=1.95$, $p<0.05$; longitudinal: $t=3.75$, $t_{0.05}=2$, $p>0.05$). 8% of microcracks were labelled with two agents, indicating propagation.

4.3.2 Three Agent Tests: Microcrack Locations

Fig. 4.13 shows the distribution of microcracks by location. For microcracks formed in the first 50,000 cycles, 94 % of them were located in interstitial bone and although this figure drops for stage 2 microcracks, less than 25 % of them were located in osteons showing that the significant majority of microcracks were found in interstitial bone ($p<0.05$).

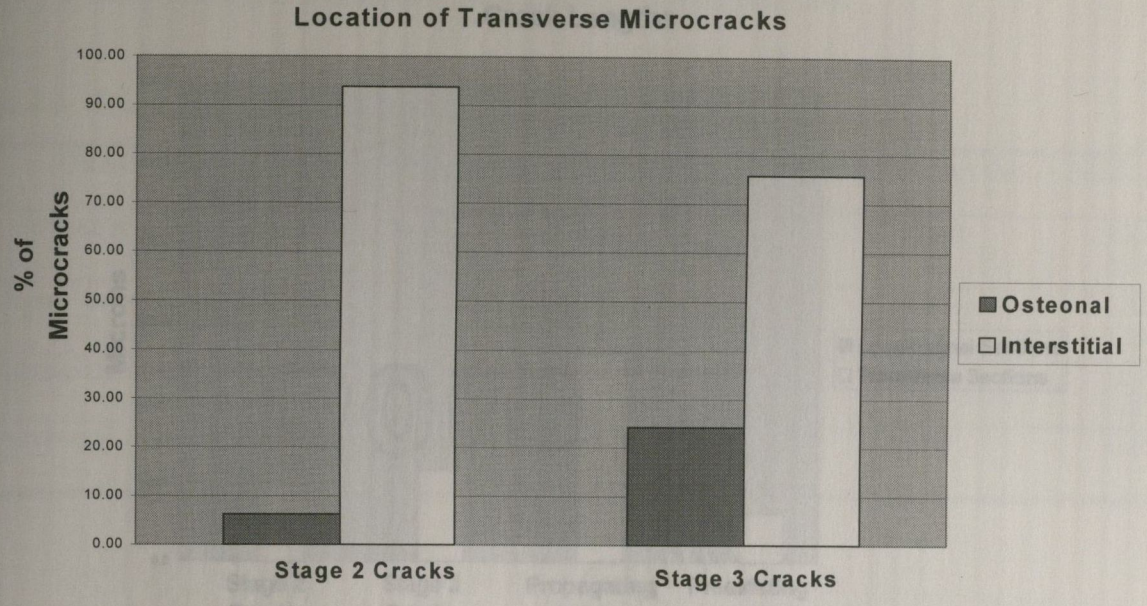

Fig. 4.13 Location of transverse microcracks

4.3.3 Three Agent Tests: Microcrack Lengths

Table 4.7 and Table 4.8 shows the data obtained from analysis of microcrack lengths for both transverse and longitudinal sections. Fig. 4.16 illustrates this data graphically.

Table 4.7 Mean crack length data obtained from transverse sections

CRACK TYPE	STAGE 2	STAGE 3	PROPAGATING	PREEXIST.
CRACK LGT (μm)	**96.5**	**115.6**	**263.9**	**61.6**
S.D.	61.8	84.4	117.2	38.78

Table 4.8 Crack length data obtained from longitudinal sections

CRACK TYPE	STAGE 2	STAGE 3	PROPAGATING	PREEXIST.
CRACK LGT (μm)	**177.2**	**249.0**	**357.3**	**50.26**
S.D.	108.8	181.1	148.2	58.4

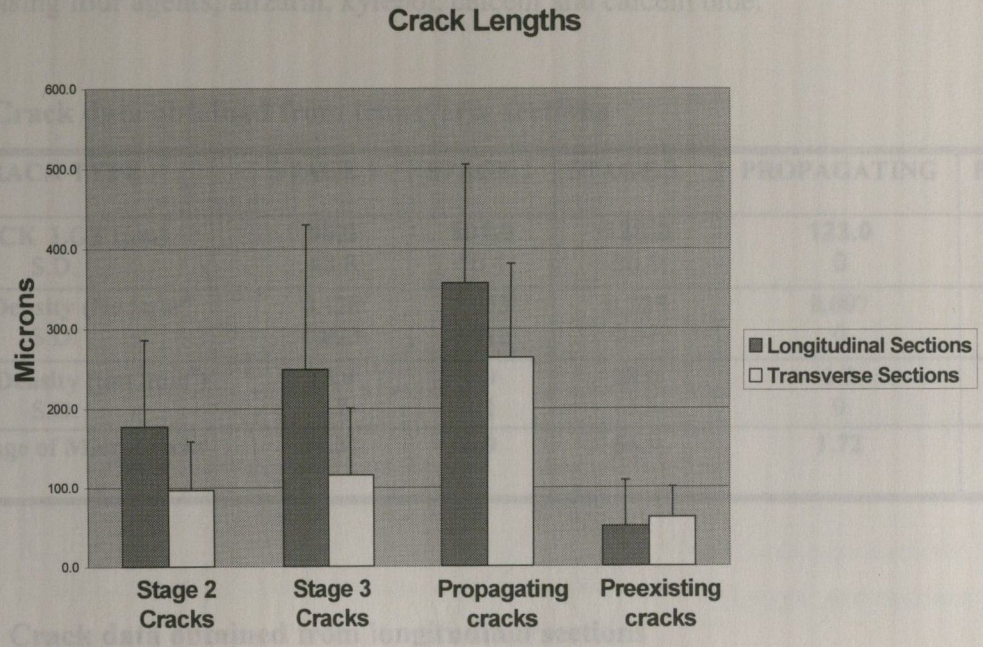

Fig. 4.14 Data obtained on microcrack lengths

Microcracks were longer in the longitudinal than in the transverse direction ($t=3.4$, $t_{0.05}=2.36$, $p<0.05$). Pre-existing microcracks were short in comparison to the other types and in general were found close to the surface of the specimen. Microcracks formed during the latter part of the test were longer than those formed during the first 50,000 cycles, with a ratio=1.2:1 in transverse sections ($t=2.66$, $t_{0.05}=1.98$, $p<0.05$) and ratio= 1.4: 1 in longitudinal sections, ($t=4.71$, $t_{0.05}=1.98$, $p<0.05$). Propagating microcracks were longer than either stage 2 or stage 3 microcracks(transverse: $t=6.74$, $t_{0.05}=1.98$, $p<0.05$; longitudinal: $t=3.99$, $t_{0.05}=1.98$, $p<0.05$). No cracks were found which had been

labelled with all three agents, and no cracks were found which had been labelled with the same agent twice, i.e labelled in different regions of a single microcrack with the same chelating agent.

4.3.4 Four agent tests

Table 4.9 and Table 4.10 show the crack data obtained from the three tests that were carried out using four agents, alizarin, xylenol, calcein and calcein blue.

Table 4.9 Crack data obtained from transverse sections

CRACK TYPE	STAGE 1	STAGE 2	STAGE 3	PROPAGATING	PREEXIST
CRACK LGT (μm) S.D.	**99.0** 43.8	**101.0** 16.1	**128.0** 60.9	**123.0** 0	**83.3** 23.0
Num. Density (No./mm$^{2)}$ S.D.	**0.128** 0.023	**0.033** 0.012	**0.225** 0.07	**0.007** 0	**0.023** 0.005
Surface Density (μm /mm^2) S.D.	**13.0** 3.7	**4.9** 1.1	**28.0** 13.3	**1.3** 0	**1.9** 1.7
Percentage of Microcracks	**29.31**	**6.9**	**56.9**	**1.72**	**5.17**

Table 4.10 Crack data obtained from longitudinal sections

CRACK TYPE	STAGE 1	STAGE 2	STAGE 3	PROPAGATING	PREEXIST
CRACK LGT (μm) S.D.	**272.8** 67.2	**242.0** 65.8	**264.8** 165.8	**243.0** 77.8	**56.0** 0
Num. Density (No./mm$^{2)}$ S.D.	**0.109** 0.032	**0.043** 0.013	**0.184** 0.115	**0.021** 0.031	**0.010** 0
Surface Density (μm /mm^2) S.D.	**27.6** 7.7	**6.9** 1.7	**46.2** 14.2	**1.8** 3.1	**0.5** 0
Percentage of Microcracks	**30.24**	**12.25**	**48.97**	**6.12**	**2.42**

When the numerical density data are compared to the equivalent data from the three agent tests, the results are found to be comparable and differences are not statistically significant, (transverse data: $t=0.6$, $t_{0.05}=2.2$, $p>0.05$; longitudinal data: $t=1.62$, $t_{0.05}=2.2$, $p>0.05$).

A similar trend was found for the surface densities of both the three agent and four agent test where again the differences were not statistically significant, (transverse data: $t=1.6$, $t_{0.05}=2.2$, $p>0.05$; longitudinal data: $t=0.73$, $t_{0.05}=2.2$, $p>0.05$).

As the differences in values were statistically insignificant, the data from the four agent test was added to the data from the three agent tests to show, how microcracks accumulated with increasing cycles. Fig. 4.15 and Fig. 4.16 show the numerical crack densities and surface crack densities plotted as a function of time. Failure is defined as the mean N_f from all the tests (90,000 cycles).

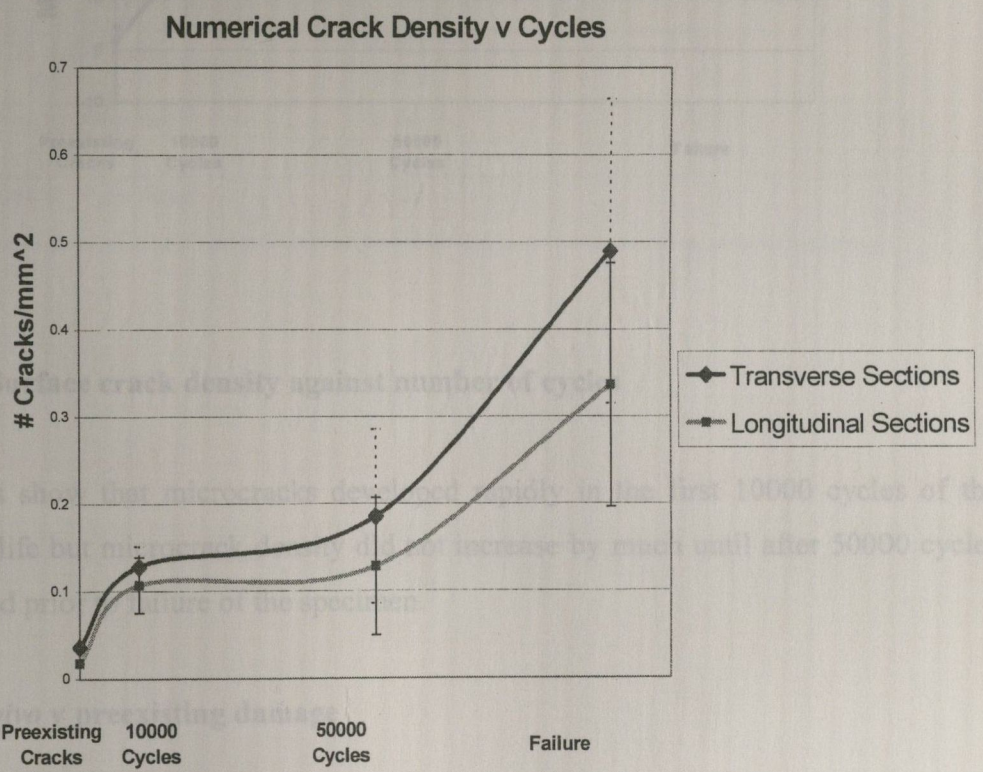

Fig. 4.15 Numerical crack densities against number of cycles

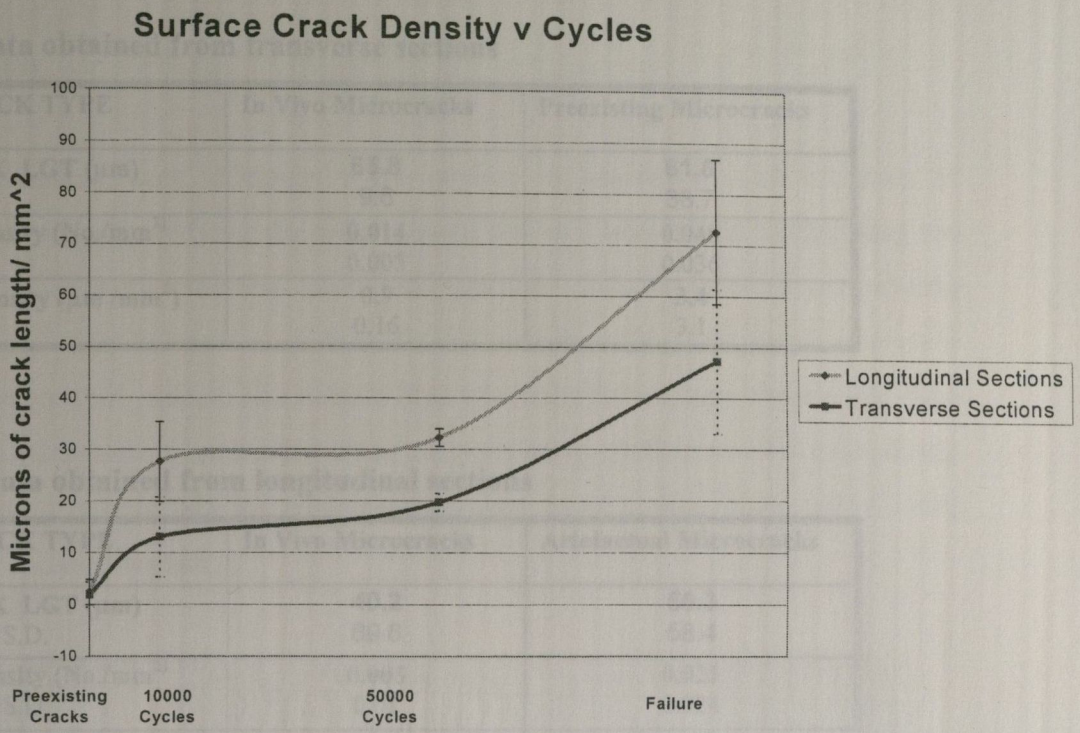

Fig. 4.16 Surface crack density against number of cycles

These plots show that microcracks developed rapidly in the first 10000 cycles of the specimens life but microcrack density did not increase by much until after 50000 cycles in the period prior to failure of the specimen.

4.3.5 *In vivo* v preexisting damage

Table 4.11 and Table 4.12 show the data obtained from the *in vivo* control studies compared to preexisting damage (*in vivo* and artefactual). Analysis showed that there was a significant difference between the greater number of artefactual microcracks than *in vivo* microcracks found (transverse data: $t=2.2$, $t_{0.05}=2.1$, $p<0.05$; longitudinal data: $t=2.1$, $t_{0.05}=2.1$, $p<0.05$).

Table 4.11 Data obtained from transverse sections

CRACK TYPE	In Vivo Microcracks	Preexisting Microcracks
CRACK LGT (μm)	**65.8** 9.6	**61.6** 38.7
Num. Density (No./mm$^{2)}$	**0.014** 0.005	**0.040** 0.036
Surface Density (μm /mm^2)	**0.9** 0.16	**3.4** 3.1

Table 4.12 Data obtained from longitudinal sections

CRACK TYPE	In Vivo Microcracks	Artefactual Microcracks
CRACK LGT (μm) S.D.	**40.2** 69.6	**50.3** 58.4
Num. Density (No./mm$^{2)}$ S.D.	**0.005** 0.01	**0.021** 0.024
Surface Density (μm /mm^2)	**1.22** 2.1	**1.4** 1.6

4.4 Discussion

The chelating agents were effective when applied in sequence. No evidence of substitution was found, verifying the work carried out in Chapter 3 in determining the optimal dye sequence for labelling microcrack growth. Alizarin labelled pre-existing microcracks and, while in some cases they did not penetrate the bone matrix extremely well, in general xylenol, calcein and calcein blue labelled microdamage clearly and were clearly distinguishable from each other when analysed using epifluorescence microscopy. Fig. 4.17 shows a calcein labelled microcrack located in interstitial bone viewed using UV and green epifluorescence.

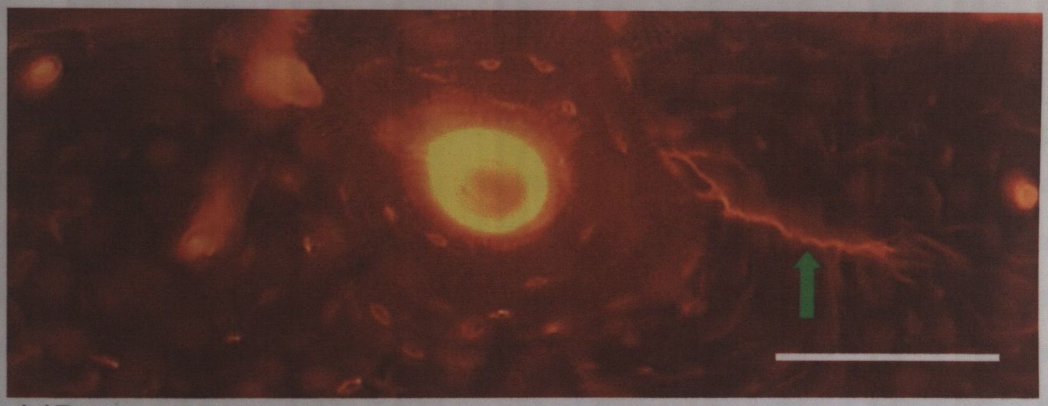

Fig. 4.17a

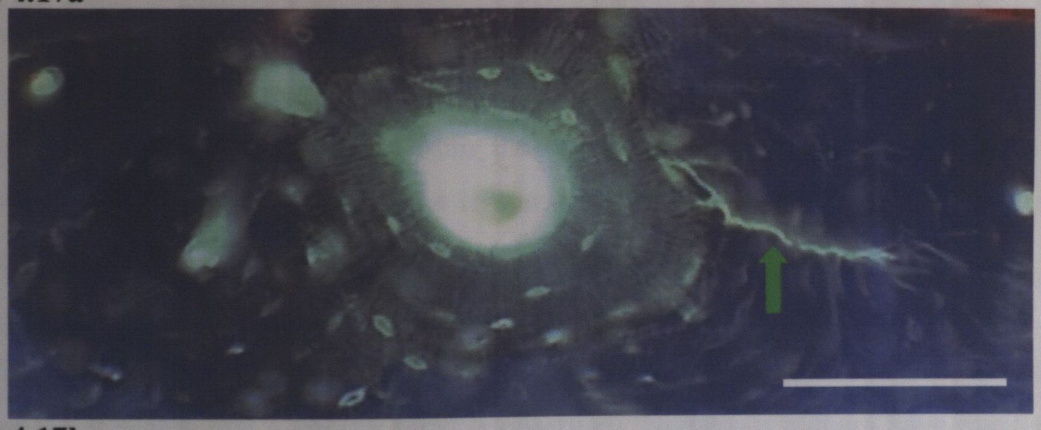

Fig. 4.17b

Fig. 4.17 Calcein labelled microcrack viewed using (a) green epifluorescence (b) UV epifluorescence. This microcrack is located in interstitial bone but part of it is found on the perimeter of a cement line surrounding a Haversian system. Bar= 100 µm.

4.4.1 Microcrack accumulation during fatigue tests

From analysis of both sets of sections in the three stain tests, it was evident that there was a greater proportion of microcracks found in transverse sections. The numerical crack density (Cr.Dn) was 0.75 ± 0.53 cracks/mm^2 for transverse sections compared to Cr.Dn.= 0.37 ± 0.26 cracks/mm^2 for longitudinal sections. This was as expected: microcracks were predicted to be longer in longitudinal than in the transverse direction so any transverse cut through a section would be more likely to cut through a microcrack than a longitudinal cut.

Only 6 % of microcracks were found to exist prior to testing and only one of a total of 54 preexisting microcracks was found to propagate during testing, suggesting that *in vivo* or artefactual microcracks did not affect the fatigue behaviour of these specimens.

In the three agent tests, a greater proportion of microcracks were found in the stage at failure than in the first 50,000 cycles. For transverse sections, the ratio was 1.9: 1 while for longitudinal sections this rose to 2.3: 1. However when an extra agent is included (four agent tests) and a reading of cracks accumulated by 10,000 cycles is taken, new observations were made. These data indicate that the microcracks formed during this set of tests initiate early during the specimens life (first 10,000 cycles) but then accumulation of more cracks is suppressed with only a slight increase occurring between 10,000 and 50,000 cycles before microcracks rapidly accumulate after 50,000 cycles eventually resulting in failure. The results from the three stain tests and four stain tests are comparable ($p>0.05$). Fig. 4.15 and 4.16 show the microcrack densities as a function of time for all the tests carried out illustrating this trend.

If Fig. 4.15 is compared to Fig. 4.1 which shows the process of failure in composite materials, it seems that a similar trend is observed. Numerous authors have mentioned the possibility of a microstructural barrier concept existing in bone (Taylor and Prendergast, 1997; Taylor, 1998; Akkus and Rimnac, 2000) with the bones microstructure allowing microcracks to initiate rapidly but because of the morphology of

osteonal bone, microcracks encounter barriers such as cement lines which suppress further growth. Fig 4.13 adds further evidence to back up this theory. 94 % of microcracks (n=144) formed during the first 50,000 cycles of tests were located in interstitial bone indicating the difficulty of microcrack growth through osteons (Fig. 4.17). In microcracks formed between 50,000 cycles and failure, this figure drops with 25% of microcracks (n=285) being found in osteons. This suggests that later in a specimen's life, there is a greater the possibility for a microcrack to break through a cement line surrounding a secondary osteon.

4.4.2 Analysis of propagating microcracks

Table 4.13 shows a comparison of lengths for microcracks formed during the first 50,000 cycles of testing (Stage 2), and those found to be propagating, i.e. those which were labelled with agents from stage 2 and stage 3. Fig. 4.18 shows an example of a propagating microcrack viewed at two different light levels to maximise the fluorescence of each of the agents.

Table 4.13 Crack Data

3 Stain Tests	Stage 2	Propagating Cracks
Longitudinal Lgt. (Mean ± S.D.)	177 ± 108 μm	357 ± 148 μm
Transverse Lgt. (Mean ± S.D.)	96 ± 62 μm	264 ± 117 μm
Ratio	2.5: 1	2.5: 1

Longitudinal lengths were found to be similar to those recorded by Burr and Martin (1993), mean length= 296 ± 257 μm. Transverse lengths and densities were also similar in length to those found in other studies, (Schaffler et al, 1989; Burr and Stafford, 1990; Lee et al, 1998). From the data obtained, it is evident that microcracks were longer in the longitudinal direction than in the transverse direction. This is not surprising and occurs commonly in composite materials when crack growth is relatively easy in one direction and difficult in the orthogonal one, due to either the type of loading or the anisotropy of

the material. It is also consistent with the prediction by Taylor and Lee (1998) who used the methods of stereology to estimate three dimensional sizes and shapes using data from two dimensional sections in the transverse and longitudinal planes.

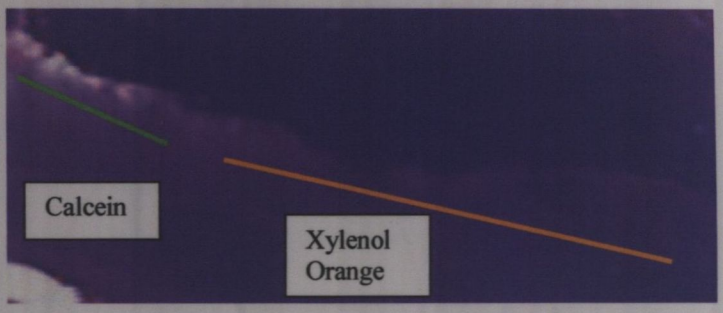

Fig. 4.18a

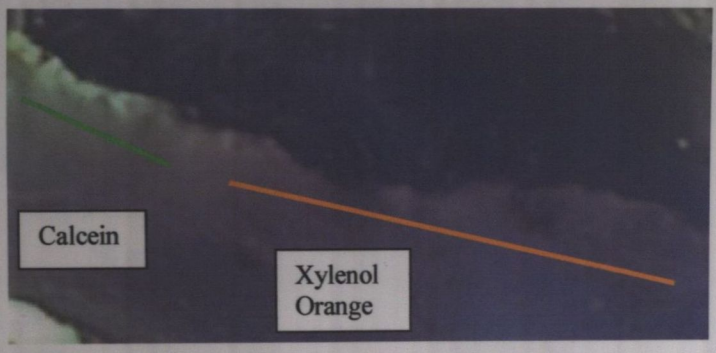

Fig. 4.18b

Fig. 4.18 Propagating microcrack stained with xylenol orange and calcein viewed (a) at high red levels in order to show xylenol stained part more clearly (b) at high green levels to show calcein stained part more effectively.

Fig. 4.19 shows a schematic of these results showing how the microcracks get longer in both directions as the test progresses.

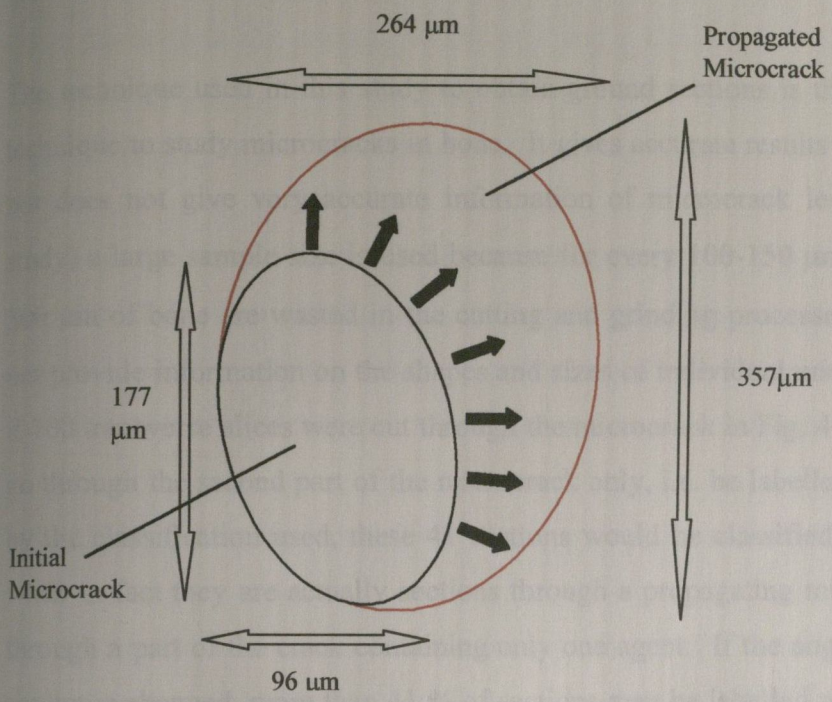

Fig. 4.19 Schematic of microcrack growth in 2 dimensions from mean data for both stage 2 and propagating microcracks

No cracks were found labelled with three agents, and no cracks had been labelled with the same agent twice, i.e labelled in different regions of single microcrack with the same chelating agent. Fig. 4.19 portrays this using the data from Table 4.13 and attempts to show how an individual microcrack may develop as the test progresses. This shows a microcrack propagating in only one direction in both the transverse plane (i.e "eastwards") and in one direction longitudinally (i.e "northwards") to reflect our observations. The microcrack grows more quickly in the longitudinal direction than in the transverse direction on average. This one-sided growth can be explained as follows. If the microcrack shown above were lying between two adjacent osteons, when it eventually developed enough energy to propagate, it would most likely break through the

cement line of whichever osteon was weakest and continue to grow in that direction preferentially. This shows that the reason that higher microcracks densities were found in transverse sections than in longitudinal sections is that there is a better chance of cutting through a microcrack in a transverse section than in a longitudinal section due to the difference in crack length in each direction.

The technique used in this study to obtain ground sections is the most commonly used technique to study microcracks in bone. It gives accurate results of microcrack densities, but does not give very accurate information of microcrack lengths unless (as in this study) a large sample size is used because for every 100-150 μm section obtained, 200-300 μm of bone are wasted in the cutting and grinding processes. Furthermore, it does not provide information on the shapes and sizes of individual microcracks. For example, if 100 transverse slices were cut through the microcrack in Fig. 4.17, 41% of them would go through the second part of the microcrack only, i.e. be labelled only with calcein. So by the classification used, these 41 sections would be classified as stage 3 microcracks when in fact they are actually sections through a propagating microcrack but have gone through a part of the crack containing only one agent. If the angle at which the sections are cut is changed, more than 41 % of sections may be labelled with only one agent. So, although only 8 % of all microcracks were shown to propagate in this study (i.e. labelled with xylenol and calcein) it would be expected that this would be an under estimate of the actual number of propagating microcracks and an overestimate of the number of microcracks which we have classified as stage 3 microcracks that are in actual fact propagating microcracks.

This indicates that to develop a more accurate quantification of micocrack development at different stages during testing, it may be worthwhile to use a geometrical or mathematical analysis to correct the figures obtained so as to assign a more accurate number of microcracks to the correct stage in which they were formed.

A complete analysis of this kind is beyond the scope of this thesis. However it can be seen that by using the conversion factors above, where 41 % of microcracks were misclassified, that the major changes would be:

(1) An increase in the number of propagating microcracks from 8% to about 15%.

(2) A decrease in the number of stage 3 cracks to about 53%.

(3) A decrease in the average length of a stage 3 microcrack, because the propagating cracks would tend to be the longest ones. This change may be enough to remove the difference in lengths between stage 2 and stage 3 as seen in Fig. 4.14.

Alternatively, by obtaining more information about the behaviour of individual microcracks i.e. their shapes, sizes and growth behaviour, it may also be possible to more accurately quantify microcracks. To attempt this, different histological techniques from the standard would be required, two such methods are developed in Chapter 5.

4.4.3 Preexisting microcracks

For the analysis of microcrack behaviour, this study classified all microcracks that existed prior to testing as "pre-existing". This term fails to differentiate between *in vivo* microcracks, which had been formed during the cow's life and artefactual cracks which had been introduced during the machining process. From the control study carried out it was found that only 29.5% of all preexisting cracks were *in vivo* cracks. This is unsurprising as the bone was taken from young cattle (2-3 years old). However, this also shows that only 4% of all microcracks found were formed by the machining process. This validates the specimen manufacture and test technique used it, as has often been suggested that the use of a CNC lathe in specimen manufacture leads to large amounts of artefactual damage and so results obtained using specimens that have been machined in this way are not always accurate.

4.5 Conclusions

(1) The chelating agents when applied in the determined sequence were found to effectively label microcracks formed at different stages during testing.

(2) Transverse sections were shown to have higher microcrack densities than longitudinal sections but this would be expected to be an artifact due to crack shape.

(3) Microcracks were found to accumulate early on in the specimens life but the rate of accumulation then slowed down until an increased rate of accumulation in the period prior to failure.

(4) Some microcracks were labelled with two agents which showed that they were propagating. The actual number of propagating microcracks is probably greater owing to the sectioning technique used; underestimate is 15% of all cracks.

(5) Bone microstructure influenced microcrack development with the vast majority of microcracks being found in interstitial bone between secondary osteons. Most microcracks (about 85%) initiated but ceased to grow at transverse lengths above 100 μm which is similar to the osteon spacing assumed by Taylor (1998a).

(6) Microcracks were shown to be 2-3 times longer in the longitudinal direction than in the transverse direction and were found to primarily grow in length parallel to the longitudinal axis of the bone.

Chapter 5

MICROCRACKS IN THREE DIMENSIONS

5.1 Introduction

Microcrack accumulation contributes to the formation of stress fractures (McBryde, 1975) and acts as a stimulus for bone remodelling (Burr and Martin, 1993; Prendergast and Taylor, 1994; Lee and Taylor, 1999a; Lee et al, 1999b; Martin, 2000). Microdamage has also been shown to accumulate with age in the femoral shaft and neck (Schaffler et al, 1989; 1995) and this contributes to fragility fractures (Sherman and Hadley, 1993).

Despite the obvious importance of microdamage in bone, the process by which microcracks initiate, propagate and ultimately coalesce leading to failure remains poorly understood. Microcracks are routinely stained with basic fuchsin in alcohol and criteria applied to exclude artefacts (Burr and Stafford, 1990; Lee at al, 1998). Electron microscopy has shown these fuchsin-stained features to be true microcracks (Burr et al, 1995). Microcracks in bone are normally analysed using two-dimensional transverse sections of bone (Frost, 1960; Burr and Stafford, 1990; Lee et al, 1998), but this technique fails to provide detailed information on the three dimensional shape and size of these microcracks. Knowledge of the true crack dimensions and variance in size are required for calculation of stress intensity values which indicate the probability of an individual microcrack propagating to cause a stress or fragility fracture (Taylor and Lee, 1998).

5.1.1 The true shape of microcracks

The initiation of microcracks in compact bone occurs without difficulty because microcracks tend to initiate in weak regions in the bone matrix. As the crack continues to grow, it encounters barriers i.e. cement lines within the microstructure which cause growth to slow and in some cases, stop completely. If growth continues, the crack

eventually becomes large (macrocrack) and its growth rate is determined by the average resistance of the material. Therefore a plot of fatigue crack growth rate (d*a*/dN, in mm/cycle) as a function of crack length (a), will show a minimum point at $a = d$: where d is the spacing of microstructural barriers (Fig. 5.1), a value of d=100μm is typical for compact bone Taylor, 1997).

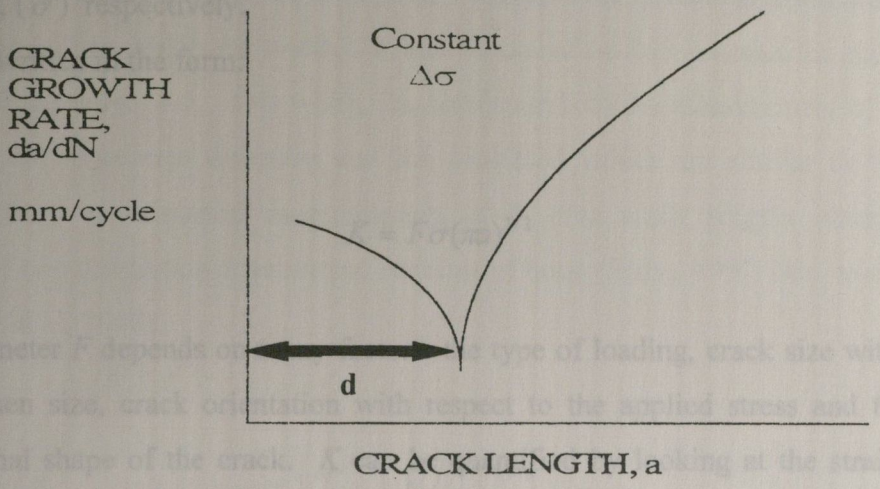

Fig. 5.1 Typical variation of fatigue crack growth rate with crack length for constant stress range. The crack growth rate is initially high because the crack initiates in a weak region in the microstructure and slows down as it encounters barriers such as grain boundaries or lamellar boundaries (Taylor, 1997).

Taylor and Prendergast (1995, 1997) proposed an equation which describes crack growth rate as a function of applied loading and crack length (Eqn. 5.1). Crack growth in bone occurs in two distinct regimes of behaviour: short crack growth which is dominated by local microstructural features and shows a decreasing rate of growth (da/dN) with increasing length and long crack growth in which crack growth rate increases with length, at a rate determined by the cyclic stress intensity range (ΔK) which is a function of applied stress range, crack length, shape and orientation.

Equation 5.1

$$\frac{da}{dN} = \left[C(\Delta K - \Delta K_{th})^n\right] + \left[C'(\Delta K)^{n'}\left[\frac{(d-a)}{d}\right]^m\right]$$

The first term gives a value of da/dN for long crack growth (a >> d) where C and n are two material constants and (ΔK_{th}) is a threshold value below which crack growth ceases. The second term gives a value of da/dN for short term crack growth where C', n' and m are material constants which govern short-crack growth and barrier resistance. In the study of fatigue crack growth, considering cycling loading where the minimum stress is zero, ΔK and the stress range, $\Delta\sigma$ are equal to the maximum stress intensity(K) and stress, (σ) respectively.

K can be written in the form:

Eq. 5.2

$$K = F\sigma(\pi a)^{1/2}$$

The parameter F depends on many factors: the type of loading, crack size with respect to specimen size, crack orientation with respect to the applied stress and the three-dimensional shape of the crack. K can be quantified by looking at the strain energy release rate (G) as a crack grows with relation to the decrease in elastic modulus (E) using the following relationship (Taylor, 1998):

Eq. 5.3

$$K = (GE)^{1/2}$$

However, this only gives an approximation for K due to the difficulty in measuring G accurately. In order to calculate F and thus K accurately, a knowledge of crack orientation and shape are required. Two dimensional crack measurements provide limited data because any random two dimensional section, tends to only cut through a section of a particular microcrack and is likely to give an underestimate of the true crack length. Therefore, accurate information of the true crack dimensions and variance in size in bone could allow for the calculation of stress intensity values which would potentially indicate the probability of an individual microcrack propagating to cause a stress or fragility fracture

5.1.2 Prediction of microcrack shape and size

Taylor and Lee (1998) used the methods of stereology to estimate three dimensional sizes and shapes using data from two dimensional sections in the transverse and longitudinal planes. They analysed experimental work which had been carried out by various authors which had measured crack lengths. Using the information, ten thousand crack-length measurements were simulated. The analysis predicted an elliptical crack shape (Fig. 5.2) in which the width, $2a$, had values of 66-113 μm and the shape factor b/a was of the order 4-5. This width, 2a, corresponds to the measurement of the crack length in the transverse direction and the predicted values are similar to the values obtained from experimental measurements of *in vivo* crack lengths obtained from analysis of two dimensional transverse sections of bone (Frost, 1960; Burr and Stafford, 1990; Lee at al, 1998).

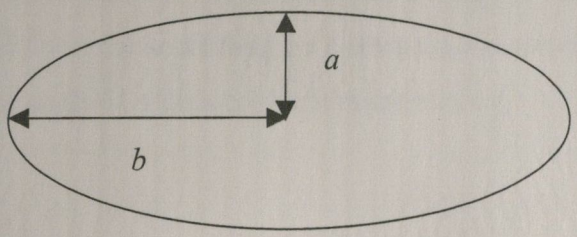

Fig. 5.2 Elliptical crack shape

The concept of an elliptical crack is common in materials science and has been shown to occur in a wide range of materials. The phenomenon occurs when crack growth is relatively easy in one direction and difficult in the orthogonal one, due to either the type of loading or the anisotropy of the material (Taylor and Lee, 1998).

5.1.3 Objectives

(1) To obtain more data on microcracks in the longitudinal, rather than transverse direction. Only one other previous study was found which looked at longitudinal crack lengths (Burr and Martin, 1993).

(2) To look at the three-dimensional nature of individual microcracks in compact bone. It was proposed to use two different methods to obtain three dimensional reconstructions of microcracks. This would allow a comparison between both techniques which determine the autenticity of the reconstructions obtained.

(3) By measuring the three dimensional shape and size of individual microcracks, to test the validity of the predicted shape and size obtained from analysis of random two dimensional sections.

5.2 Materials and methods

5.2.1 Preparation of samples

The rib is continuously cyclically loaded during life and this leads to the formation of significant amounts of microdamage. The use of human rib sections in this study allowed comparison with previous research, including the one other study found in the literature on the behaviour of microcracks in the longitudinal direction (Burr and Martin, 1993).

The left ninth rib was excised from nine embalmed cadavers. The subjects ranged in age from 69-92 years (mean 82.11, S.D. 6.56); four were male and five were female. No evidence of trauma or metastatic disease was found in the chest walls or ribs. Using a diamond saw (Struers Minitom, Copenhagen, Denmark), one 0.5 cm block and one 1 cm block were cut from each rib, commencing 1cm distal to the tubercle. The first set of blocks were used for serial sectioning on a sledge macrotome while the second set of blocks were used for analysis with a confocal microscope.

5.2.2 Staining

One per cent solutions of basic fuchsin were prepared in 80%, 90% and 100% ethanol. The blocks of rib were stained in basic fuchsin using the following procedure (Burr and Hooser, 1995; Lee et al, 1998). After rinsing under running tap-water to remove the fatty marrow, specimens were fixed overnight in 70% ethanol and bulk stained in 4ml of the following solutions in individual vials and placed in a desiccator (50 mm Hg) vacuum:

(1) 1% basic fuchsin in 80% ethanol (ETOH) for 2 hours;

(2) Change solution;

(3) 1% basic fuchsin in 80% ETOH for 2h;

(4) Repeat steps 1-3 with 1% basic fuchsin in 90% ETOH;

(5) Repeat steps 1-3 with 1% basic fuchsin in 100% ETOH;

(6) Rinse in 100% ETOH for 1hour to remove **excess** stain.

5.2.3 Preparation of blocks for serial sectioning

In order to obtain a three dimensional reconstruction of microcracks from serially sectioned slices of bone, a technique was required for the serial sectioning of compact bone. For serial sections to be suitable for this purpose, they must be thin (10-20μm) and of consistently high quality. In most pathology laboratories, the standard technique of obtaining serial sections of compact bone is by first decalcifying them and then sectioning on a standard microtome. However, in this study decalcification obviously cannot be used as it would dissolve the fuchsin staining the microcracks.

Mineralised bone can be cut with macrotome knives but it requires special support to avoid cracking or crumbling. Standard histological techniques such as soft embedding with paraffin wax or nitrocellulose are inadequate to prevent the mineralised tissue crumbling as it is being cut. Additional support or a harder, tougher embedding medium, which has similar material properties to the bone itself is required (Schenk et al, 1984). Methylmethacrylate (MMA) when used with the right amount of softener (to prevent the resin being too brittle) and a suitable catalyst has the required properties. To cut serial sections of calcified bone, they must first be embedded in the resin and then sectioned on a sledge macrotome before being mounted on glass slides.

5.2.4 Embedding of bone specimens in methylmethacrylate.

The following protocol was developed by carrying out 'trial and error' experiments in the laboratory. Before embedding, the bone specimens had to be dehydrated in separate glass vials to facilitate uniform polymerisation of the resin. Specimens were dehydrated using the following protocol:

80% ethanol solution- 4 days;
95% ethanol solution- 1 day;
100% ethanol solution- 1 day;
100% ethanol solution- 1 day;
Acetone- 2 days;

Following dehydration, the specimens were infiltrated with MMA (Merck-Schuchardt, Hohenbrunn, Germany) to allow the solution to fully penetrate the bone matrix prior to embedding. Initial tests showed that if bone specimens were insufficiently infiltrated, bone tended to separate from the resin during sectioning and poor quality sections were obtained. The solution used for the infiltration was the same as that for embedding. It consisted of 200 ml MMA monomer, 50 ml softener (dibutyl phthalate, Merck-Schuchardt, Hohenbrunn, Germany), that prevented the finished polymer being too brittle, and 50 g of the catalyst (benzoyl peroxide, BDH Laboratory Supplies, Poole, UK), which caused polymerisation when the temperature was increased. The rib sections were placed in glass vials containing the solution in a vacuum dessicator (50 mm Hg). They were infiltrated for 3 days with the solution changed daily. All glassware was clean and dry throughout the infiltration stage.

Infiltrated specimens were then completely immersed in MMA solution in a clean glass vial for embedding. The vial was placed to the vacuum dessicator for three hours (to ensure no bubbles had been trapped in the solution) before being heated in an oven at 55°C for three days. The embedding procedure was developed by varying the embedding times and temperatures to optimise the resin obtained. Too low a temperature yielded a soft resin while, if the temperature was too high, the solution began to boil and generated large numbers of bubbles.

5.2.5 Sectioning of specimens using a sledge macrotome

The sledge macrotome (LKB 2260, Germany) (Fig. 5.3) is an automatic heavy-duty sledge macrotome which, because of its stability, is suitable for the sectioning of hard tissue. It consists of a main cutting unit with a D-profile steel knife. The knife is mounted on vertical supporting pillars above the specimen sledge which is motor driven in the horizontal plane. A stepping motor feeds the knife downwards to the specimen before each cutting stroke and provides an automatic 60 μm retraction during the return stroke to protect the specimen.

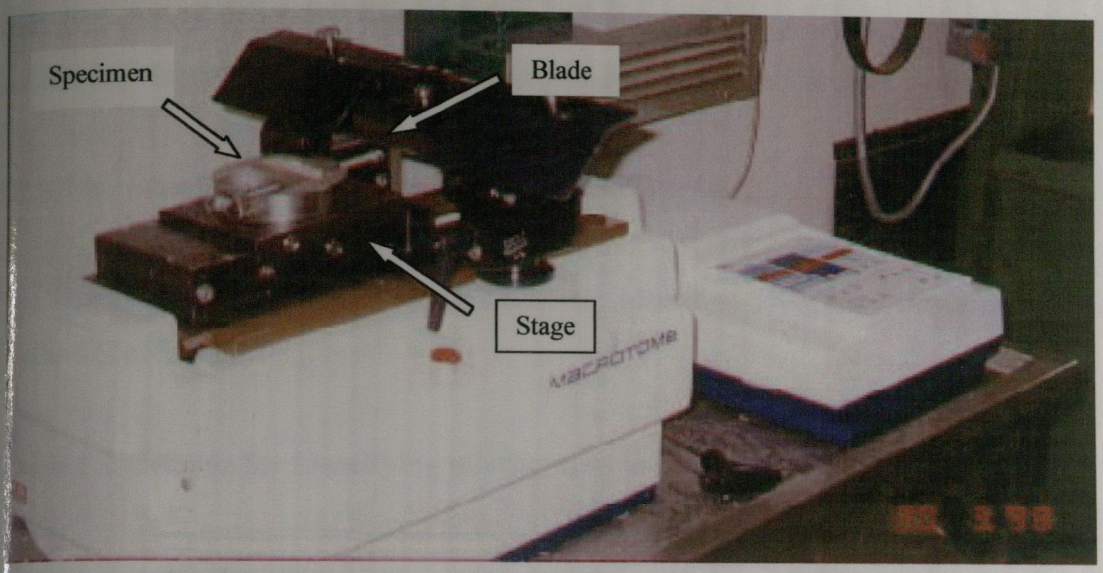

Fig. 5.3 Sledge macrotome

Variables such as cutting speed, sectioning angle and section thickness have a large bearing on the quality of sections obtained. From tests carried out, the optimum settings for these parameters were determined to be:

Cutting speed: 1-2 mm/s

Depth of cut: 7-15 μm

Clearance angle: 9-10°

Bone is an anisotropic material so its mechanical properties depend on the direction of applied loading. Long bones, such as the tibia, are stronger and stiffer in the longitudinal direction, rather than across the bones axis. Consequently it might be expected that it would be easier to section specimens along the longitudinal axis rather than across the grain. When it was attempted to cut the specimens in the transverse plane, the bone tended to fragment and it was difficult to obtain good quality sections. Indeed in some cases, it was noted that sectioning in the transverse plane damaged to the surface of the macrotome knife. Therefore, sectioning on the macrotome was carried out along the longitudinal axis.

The embedded blocks were mounted on the sledge macrotome and 10 μm serial sections of bone were cut through a depth of 250 μm (i.e. 25 sections). Specimens were removed from the blade using forceps and a soft artists brush. The sections were soaked in 90% ethanol which allowed the polymer surrounding the bone to soften and any folds

or creases were unfurled and flattened using the brush and forceps. The sections were then transferred to glass slides and mounted with DPX mounting medium (BDH Laboratory Supplies, Poole, UK) under a coverslip and allowed to dry.

5.2.6 Identification and reconstruction of microcracks

The slides were analysed and microcracks were identified using the fluorescence-aided method (Table 5.1).

Table 5.1 Criteria for identifying microcracks in bone (Lee et al, 1998)

Step 1: Fluorescence microscopy - green incident light (G – 2A filter block, λ=546 nm), x125 magnification: Candidate crack should be intermediate in size, being larger than canaliculi but smaller than vascular canals.
Step 2: Fluorescence microscopy - green incident light (G – 2A filter block, λ=546 nm), x125 magnification: Candidate crack should have a sharp border, with fluorescence of chelating agent within crack borders evident.
Step 3: Fluorescence microscopy - UV incident light (λ=365 nm), x125 magnification: Candidate crack should be stained through the depth of the section.
Step 4: Light microscopy, x250 magnification: When the depth of focus is changed, the edges of the crack can be observed to be more deeply stained than the intervening space.

Having confirmed the presense of an individual microcrack in a serial section and determined that it was not artefactual, the serial slices immediately preceding and following on from the section in question were examined for the presence of the same microcrack. This technique was repeated through the entire depth of the microcrack. Microcrack images were then transferred to a HP PIII Brio personal computer (Hewlett Packard, Grenoble, France) using a CCD colour video camera (Optronics Engineering, Goleta, Ca), reference points were noted on each slice by microcrack location in relation to the corners of the section being analysed and using *Surfdriver* ™ computer software (John. A Burns School of Medicine, University of Hawaii, Honolulu, Hawaii) the serial slices were reconstructed into three-dimensional images of each individual microcrack.

This software initially allowed for a 'skeletal' reconstruction of the microcrack with all the individual slices evident and then, a covering or skin was formed over the sections, so that the true shape of the crack was apparent. Measurements of crack lengths in both transverse and longitudinal directions were made from the reconstructed images using image analysis software (Scion Image™, Scion Corporation, Frederick, Maryland, USA).

5.2.7 Preparation of ground sections for LSCM analysis

The second set of blocks (1 cm) were rehydrated in distilled water for 24 hours after staining. It has been shown (Frost, 1960; Burr and Stafford, 1990) that immediate sectioning after staining in ethanol results in destruction of specimens. Blocks were then secured in a diamond saw (Struers Minitom, Copenhagen, Denmark), 250 μm longitudinal sections were cut and handground to between 100 and 150 μm and mounted using the following technique (Frost, 1958):

1. Specimen was placed in a small clamp and approximately 250μm was cut using a diamond saw (Struers Miniton, Copenhagen, Denmark).

2. A sheet of No. 400 silicon carbide paper was placed on a flat surface under running water and the section was placed upon it. Another piece of paper was wrapped around a glass slide and the section was manually ground down between the two pieces of paper in a circular fashion using light pressure.

3. This grinding was continued and periodically the thickness was checked using a micrometer screw until the required thickness (100-150μm) had been obtained

4. Specimens were agitated in 0.01% dish detergent in a beaker, placed in a Coors porcelain funnel with fixed perforated plate and washed in distilled water.

5. Specimens were then air dried and mounted using DPX mounting medium (BDH Laboratory Supplies, Poole, UK) and a coverslip.

Hand grinding was used to obtain sections of high quality which were a lot thicker than the macrotome cut sections. The advantage of this method is that it is simple, quick and

can be used to obtain transverse sections of compact bone which proved extremely difficult using the macrotome. This technique was developed by Frost (1958) and in this study was used initially as a control to test the quality of the sections obtained from the macrotome. The main drawback with the technique is that the sections are too thick to be of use as serial sections for 3D reconstruction purposes. The diamond saw blade is 250 μm in width and the minimum thickness of section that can be obtained is 200-250 μm thus 500 μm of bone was used to obtain one 150 μm thick section.

5.2.8 Examination of ground sections using LSCM

Laser scanning confocal microscopy (LSCM), which combines fluorescence microscopy, laser light illumination and computer imaging, was used to visualise microcracks. The Dept. of Anatomy in the Queen's University of Belfast, Northern Ireland made a Leica TCS/NT confocal microscope available for use in this study, with assistance provided by their technical staff.

This microscope was equipped with a krypton/argon laser as the source for the ion beam and was used to examine the sections for fluorescence of fuchsin-stained microcracks. The fuchsin-stained samples were imaged by excitation at 647 nm with a 664-696 nm long-pass emission filter. Individual microcracks were identified on the surface of each section. The laser was then focussed at different depths through the entire depth of the section generating a series of individual slices at 8μm intervals and a single microcrack was reconstructed into a 3-D image. The software allowed the reconstructed image to be rotated through 360° in order to show the crack shape. All the settings on the confocal microscope: objective lens used, wavelength of channels, readings on the photomultipler tubes, depth of Z-scan, strength of laser and format of acquistion were standardised and recorded for each data set acquisition. With the confocal microscope it is possible to reproduce settings from one experiment to another. While there was appropriate software in the system to maintain laser stability and strength through a depth of 200 μm, our observations were restricted to a maximum depth of 100-160 μm to avoid tissue attenuation of laser beam penetration and emission light.

The ground sections were then examined using epifluorescence microscopy (Table 5.1) and microcracks identified. The microcrack images were transferred to a HP PIII Brio personal computer (Hewlett Packard, Grenoble, France) using a CCD colour video camera (Optronics Engineering, Goleta, Ca) and the length of each microcrack was measured (Scion Image™, Scion Corporation, Frederick, Maryland, USA). Finally, the area of each section was determined by transferring the image of each section to the PC using a CCTV video camera (Panasonic, Japan) and measuring it using the same analysis software, having initially calibrated the software using a graticule containing a scale bar. The results were tabulated in the form of: (i) number of cracks occurring per section, (ii) crack numerical density (number of cracks occurring per mm^2) and (ii) mean longitudinal crack length (Lee et al, 2000b).

5.3 Results

5.3.1 Serial Sectioning Technique

The reconstructions obtained using the serial sectioning technique are shown below. Figure 5.4 shows a microcrack reconstructed from serial sections rotated through 0, 45 and 90 degrees. In each case, a 'skeletal' image shows the initial reconstruction with all the individual sections present while the 'covered' image shows the reconstructed crack when a 'skin' has been placed around the sections.

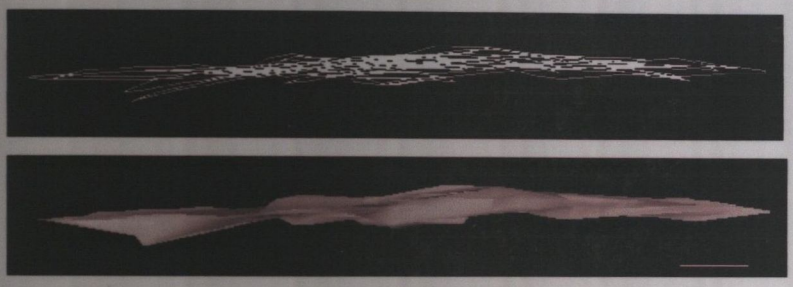

Fig. 5.4a 0 degrees

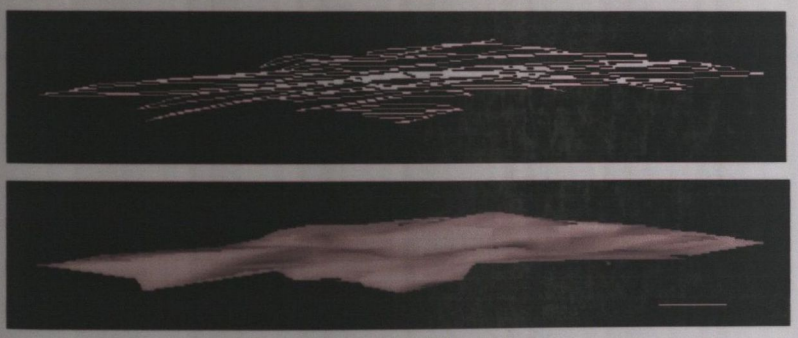

Fig. 5.4b 45 degrees

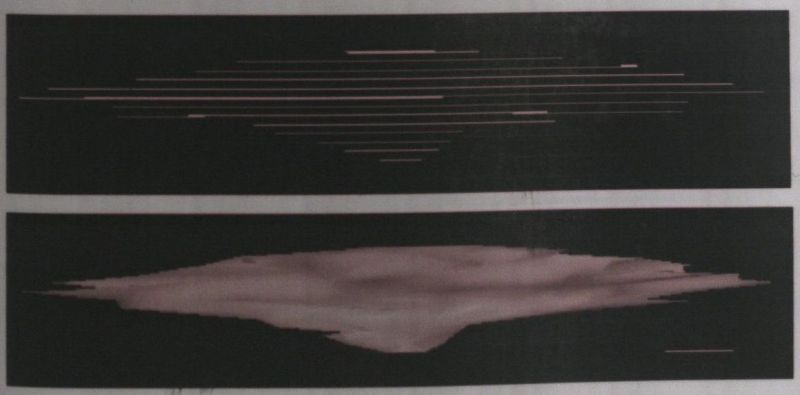

Fig. 5.4c 90 degrees

Fig. 5.4 Lateral view of a microcrack reconstructed from serial sections, in 'skeletal' and 'covered' forms, rotated through 0, 45 and 90 degrees. Bar, 50 µm.

Table 5.2 summarises the data obtained from the crack reconstructions obtained from serial sections. The average crack length in the longitudinal direction was 404 ± 145 μm [mean ± S.D.], the crack width or length in the transverse direction was 97 ± 37 μm and crack thickness was 9 ± 3 μm (n = 9). This resulted in a mean aspect ratio of longitudinal: transverse length of 4.6: 1 (S.D. 2.2).

Table 5.2 Data obtained from reconstructed serial sections on microcrack lengths in both transverse and longitudinal planes

Crack. No.	Longitudinal Lgt. (μm)	Transverse Lgt. (μm)	Ratio L:T	Thickness (μm)
1	559.29	79.37	7.0	8.93
2	553.03	82.71	6.7	5.05
3	241.95	55.55	4.4	5.36
4	543.17	96.28	5.6	9.62
5	206.19	75.49	2.7	7.14
6	337.74	180.96	1.9	11.29
7	252.91	120.0	2.1	13.95
8	481.84	110.56	4.4	13.16
9	459.15	69.02	6.7	7.14
Mean	**403.92**	**96.66**	**4.6**	**9.12**
S.D.	144.66	37.48	2.2	3.30

5.3.2 Confocal microscopy technique

Cracks were found to be sheet-like defects and were approximately elliptical in shape. A microcrack viewed using LSCM is shown in Figure 5.5. The fuchsin-stained cracks generally ran parallel to the longitudinal axis of the rib and were most commonly located in interstitial bone parallel to Haversian systems. Figure 5.6 shows the same microcrack viewed at different intervals through the section. Beginning with the initial slice (bottom right hand corner), and following the arrows, it can be seen that initially the crack was indistinct (white arrow) but progressing through the sections, it became clearer and clearer before becoming less distinct again indicating that the laser has gone through the entire width of the crack. A reconstruction of this dataset of images is shown in Figure 5.7, with the crack rotated in order to show the three-dimensional crack

shape. Another microcrack reconstructed from LSCM is shown in Figure 5.8.

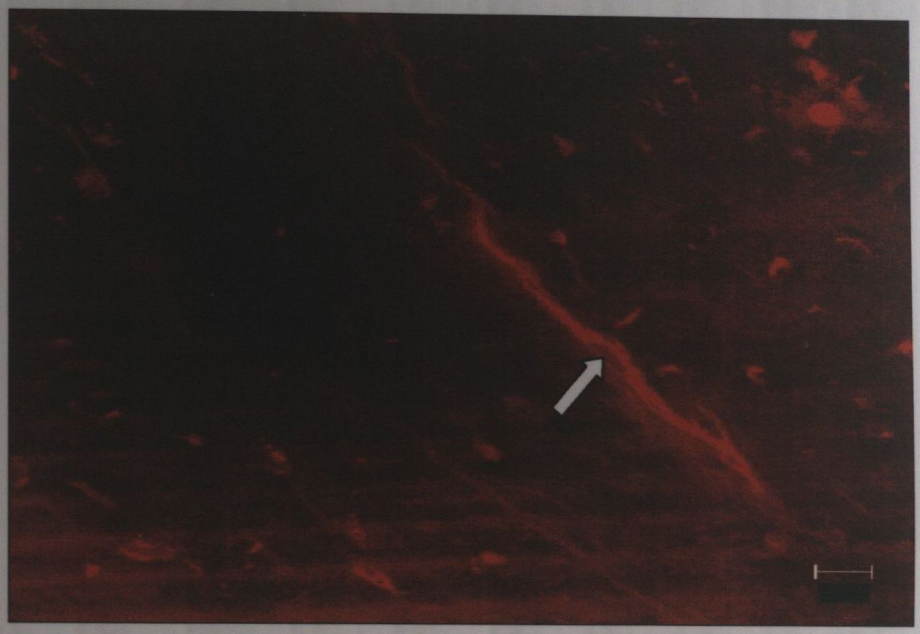

Fig. 5.5 Fuchsin-stained microcrack (white arrow) viewed using LSCM. Bar, 50μm.

Fig. 5.6 Dataset of images of microcrack (arrow) visualised in Fig. 5.5 at 8μm intervals through the section beginning at bottom right hand section (white arrow) and following black arrows through the depth of the section. Bar, 250μm.

Fig. 5.7 Reconstructed microcrack obtained from dataset of images (Fig. 5.6). The crack has been rotated to show its three-dimensional shape. Bar, 50μm.

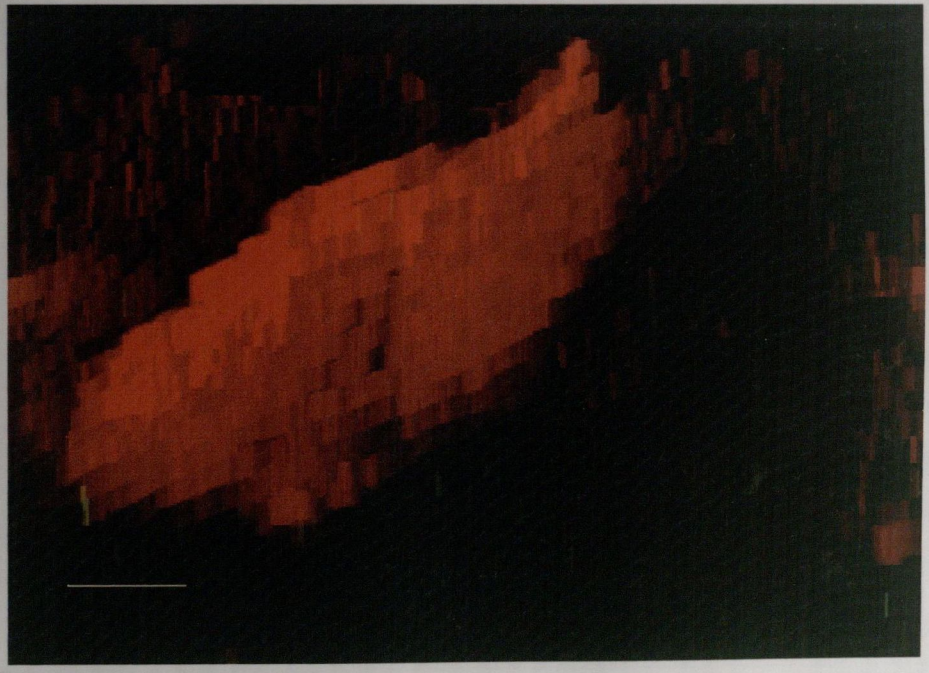

Fig. 5.8 A reconstructed microcrack obtained using a gallery of LSCM images. Bar, 100μm.

5.3.3 Data obtained using epifluorescence microscopy

Basic fuchsin was found to label microdamage clearly in all samples. Artefactual damage was differentiated from *in vivo* microdamage by the absence of dye in the candidate crack or failure to satisfy the required criteria (Table 5.1). Figure 5.9 shows an example of a microcrack viewed using: (a) green and (b) UV epifluorescence. Under green incident light, basic fuchsin fluoresced orange and under UV incident light, fluoresced purple.

Data obtained using the fluorescence-aided method are summarised in Table 5.3. A total of 92 cracks were identified. The mean number of cracks per section was 10.2 ± 6.9 [mean ± S.D.]. The mean crack density was 0.12 ± 0.10 cracks/ mm^2 and the mean longitudinal crack length was found to be 371 ± 211μm.

Table 5.3 Microcrack number, density (Cr.Dn.) and length (Cr.Le.) in longitudinal sections. This data was obtained from analysis of sections using epifluorescence microscopy.

Sample	No.	Cr.Dn. (no./mm^2)	Cr.Le. (μm)
1	8	0.073	483.50
2	11	0.091	436.02
3	8	0.077	401.46
4	24	0.295	391.14
5	8	0.069	245.86
6	3	0.385	358.79
7	4	0.045	285.39
8	19	0.293	324.17
9	7	0.097	176.81
Average	**10.22**	**0.12**	**370.75**
S.D.	6.92	0.10	211.01

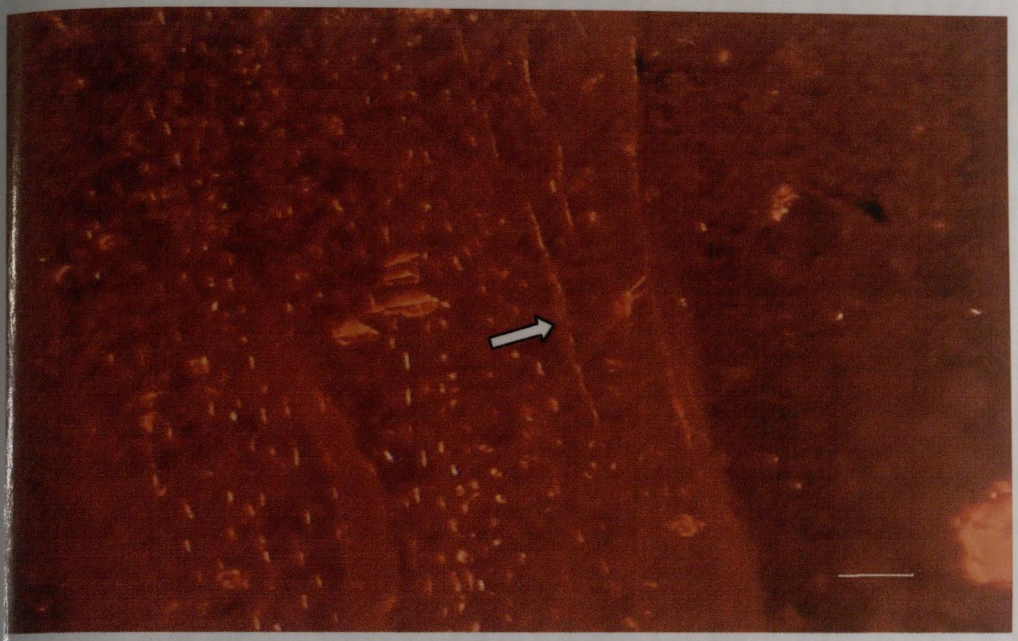

Fig. 5.9a

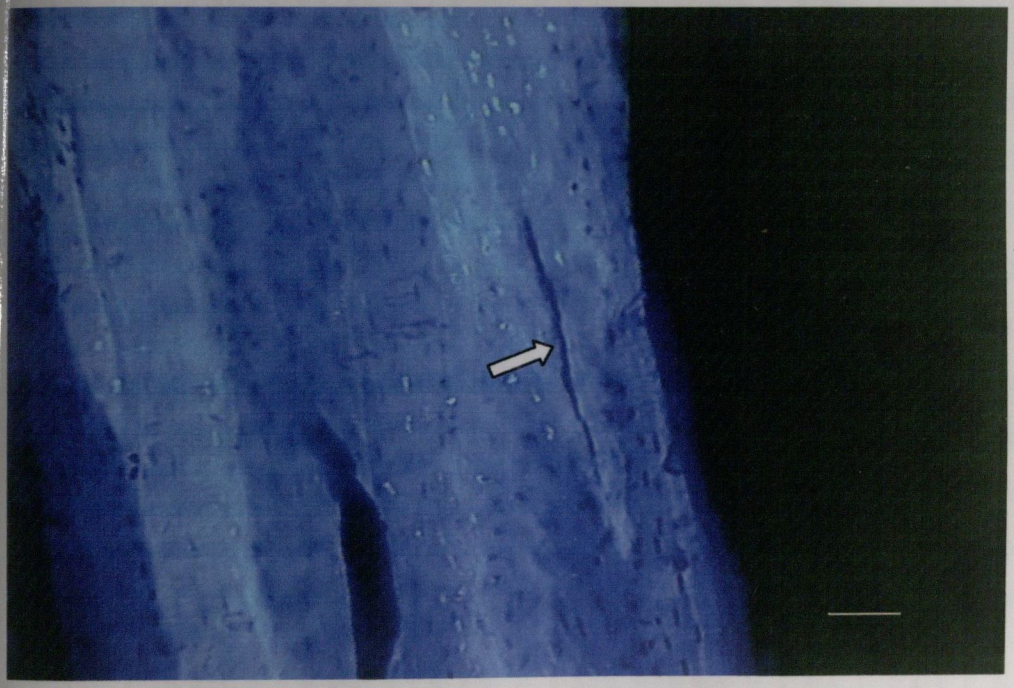

Fig. 5.9b

Fig. 5.9 Microcrack (arrow) viewed using (a) green (b) UV epifluorescence. Bar, 100µm.

5.4 Discussion

While LSCM has previously been used to study microdamage in trabecular bone (Fazzalari et al, 1998), the morphology of *in vitro* microcracks in fatigue-tested compact bone (Zioupos and Currey, 1994) and dense arrays of ultra-microcracks in human tibiae (Boyce et al, 1998), little data exist regarding *in vivo* longitudinal microcracks in compact bone.

Confocal microscopy combines fluorescence microscopy, laser light illumination and computer image processing. The advantage of this technique over conventional microscopy methods is that it shows a much improved spatial resolution, because the laser can be focussed with high precision onto the actual microcrack being examined and this allows elimination of the out-of-focus image from the image focal plane (Fazzalari et al, 1998). This property of the confocal microscope allowed the fuchsin-stained microcracks to be highlighted from the surrounding matrix.

Once a microcrack had been identified, a series of slices was made at intervals through the bulk sample and using computer processing, a complete three-dimensional image of the microcrack was created. While the laser strength and stability of the confocal microscope can be maintained through a depth of 200 μm, imaging of compact bone samples was limited to a maximum depth of 100-160 μm to avoid bone tissue attenuation of both the laser beam penetration and the emission light. No quantitative data were obtained on three-dimensional crack measurements from the confocal-reconstructive technique as it was only possible to measure part of the crack width because once a crack had been identified on the surface of a section, it was not possible to determine how much of the crack had been cut away during the sectioning process.

Both LSCM and serial sectioning showed similar results regarding the shape of microcracks in bone. They were found to be three-dimensional, sheet-like defects. This is consistent with the study by Fazzalari et al (1998). Using both reconstruction techniques, they were approximately elliptical in shape. This is consistent with crack shapes found in other materials (Miller and de los Rios, 1986) and arises when crack growth is relatively easy in one direction but difficult in the orthogonal one, due either

to the type of loading or the anisotropy of the material (Taylor and Lee, 1998). From the reconstructions (n = 9) obtained from the serial sectioning method where it was possible to measure the crack widths because the entire crack geometry was known (Table 5.3), the average crack length in the longitudinal direction (i.e. the major axis of the ellipse) was found to be 404 ± 145μm (mean ± S.D.) while the crack width, or length in the transverse direction was 97 ± 37μm (i.e. minor axis of the ellipse). This resulted in a mean aspect ratio of longitudinal: transverse length of 4.6. (S.D. 2.2). This was consistent with the theoretical prediction of an elliptical crack shape with axis ratio of 5:1 (Taylor and Lee, 1998) and the results are comparable with the observations by Burr and Martin (1993) which suggested that microcracks are 4-6 times longer in the longitudinal direction than in cross section.

The epifluorescence technique yielded a mean numerical crack density of 0.12 ± 0.10 cracks/ mm^2. This was similar in range to previous studies (Burr and Stafford, 1990; Lee at al, 1998). Microcracks were shown to average 371 ± 211 μm in length along the longitudinal axis (n = 92) which is consistent with the one previous study on longitudinal crack lengths (Burr and Martin, 1993) which found a longitudinal crack length of 296 ± 257μm. In general, microcracks ran parallel to the longitudinal axis of the rib and were most commonly located in interstitial bone parallel to Haversian systems. This again was consistent with previous work on location of *in vivo* microcracks in human tibiae (Boyce et al, 1998).

In transverse sections, the microcracks observed in this (Table 5.3) and other studies on human rib (Frost, 1960; Burr and Stafford, 1990; Lee et al, 1998; Lee et al, 2000) are similar to those found in the femoral neck and shaft (Schaffler et al, 1989, 1995) and to those seen in fatigue-tested bone (Fyhrie and Schaffler, 1994; Choi et al, 1994). By measuring the dimensions of microcracks in three dimensions, we have gained insight into the true sizes and shapes of microcracks in compact bone. This offers the possibility of calculating stress intensity values, which determine the risk of fracture occurring from a particular microcrack. The development of these techniques provides a potential tool for the prediction of fatigue fractures in bone.

5.5 Conclusions

The techniques used provide new data on the three dimensional shape of microcracks in compact bone:

(1) Serial sectioning of methylmethacrylate embedded rib sections and laser scanning confocal microscopy were found to show similar results regarding the shape of microcracks in bone.

(2) Microcracks were elliptical in shape with aspect ratio of longitudinal length: transverse width of 4.4:1. This was consistent with theoretical prediction of microcrack shape from a model developed from analysis of random two dimensional sections (Taylor and Lee, 1998). This model predicted an aspect ratio of 5:1.

(3) Basic fuchsin was found to clearly label microcracks in all samples. The data obtained on longitudinal crack lengths and densities were consistent with the study by Burr and Martin (1993). This was the one previous study found in the literature which analysed microcracks in longitudinal rather than in transverse sections.

Chapter 6

DISCUSSION

6.1 The fatigue behaviour of bone

The work carried out in Chapter 2 has led to the establishment of a repeatable, standardised technique whereby repeatable fatigue tests can be conducted which allows cyclic deflection to be monitored during the course of a fatigue test. The specimen geometry used was devised from a similar technique developed by Keaveny et al (1994a) which was used for testing trabecular bone. Specimens were cylindrical in cross section (Fig. 2.3) which minimised stress concentrations and the machining process was not found to introduce significant amounts of artefactual damage. The test rig designed (Fig. 2.4) was simple but effective. Parallel aluminium plates into which depressions had been machined to accommodate the specimens' end caps, helped to avoid errors in the axial alignment of the specimens and brass end caps were attached to the specimens before testing to facilitate loading without contact damage.

A number of specimens failed before the predicted reduction in stiffness had taken place. The failure pattern was similar in all specimens, with the main fracture crack occurring in the gauge length of the specimen at an approximate angle of 45^0 to the specimen axis further endorsing the design of the specimen. The average life for the specimens was 36000 cycles (S.D. 38000). Although there was variation in fatigue life over three orders of magnitude from specimen to specimen, this degree of scatter is similar to that found by other authors (Table 2.1). This suggests that the scatter is not due to inadequacies in the testing technique but is due to the bone material itself. Although the specimens tested were of exactly the same dimensions and all came from the mid diaphysis of bovine tibiae, other factors such as orientation of the bone lamellae, porosity, degree of mineralisation etc. could explain the large variation in fatigue life from specimen to specimen. This further indicated that more work needed to be carried out to look at the

process by which microcracks initiate and grow in compact bone and how the bones microstructure influences the ability of individual cracks to develop.

When the experimental data was compared to the theoretical model (Taylor, 1998a), the fatigue strength at a time to failure of 100,000 cycles, was found to be 91.84 MPa. This value compared favourably with the value of 95.61 MPa predicted for the fatigue life by Taylor's model (1998a). This model was devised from statistical analysis of previous data. The intention of the model was to show that data from various sources, tested in a variety of different ways can be linked and shown to tell a similar story (Taylor et al, 1999b) and from this certain predictions can be made. One of the weaknesses with the model is that it assumes that failure will always occur from the weakest point in the specimen and this may not always be the case. However, these initial experimental results appear to have validated the accuracy of the model as it appears to be able to predict the strength of bovine bone in compression by combining the effects of specimen size, temperature and loading frequency.

The chelating agents were found to label microcracks effectively when applied to the specimens during testing. This was the first study to use the agents to label microdamage in compact rather than trabecular bone. Histological examination showed that the agents worked effectively when applied individually but some problems began to emerge with the application of the agents in sequence. As had been shown previously (Lee, 1997; Lee et al, 2000a; O'Brien et al, 1998) substitution of certain agents took place when an apparently 'stronger' agent (having a greater affinity for calcium) was sequentially applied e.g. calcein blue followed by alizarin. This indicated once again the necessity for a chemical analysis to be carried out in order to determine the binding constants for each of the five chelating agents and so determine an optimal application sequence which would minimise substitution.

6.2 Refinement of detection technique

The most common method of microcrack detection in bone has been the use of transmitted light microscopy, either alone or using a penetrant dye in order to allow differentiation of microdamage from the surrounding bone matrix. Frost (1960) introduced the concept of bulk staining of bone in basic fuchsin to label microcracks and this agent remains the most commonly used. Burr and Stafford (1990) modified Frost's criteria (1960) for identifying microcracks. This process has been successfully use to detect microcracks both *in vitro* (Akhter et al, 1993) and *in vivo* (Mori and Burr, 1993; Lee, 1995).

Zioupos and Currey (1994) introduced the idea of using a fluorescent dye, or fluorochrome to label microcracks. Basic fuchsin also fluoresces under ultra violet light and Lee et al (1998) utilised the fluorescent properties of basic fuchsin, in addition to bulk-staining, to detect microdamage. This study improved the technique of crack detection using basic fuchsin by varying the magnification and light type when sections were examined under a fluorescent microscope.

Rahn (1977) developed a dosage regime and sequence of fluorochrome administration (Table 3.3) which allowed for a series of five fluorescent chelating agents to appear equally bright under the microscope in order to facilitate histological examination. This regime has been used in a number of previous *in vivo* studies in order to demonstrate bone remodelling under conditions of altered mechanical loading (Lanyon et al, 1982; Burr et al, 1989; Lee, 1995). Stover et al (1993) was the first author to use the fluorochromes to label microcracks. They showed that *in vivo* microdamage could be successfully labelled using calcein. Lee et al (2000a) was the first study to show that the chelating agents could be used to label *in vitro* microdamage. This work however, detected some problems with the use of chelating agents in monitoring crack propagation whereby different agents tended to substitute each other when applied in sequence and a further study (O'Brien et al,1998) showed similar problems.

The ion chromatography tests carried out in Chapter 3 emphasised the chelating agents ability to bind to exposed to calcium. In this laboratory situation, the amount of calcium in a calcium chloride solution was measured, and the amount of calcium left, after application of each chelating agent, was then measured using ion chromatography. This showed that alizarin (A) had the greatest affinity for calcium, followed by by xylenol orange (X), calcein blue (CB), calcein (C) and oxytetracycline (O). Confirmatory tests were carried out using bone in which scratches had been made to simulate the process of crack development by exposing fresh calcium on the bone surface. From these tests, it was found that C had a greater affinity for calcium than CB. On application of the agents in the reverse order, CB was found to slightly substitute C but when the concentration of CB was reduced from 0.0005M to 0.0001M substitution did not take place. Oxytetracycline was found to work well as an individual agent. However, when applied in sequence, it was substituted to some extent by each of the agents while paradoxically it also substituted all of the other agents with the exception of alizarin. For this reason it was decided to exclude the agent from sequential labelling of microcracks.

Rahn (1977) developed a dosage regime and sequence of fluorochrome administration *in vivo* (Table 3.3) which allowed for the five agents to appear equally bright under the microscope to facilitate histological examination. Lee et al (1997, 2000a) used 1% solutions of the five agents. The concentrations used in these tests were the lowest possible, so as to prevent bleeding of the agents into the bone matrix, which allowed all agents to fluoresce clearly while still allowing chromatograms to be obtained. Tests were carried out using the *in vivo* dosage regime (Rahn, 1977) but results were inferior to those obtained using concentrations established in this study. A and X were found to be difficult to differentiate from each other. Both agents appeared as a red/ orange colour and X may have been displaced A to a minor extent. Similarly, calcein blue was found to displace calcein making differentiation again difficult. This final analysis has shown that the technique of sequential labelling has been successfully refined and the optimal concentrations and application sequence for the four chelating agents has been established.

6.3 The formation and growth of microcracks

Having refined the detection technique, the next step, was to apply the agents in the determined sequence before, and at different intervals during mechanical testing to study microcrack initiation, propagation and accumulation in bone. Numerous studies have looked at the fatigue behaviour of bone, and at microcrack densities both *in vivo* and *in vitro* and how microcracks effect the fatigue behaviour of bone (Chapter 4, Section 4.1). The process by which microcracks initiate, grow and interact with the bone microstructure remains poorly understood and little work has looked at the stages during a bone's life in which microcracks initiate, accumulate and ultimately bring about failure.

In attempting to understand the process, previous workers (Burr et al, 1995; Boyce et al, 1996, Forwood and Parker, 1989) have performed fatigue tests, stopping the tests prior to failure to allow histological analysis of damage developed before fracture. The only study to have looked at the process of initiation, propagation and growth of individual microcracks was Akkus and Rimnac (2000). They investigated microcrack growth of individual surface microcracks in human cortical bone using a video microscopy system. The limitations of their work include the fact that they only looked at surface cracks and also disregarded microcracks that did not run in straight lines and they did not look at the actual mechanisms by which microcrack growth was arrested. Their results however, do support the concept of a microstructural barrier effect existing for cortical bone tissue whereby the morphology of osteonal bone appears to provide an abundance of crack initiation sites but its structure prevents or slows crack growth (Taylor and Prendergast, 1997; Taylor, 1998).

The chelating agents, in general, were found to label microcracks effectively. Some problems were encountered with the degree to which the agents were able to penetrate bone. However, no evidence of substitution was found, thus validating the refinement results (Chapter 3). A small number of microcracks were shown to propagate as they were labelled with two chelating agents. However as suggested in Chapter 5, this is likely to be an underestimate of the actual number of propagating microcracks, with

many which had been classified as being stage 2 or stage 3 microcracks actually being sections through a propagating microcrack. This is due to the amount of bone wasted in the attainment of one 150 μm thick section. Fig. 6.1 shows an example of a propagating microcrack labelled initially with xylenol orange and then with calcein, showing it to have been formed during the first part of the test and grown further during the second part of the test.

The results indicate that microcracks initiate early on during the bone's life (first 10,000 cycles) but then accumulation of more cracks is suppressed, with only a slight increase in microcrack density occurring between 10,000 and 50,000 cycles, before microcracks rapidly accumulate after 50,000 cycles, eventually resulting in failure. This is consistent with the microstructural barrier concept, where the bone's microstructure would be expected to allow microcracks to initiate rapidly but, because of the morphology of osteonal bone, microcracks encounter barriers which suppress further growth before eventually a single microcrack develops enough energy to overcome the barrier and grow further.

The results obtained from the location of transverse microcracks showed that the majority of microcracks (94%) formed during the first 50,000 cycles of tests were located in interstitial bone indicating the difficulty of microcrack growth through osteons. This figure dropped in the latter part of the specimen's life with 25% of microcracks being found in osteons. This again suggests that late in the bone's life, microcracks have a greater potential to break through a cement line. It was also evident from the failed specimens that the main macrocrack, which caused failure, often tended follow Volkmann's and Haversian canals. This suggests that although small microcracks tend to slow down or cease growing completely when they encounter barriers to growth such as cement lines, when a crack is propagating rapidly and does manage to break through, it will take advantage of voids or cavities in the material, whose orientation facilitates growth.

Only a small number of pre-existing cracks were found in specimens. From the control study, it was evident that less than 30% of these cracks were *in vivo* microcracks formed during the cow's life, suggesting that the remainder were small microcracks induced by the machining process. From histological examination, it appeared that the presence of these machining artefacts did not lead to damage accumulation and any cracks formed from these artefacts were minute and did not propagate further. This shows that the use of a CNC lathe during machining of a test specimen does not result in large quantities of artefactual cracks, which might affect the fatigue behaviour of the specimen.

Microcracks were found to be 2-3 times longer in longitudinal than in transverse sections. This is a common occurrence in anisotropic materials, and arises when microcracks find it easier to grow in one direction than in the orthogonal direction. Fig. 4.17 shows a representation of how microcracks may develop in size in both transverse and longitudinal directions. This crack shape was predicted from analysis of all the microcrack lengths in both transverse and longitudinal sections. However, to better predict the three-dimensional shapes of microcracks, a technique would be required which would allow analysis of the shape and size of individual microcracks. Such techniques were employed in Chapter 5.

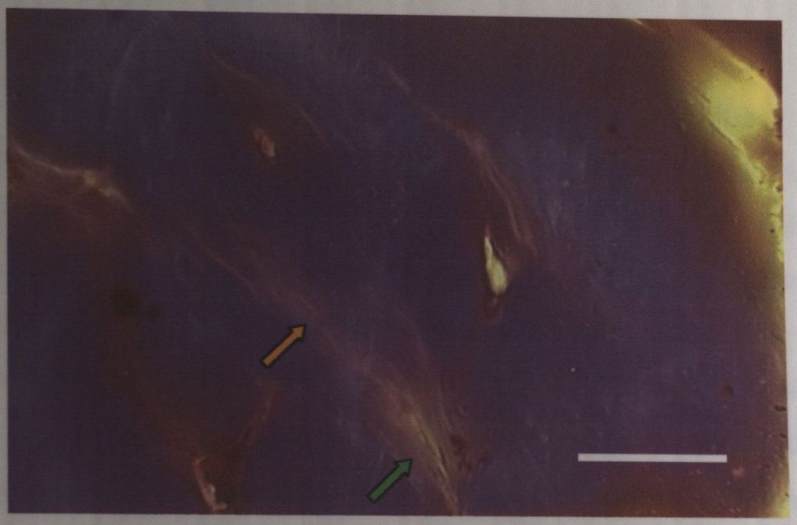

Fig. 6.1 Example of propagating microcrack, initially stained with xylenol and then stained with calcein showing it, to have been formed during the first 50,000 cycles and then to have grown further between 50,000 cycles and failure. Other xylenol orange labelled microcracks can also be seen in the image. Bar=100 μm.

Fig. 6.2a

Fig. 6.2b

Fig. 6.2 A comparison between the two reconstructive techniques (a) reconstruction obtained using laser scanning confocal microscopy (b) reconstruction obtained using serial sectioning method.

6.4 Microcracks in three dimensions

Microcracks in bone are normally analysed using two-dimensional transverse sections of bone (Frost, 1960; Burr and Stafford, 1990; Lee et al, 1998). However, microcracks are longer in the longitudinal direction than in the transverse direction (Burr and Martin, 1993; O'Brien et al, 2000) which suggests that measurements of microcracks in transverse sections are actually a measure of a crack's *width* rather than its *length.* Furthermore, two dimensional measurements fail to provide detailed information on the true shape and size of these microcracks. Knowledge of the true crack dimensions and variance in size may allow for a more accurate calculation of stress intensity values which indicate the probability of an individual microcrack propagating to cause a stress or fragility fracture (Taylor and Lee, 1998).

The work carried out used two different methods to develop three-dimensional reconstructions of individual microcracks. This allowed comparison between the techniques used and the results obtained and provided a more accurate result as to the true three dimensional shape of microcracks in bone. The use of confocal microscopy in microcrack identification is a relatively new one. Laser scanning confocal microscopy (LSCM) has the advantage of visualising a very thin plane of the section and the image has a high spatial resolution as a result of suppressing the glare associated with the out-of-focus areas of the section. LSCM has previously been used to study microdamage in trabecular bone (Fazzalari et al, 1998), the morphology of *in vitro* microcracks in fatigue-tested compact bone (Zioupos and Currey, 1994) and dense arrays of ultra-microcracks in human tibiae (Boyce et al, 1998). Fazzalari's study (1998) is the only one, which has attempted to look at microcracks in three dimensions. This study did not obtain quantative data and concluded that microcracks were actually three dimensional "sheet-like" defects in the bone matrix.

Basic fuchsin bulked-stained blocks of human rib were used in this study. Both techniques, LSCM and serial sectioning of methylmethcrylate-embedded rib sections showed similar results. Microcracks were found to be three dimensional defects and

were shown to be elliptical in shape. Fig. 6.2 shows a comparison between microcracks reconstucted using both techniques. The serial sectioning technique allowed the attainment of quantative data and the ratio of longitudinal length to transverse width was found to be 4.6: 1. This was consistent with the prediction of an elliptical crack shape with axis ratio of 5:1 which had been obtained from analysis of random two dimensional sections (Taylor and Lee, 1998). The results are also comparable with the prediction made in Chapter 4 of this study (Fig. 4.19) and also with the observations by Burr and Martin (1993) that microcracks are 4-6 times longer in the longitudinal direction than in cross section.

Epifluorescence microscopy of the ground sections which had been used for the LSCM analysis showed a mean microcrack density of 0.12 ± 0.10 cracks/ mm^2. This was similar in range to previous studies which had looked at *in vivo* microcracks (Burr and Stafford, 1990; Lee at al, 1998). It was considerably lower then the mean longitudinal density found in the fatigue tested bovine specimens (0.37 ± 0.2 cracks/ mm^2). Microcracks were shown to average 371 ± 211 μm in length along the longitudinal axis (n = 92) which is consistent with the one previous study on *in vivo* longitudinal crack lengths (Burr and Martin, 1993). Surprisingly this mean value is greater then the mean longitudinal length found in the bovine specimens after fatigue testing (279 ± 132 μm). The aspect ratio of the *in vivo* cracks was also greater than that found for *in vitro* microcracks. This may be indicative of the role of microcrack repair in living bone and the difference between cracks that grow *in vivo*, at lower stresses than cracks which grow during mechanical tests. It could also be indicative of how the differences in the microstructure in bovine bone (used for the mechanical tests) and human bone (used for the *in vivo* study) promote microcrack growth. Longitudinal microcracks in human rib were found to run parallel to Haversian systems and to the longitudinal axis of the rib, again showing how microcracks will take advantage of the path of least resistance.

6.5 Future work

The work carried out in this thesis has led to the development of a technique, which allows microcrack growth during the course of a mechanical fatigue test to be studied. The fluorescent chelating agents were again found to be excellent markers of microcracks in compact bone. The only drawback with their use was, in a small number of cases, of poor penetration of dense cortical bone. This may have led to an underestimate of microcrack density and length in some cases. This might be overcome, by developing a rig which allows the bone specimens to be immersed in a bath of a chelating agent under vacuum during testing.

The results obtained have provided a new insight into the process by which the development of microcracks influences the fatigue behaviour of bone. This work has shown the process by which microcracks initiate and propagate in bone and how their development at different stages ultimately brings about failure. Information too, has been obtained on microcracks in the longitudinal direction and also on the three dimensional size and shapes of microcracks in bone. Following on from this, worthwhile future studies might involve studying how microcrack growth is influenced by differing microstructure in bone from different species, for example, in species where Haversian systems are not prevalent. The fatigue behaviour of bone in compression was looked at in this study. However, it may be worthwhile to develop an insight into how the fatigue strength of bone is affected by different types of loading, such as tension, bending or torsion. Most mechanical testing of bone involves test specimens, which have been manufactured using various machining process. To be completely sure of how bone reacts with mechanical loading, knowledge of the behaviour of whole bones subjected to mechanical testing may be a more accurate representation of their behaviour in an *in vivo* situation.

This study used laser scanning confocal microscopy to look at fuchsin stained samples of bone. However, it has barely approached the confocal microscope's capabilities. The technique allows fluorochrome labelled microcracks to be highlighted from the

surrounding matrix with extraordinary clarity. Its potential in the area of fluorochrome labelled microcrack analysis is great and much thought should be given to how to maximise its ability.

Finally, the majority of the work in this project was carried out by an engineer working in a medical school. With the development of new insights into the fatigue behaviour of bone, much more effort needs to be applied to the clinical importance of microcracks in bone. The coming decade, 2000-2010 has been given the title of the Bone and Joint Decade. Its aim, is to increase the awareness of society to the suffering and cost due to muskoloskeletal disease and to influence governments at national and international levels to increase the organisation and resources devoted to its treatment. Such a task can only be accomplished by world-wide, multidisciplinary efforts (Horan, 1999). Further research into the area should be carried out with long term clinical development in mind. The possibility of developing an agent, which chelates to exposed calcium but also shows up under radiological imaging might be a first step. The further development and improvement of Micro CT (Computed Topography) may help this to be realised and enable microdamage to be measured clinically and used to help predict and prevent stress and fragility fractures.

6.6 Conclusions

1. A repeatable *in vitro* testing protocol has been established which allows compact bone specimens to be tested in compression.
2. Specimens were found to have a mean life of 36,000 cycles to failure at 100 MPa. The degree of scatter regarding number of cycles to failure was similar to that observed by other authors. This has validated the accuracy of the predictive model (Taylor, 1998a).
3. The technique of sequentially applying chelating agents to specimens of bone has been refined to prevent the problem of substitution occurring. The new technique, allows microcrack growth at different stages during a mechanical fatigue test to be studied. The established sequence of application is: alizarin - xylenol orange – calcein - calcein blue.

4. Microcracks were found to accumulate early on in a specimen's life but the rate of accumulation then slows down until an increased rate of accumulation in the period prior to failure. Bone microstructure greatly influences microcrack growth with the vast majority of microcracks being found in interstitial bone between Haversian systems. Microcracks have been shown to grow in length primarily in the longitudinal direction, parallel to Haversian systems and the longitudinal axis of the bone. These results support the concept of a microstructural barrier effect existing in bone.

5. Two separate techniques have been developed to look at the three dimensional shape of *in vivo* microcracks in bone.

6. *In vivo* Microcracks are elliptical in shape, being longer in the longitudinal than in the transverse direction.

Chapter 7

REFERENCES

Agarwal, B.D. and Broutman, L.J. (1980) *Analysis and performance of fiber composites*, New York: John Wiley and Sons.

Akkus, O. and Rimnac, C.M (2000) Short fatigue crack growth in human cortical bone. *Personal communication.*

Atkinson, P.J. and Hallsworth, A.S. (1982) The spatial structure of bone. In: Harrison, R.J. and Navaratum, V. (Eds.) *Progress in Anatomy*, Vol. 2, Cambridge, UK: Cambridge University Press, 179-199.

Balena, R., Toolan, B.C., Shea, M., Markatos, A., Myers, E.R., Lee, S.C., Opas, E.E., Seedor, J.G., Klein, H. and Frankfield, D. (1993) The effects of 2-year treatment with the aminobisphosphonate alendronate on bone metabolism, bone histomorphometry and bone strength in ovariectomized non-human primates. *Journal of Clinical Investigation* **92:** 2577-2586.

Bentolila, V., Boyce, T.M., Fyhrie, D.P., Drumb, R., Skerry, T.M. and Schaffler, M.B. (1998) Intracortical remodeling in adult rat long bones after fatigue loading. *Bone* **23:** 275-281.

Boyce, T.M., Fyhrie, D.P., Brodie, F.R. and Schaffler, M.B. (1996) Residual mechanical properties of human cortical bone following fatigue loading. *Transactions of the American Society of Biomechanics* **20:** 23-24.

Boyce, T.M., Fyhrie, D.P., Glotkowski, M.C., Radin, E.L. and Schaffler, M.B. (1998) Damage type and strain mode associations in human compact bone bending fatigue. *Journal of Orthopaedic Research* **16:** 322-329.

Burr, D.B., Martin, R.B., Schaffler, M.B. and Radin, E.L. (1985) Bone remodeling in response to *in vivo* fatigue microdamage. *Journal of Biomechanics* **18**: 189-200.

Burr, D.B., Schaffler, M.B., Yang, K.H., Wu, D.D., Lukoschek, M., Kandzari, D., Sivaneri, N., Blaha, J.D. and Radin, E.L. (1988) The effects of altered strain environments on bone tissue kinetics. *Bone* **10**: 215-221.

Burr, D.B. and Stafford, T. (1990) Validity of the bulk-staining technique to separate artifactual from *in vivo* bone microdamage. *Clinical Orthopaedics and Related Research* **260**: 305-308.

Burr, D.B. and Martin, R.B. (1993) Calculating the probability that microcracks initiate resorption spaces. *Journal of Biomechanics* **26**: 613-616.

Burr, D.B. and Hooser, M. (1995) Alterations to the en bloc basic fuchsin staining protocol for the demonstration of microdamage produced *in vivo*. *Bone* **17**: 431-433.

Burr, D.B., Turner, C.H., Naick, P., Forwood, M.R. and Pidaparti, R.M.V. (1995) Does microdamage accumulation affect the mechanical properties of bone? *Proceedings of the Orthopaedic Research Society* **41**: 127 (Abstract).

Burr, D.B. (2000) Damage detection and behaviour in bone. In: Prendergast, P.J., Lee, T.C. and Carr, A.J. (Eds.) *Proceedings of the 12th Conference of the European Society of Biomechanics* , Dublin: Royal Academy of Medicine in Ireland.

Burstein, A.H., Currey,J.D., Frankel, V.H., and Reillly, D.T. (1972) The ultimate properties of bone tissue: the effects of yielding. *Journal of Biomechanics* **5:** 35-44.

Burstein, A.H., Zika, J.C., Heiple, K.G. and Klein, L. (1975) Contribution of collagen and mineral to the elastic-plastic properties of bone. *Journal of Bone and Joint Surgery* **57A**: 956-961.

Caler, W.E. and Carter, D.R. (1989) Bone creep- fatigue damage accumulation. *Journal of Biomechanics* **22:** 625-635.

Carter, D.R. and Hayes, W.C. (1976) The fatigue life of compact bone. I: Effects of stress amplitude, temperature and density. *Journal of Biomechanics* **9:** 27-34.

Carter, D.R. and Hayes, W.C. (1977a) The compressive behaviour of bone as a two-phase porous structure. *Journal of Bone and Joint Surgery* **59A:** 954-962.

Carter, D.R. and Hayes, W.C. (1977b) Compact bone fatigue damage: a microscopic examination. *Clinical Orthopaedics and Related Research* **127:** 265-274.

Carter, D.R., Harris, W.H., Vasu, R. and Caler, W.E. (1981) The mechanical and biological response of cortical bone to *in vivo* strain histories. In: Cowin, S.C. (Ed.) *Mechanical Properties of Bone*, New York: American Society of Mechanical Engineers.

Carter, D.R., Caler, W.E., Spengler, D.M. and Frankel, V.H. (1981) Fatigue behaviour of adult cortical bone: the influence of mean strain and strain range. *Acta Orthopaedica Scandinavia* **52:** 1579-1586.

Carter, D.R. (1982) The relationship between *in vivo* strains and cortical bone remodeling. *CRC Critical Reviews in Biomedical Engineering* **8**: 1-28.

Carter, D.R. and Caler, W.E. (1983) Cycle-dependant and time-dependant bone fracture with repeated loading. *Journal of Biomechanical Engineering* **105:** 166-170.

Chamay, A. and Tschantz, P. (1972) Mechanial influences in bone remodeling. Experimental research on Wolff's Law. *Journal of Biomechanics* **5:** 173-180.

Choi, K. and Goldstein, S.A. (1992) A comparison of the fatigue behaviour of human trabecular and cortical bone tissue. *Journal of Biomechanics* **25**: 1371-1381.

Choi, K., Fyhrie, D.P. and Schaffler, M.B. (1994) Failure mechanisms of compact bone in bending: a microstructural analysis. *Proceedings of the Orthopaedic Research Society* **19**: 425.

Cooper, C. (1993) The epidemiology of fragility fractures: is there a role for bone quality? *Calcified Tissue International* **53 (Suppl 1):** S23-S26.

Corondan, G. and Haworth, W.L. (1986) A fractographic study of human long bone. *Journal of Biomechanics* **19:** 207-218.

Cowin, S.C., Weinbaum, S. and Zeng, Y. (1995) A case for bone canaliculi as the anatomical site of strain generated potentials. *Journal of Biomechanics* **28**: 1281-1297.

Currey J.D. (1984) *The Mechanical Adaptations of Bones.* Princeton: Princeton University Press.

Daffner, R.H. (1978) Stress fractures: current concepts. *Skeletal Radiology* **2**: 221-229.

Daffner, R.H., Martinez, S., Gehweiler, J.A.Jr. and Harrelson, J.M. (1982) Stress fractures of the proximal tibia in runners. *Radiology* **142**: 63-65.

Daffner, R.H. and Pavlov, H. Stress fractures: current concepts. *American Journal of Roentgenology* **159:** 245-252.

Deisseroth, K.B. and Hogan, H.A. (1995) Characterisation of three-dimensional osteon geometries in haversian cortical bone tissue. *Advances in bioengineering* **31:** 341-342.

Evans, F.G. and Riolo, M.L. (1970) Relations between the fatigue life and histology of adult femoral bone. *Journal of Bone and Joint Surgery* **52A**: 1579-1586.

Fazzalari, N.L., Forwood, M.R., Manthey, B.A,, Smith, K. and Kolesik, P. (1998) Three-dimensional confocal images of microdamage in cancellous bone. *Bone* **23**: 373-378.

Forwood, M.R. and Parker, A.W. (1989) Microdamage in response to repetitive torsional loading in the rat tibia. *Calcified Tissue International* **45:** 47-53.

Frasca, P. (1981) Scanning electron microscopy studies of ground substance in the cement lines, resting lines, hypercalcified rings and reversal lines of human cortical bone. *Acta Anatomica* **109:** 115-121.

Frost, H.M. (1958) Preparation of thin undecalcified bone sections by rapid manual method. *Stain Technology* **33:** 273-277.

Frost, H.M. (1960) Presence of microscopic cracks in vivo in bone. *Henry Ford Hospital Bulletin* **8**: 25-35.

Frost, H.M. (1963) Measurement of human bone formation by means of tetracycline labeling. *Canadian Journal of Biochemistry and Physiology* **41**: 31-42.

Frost, H.M. (1966) Relation between bone-tissue and cell population dynamics, histology and tetracycline labelling. *Clinical Orthopaedics* **49**: 65-75.

Frost, H.M. (1969) Tetracycline-based analysis of bone remodeling. *Calcified Tissue Research* **3**: 211-237.

Frost, H.M. (1973) *Bone remodeling and its relationship to metabolic bone diseases*, Springfield: Charles C. Thomas.

Frost, H.M. (1986) *Intermediary organization of the skeleton*, Boca Raton: CRC Press.

Fyhrie, D.P. and Schaffler, M.B. (1994) Failure mechanisms in human vertebral cancellous bone. *Bone* **15**: 105-109.

Fyhrie, D.P. and Vashishth, D. (2000) Bone stiffness predicts strength similarly for human vertebral cancellous bone in compression and for cortical bone in tension. *Bone* **26**: 169-173.

Gibson, L.J. (1985) The mechanical behaviour of cancellous bone. *Journal of Biomechanics* **18**: 317-328.

Gibson, L.J. and Ashby, M.F. (1988) *Cellular Solids - structures and properties*, Oxford: Pergamon Press.

Gibson, L.J. and Ashby, M.F. (1997) *Cellular Solids - structures and properties*, 2nd *Edition,* Cambridge: Cambridge University Press.

Goldring, S.R., Clark, C.R. and Wright, T.M. (1993) Editorial. The problem in total joint arthroplasty: aseptic loosening. *Journal of Bone and Joint Surgery* **75-A**: 539-546.

Goldstein, S.A. (1987) The mechanical properties of trabecular bone; dependence on anatomical location and function. *Journal of Biomechanics* **20**: 1055-1061.

Goldstein, S.A., Goulet, R. and McCubbrey, D. (1993) Measurement and significance of three-dimensional architecture to the mechanical integrity of trabecular bone. *Calcified Tissue International* **53 (SUPPL 1)**: S127-S133.

Goodship, A.E., Lanyon, L.E. and MacFie, H. (1979) Functional adaptation of bone to increased stress. An experimental study. *Journal of Bone and Joint Surgery* **61-B**: 539-546.

Gray, R.J and Korbacher, G.K. (1974) Compressive fatigue behaviour of bovine compact bone. *Journal of Biomechanics* **7**: 287-292.

Guo, X.E., Gibson, L.J. and McMahon, T.A. (1993) Fatigue of trabecular bone: avoiding end-crushing artifacts. *Proceedings of the Orthopaedic Research Society* **18**: 584 (Abstract).

Haddad, P.R. and Jackson, P.E. (1990) Ion chromatography: principles and applications, Amsterdam: Elsevier Science Publishers.

Hall, B.K. (1991) Historical overview of studies on bone growth and repair. In: Hall, B.K. (Ed.) *Bone, Vol. 1*, Boca Raton: CRC Press.

Hardiman, D.A. (1998) Bone morphology and microcracks in compact bovine bone, *BAI Thesis, University of Dublin.*

Harris, W.H., Jackson, R.H. and Jowsey, J. (1962) The *in vivo* distribution of tetracyclines in canine bone. *Journal of Bone and Joint Surgery* **44A**: 1308-1312.

Hayes, W.C. and Gerhart, T.N. (1985) Biomechanics of bone: Applications for assessment of bone strength. In: Peck, W.A. (Ed.) *Bone and mineral research,* 259-294, Amsterdam: Elsevier Science Publishers.

Hayes, W.C. (1991) Biomechanics of cortical and trabecular boe: implications for assessment of fracture risk. In: Maow, V.C. and Hayes, W.C. (Eds.) *Basic orthopaedic biomechanics*, New York: Raven Press.

Hayes, W.C. and Myers, E.R. (1995) Biomechanics of fractures. In: Riggs, B.L. and Melton, L.J.III (Eds.) *Osteoporosis - etiology, diagnosis and management*, 2nd edn. Philadelphia: Lippincott - Raven.

Hayes, W.C. and Bouxsein, M.L. (1997) Biomechanics of cortical and trabecular bone: Implications for assessment of fracture risk. In: Maow, V.C. and Hayes, W.C. (Eds.) *Basic orthopaedic biomechanics:* 69-107, Philadelphia: Lippincott-Raven Publishers.

Heaney, R.P. (1993) Is there a role for bone quality in fragility fractures? *Calcified Tissue International* **53 (Suppl 1)**: S3-S6.

Hirano, T., Turner, C.H., Forwood, M.R., Johnston, C.C. and Burr, D.B. (2000) Does suppression of bone turnover impair mechanical properties by allowing microdamage accumulation. *Bone* **27**: 13-20.

Horan, F. (1999) The bone and joint decade – 2000 to 2010. *Journal of Bone and Joint Surgery* **81-B:** 377-379.

Huja, S.S., Hasan, M.S., Pidaparti, R., Turner, C.H., Garetto, L.P. and Burr, D.B. (1999) Development of a fluorescent light technique for evaluating microdamage in bone subjected to fatigue loading. *Journal of Biomechanics* **32:** 1243-1249.

Huheey, J.E. (1983) *Inorganic chemistry: principles of structure and reactivity*, 3rd edn., New York: Harper & Row.

Jepsen, K.J.; Davy, D.T. and Krzypow, D.J. (1999) The role of the lamellar interface during torsional yielding of human cortical bone. *Journal of Biomechanics* **32:** 303-310.

Johnell, O. (1997) The socioeconomic burden of fractures: today and in the 21st century. *American Journal of Medicine* **103(2A):** 20-65.

Johnson, A.W., Weiss, C.B.Jr. and Wheeler, D.L. (1994) Stress fractures of the femoral shaft in athletes - more common than expected. A new clinical test. *American Journal of Sports Medicine* **22**: 248-256.

Kanis, J.A. (1993) *Assessment of fracture risk and its application to screening for postmenopausal osteoporosis. WHO Collaborating centre for Metabolic Bone Disease, WHO Technical Report Series XXX*, Berne: European Foundation for Osteoporosis and Bone Disease.

Keaveny, T.M., Wachtel, E.F., Guo, X.E. and Hayes, W.C. (1994a) Mechanical behaviour of damaged trabecular bone. *Journal of Biomechanics* **27**: 1309-1318.

Keaveny, T.M., Guo, X.E., Wachtel, E.F., McMahon, T.A. and Hayes, W.C. (1994b) Trabecular bone exhibits fully linear elastic behavior and yields at low strains. *Journal of Biomechanics* **27**: 1127-1136.

Kimmel, D.B., Heaney, R.P., Avioli, L.V., Chesnut, C.H., Recker, R.R., Lappe, J.M. and Brandenburger, G.H. (1991) Patellar ultrasound velocities in osteoporotic and normal subjects of equal forearm or spinal bone density. *Journal of Bone and Mineral Research.* **6:** S169.

King, A.I. and Evans, F.G. (1967) Analysis of fatigue strength of human compact bone by the Weibull method. *7th Conference of Medical and Biological Engineering, Stockholm.*

Lafferty, J.F. and Raju, P.V. (1979) The influences of stress frequency on the fatigue strength of cortical bone. *Journal of Biomedical Engineering* **101:** 112-113.

Lamberg-Allardt, C., Karkkainen, M., Seppanen, R. and Bistrom, H. (1993) Low serum 25-hydroxyvitamin D concentrations and secondary hyperparathyroidism in midddle-aged white strict vegetarians. *American Journal of Clinical Nutrition* **58:** 684-689.

Landis, W.J. (1995) The strength of a calcified tissue depends in part on the molecular structure and organization of its constituent mineral crystals in their organic matrix. *Bone* **16**: 533-544.

Landis, W.J. (1996) Ionic constituents of compact bone. *Personal communication.*

Lane, J.M., Riley, E.H. and Wirganowicz, P.Z. (1996) Osteoporosis: diagnosis and treatment. *Journal of Bone and Joint Surgery* **78-A:** 618-632.

Lanyon, L.E., Goodship, A.E., Pye, C.J. and MacFie, J.H. (1982) Mechanically adaptive bone remodeling. *Journal of Biomechanics* **15**: 141-154.

Lanyon, L.E. (1991) Biomechanical properties of bone and response of bone to mechanical stimuli: functional strain as a controlling influence on bone modeling and remodelling behaviour. In: Hall, B.K., (Ed.) *Bone, Volume 3*, Boca Raton: CRC Press.

Lee, T.C. (1995) Functional adaptation in compact bone, Ph.D. Thesis, *University of Dublin.*

Lee, T.C. (1997) Detection and accumulation of microdamage in bone, M.D. Thesis, *University of Dublin.*

Lee, T.C., Myers, E.R. and Hayes, W.C. (1998) Fluorescence-aided detection of microdamage in compact bone. *Journal of Anatomy* **193**: 179-184.

Lee, T.C. and Taylor, D. (1999a) Bone remodelling: should we cry Wolff? *Irish Journal of Medical Science* **168:** 102-105.

Lee, T.C., Noelke, L., McMahon, G.T., Mulville, J.P. and Taylor, D. (1999b) Functional adaptation in bone. In: Pedersen, P. and Bendsoe, M.P.(Eds.) *Synthesis in BioSolid Mechanics.* Dortrecht: Kluwer Academic Publishers.

Lee, T.C., Arthur, T.L., Gibson, L.J. and Hayes, W.C. (2000a) Sequential labelling of microdamage in bone using chelating agents. *Journal of Orthopedic Research* **18:** 322-325.

Lee, T.C., O'Brien, F.J. and Taylor, D. (2000b) The nature of fatigue damage in bone. *International Journal of Fatigue* (in press).

Liberman, U.A., Weiss, S.R., Broll, J., Minne, H.W., Quan, H., Bell, N.H., Rodriguez-Portales, J., Downs, R.W.Jr., Dequeker, J., Favus, M., Seeman, E., Recker, R.R., Capizzi, T., Santora, A.C., Lombardi, A., Shah, R.V., Hirsch, L.J. and Karpf, D.B. (1995) Effect of oral alendronate on bone mineral density and the incidence of fractures in postmenopausal osteoporosis. *New England Journal of Medicine* **333:** 1437-1443.

Lin, J.H. (1996) Bisphosphonates: a review of their pharmacokinetic properties. *Bone* **18**: 75-85.

Maow, V.C. and Hayes, W.C. (1997) *Basic orthopaedic biomechanics,* Philadelphia: Lippincott-Raven Publishers.

Martin, R.B. and Burr, D.B. (1982) A hypothetical mechanism for the stimulation of osteonal remodelling by fatigue damage. *Journal of Biomechanics* **15**: 137-139.

Martin, R.B. and Burr, D.B. (1989) *Structure, function and adaptation of compact bone*, New York: Raven Press.

Martin, R.B., Burr, D.B. and Sharkey, N.A. (1998) *Skeletal Tissue Mechanics*, New York: Sprenger-Verlag.

Martin, R.B. (2000) Toward a unifying theory of bone remodelling. *Bone* **26:** 1-6.

Martini, F.H. (1992) *Fundamentals of Anatomy and Physiology,* New Jersey: Prentice Hall.

Mashiba, T., Hirano, T., Turner, C.H., Forwood, M.R., Johnston, C.C. and Burr, D.B. (2000) Suppressed bone turnover by bisphosphonates increases microdamage accumulation and reduces some biomechanical properties in dog rib. *Journal of Bone and Mineral Research* **15:** 613-620.

McBryde, A.M. (1975) Stress fractures in athletes. *Journal of Sports Medicine* **3:** 212-217.

Melton, L.J., Kan, S.H., Fyre, M.A., Wahner, H.W., O'Fallon, W.M. and Riggs, B.L. (1989) Epidemology of vertebral fractures in women. *American Journal of Epidemology*, **129:** 1000-1011.

Melton, L.J.III (1996) Epidemiology of hip fractures: Implications of the exponential increase with age. *Bone* **18 (Suppl.):** 121S-125S.

Michel, M.C., Guo, X.E., Gibson, L.J., McMahon, T.A. and Hayes, W.C. (1993) Compressive fatigue behaviour of bovine trabecular bone. *Journal of Biomechanics* **26**: 453-463.

Milgrom, C., Giladi, M., Simkin, A., Rand, N., Kedem, R., Kashtan, H., Stein, M. and Gomori, M. (1989) The area moment of inertia for the tibia: a risk factor for stress fractures. *Journal of Biomechanics* **22**: 1243-1248.

Miller, E.H., Schneider, H.J., Bronson, J.L. and McLain, D. (1975) A new consideration in athletic injuries. The classical ballet-dancer. *Clinical Orthopaedics and Related Research* **111**: 191.

Miller, K.J. and De los Rios, E.R. (1986) The behaviour of short fatigue cracks, London: *Mechanical Engineering Publications.*

Mori, S. and Burr, D.B. (1993) Increased intracortical remodeling following fatigue damage. *Bone* **14**: 103-109.

Moskilde, L. (1988) Age-related changes in vertebral trabecular bone architecture - assessed by a new method. *Bone* **9**: 247-250.

Muir, P., Johnson, K.A. and Ruaux-Mason, C.P. (1999) *In vivo* matrix microdamage in a naturally occurring canine fatigue fracture. *Bone* **25:** 571-576.

Nunamaker, D.M.; Butterwerk, D.M.; Provost, M.T. (1990) Fatigue fractures in thoroughbred reacehorses: relationships with age. *Journal of Orthopaedic Research* **8:** 604-611.

Obrant, K. (1989) Editorial: Increasing age-adjusted risk of fragility fractures: a sign of increasing osteoporosis in successive generations? *Calcified Tissue International* **44**: 157-167.

O'Brien, F.J. (1997) Fatigue cracks in bone, BAI Thesis, *University of Dublin.*

O'Brien, F.J., Pellegrini, F., Dickson, G., Lee, T.C. and Taylor, D. (1998) Morphology of fatigue microcracks in compact bone. *Irish Journal of Medical Science* **167:** 276

O'Brien, F.J., Taylor, D, Dickson, G.R. and Lee, T.C. (2000) Visualisation of three-dimensional microcracks in compact bone. *Journal of Anatomy* **197:** 413-420.

Odgaard, A. and Linde, F. (1991) The underestimation of Young's modulus in compressive testing of cancellous bone specimens. *Journal of Biomechanics* **24**: 691-698.

Ott, S.M. (1993) When bone mass fails to predict bone failure. *Calcified Tissue International* **53 (Suppl 1)**: S7-S13.

Pais, M.J. and Wang, F. (1989) Stress injuries. In: Tehranzedah, J., Serafini, A.N. and Pais, M.J. (Eds.) *Avulsion and stress injuries of the musculoskeletal system*, New York: Kargen.

Pal, B. (1999) Questionnaire survey of advice given to patients with fractures. *Bone and Mineral Journal* **318:** 176-177.

Park, H.C. and Lakes, R.S. (1986) Cosserat micromechanics of human bone: strain redistribution by a hydration sensitive constituent. *Journal of Biomechanics* **19**: 385-397.

Pattin, C.A., Caler, W.E. and Carter, D.R. (1996) Cyclic mechanical property degradation during fatigue loading of cortical bone. *Journal of Biomechanics* **29:** 69-79.

Pellegrini, F. (1997) Bovine bone crack detection using chelating agents, BAI Thesis, *University of Dublin.*

Pester, S. and Smith, P.C. (1992) Stress fractures in the lower extremities of soldiers in basic training. *Orthopaedics Review* **21**: 297-303.

Piekarski, K. (1973) Analysis of bone as a composite material. *Journal of Biomechanics* **11**: 557-565.

Prendergast, P.J. and Taylor, D. (1992) Design of intermedullary prostheses to prevent bone loss: predictions based on damage-stimulated remodelling. *Journal of Biomedical Engineering* **14**: 499-506.

Prendergast, P.J. and Taylor, D. (1994) Prediction of bone adaptation using damage accumulation. *Journal of Biomechanics* **27**: 1067-1076.

Prendergast, P.J. and Huiskes, R. (1996) Microdamage and osteocyte-lacuna strain in bone: a microstructural finite element analysis. *Journal of Biomechanical Engineering* **118:** 240-246.

Price, P.A., Parthemore, J.G. and Deftos, L.J. (1980) New biochemical marker for bone. *Personal communication.*

Prina Mello, A. (1998) Fatigue properties of bone, BAI Thesis, *University of Dublin.*

Radin, E.L., Parker, H.G., Pugh, J.W., Steinberg, R.S., Paul, I.L. and Rose, R.M. (1973) Responses of joints to impact loading - III. Relationships between trabecular microfractures and cartilage degeneration. *Journal of Biomechanics* **6**: 51-57.

Radin, E.L., Rubin, C.T., Thrasher, E.L., Lanyon, L.E., Crugnola, A.M., Schiller, A.S., Paul, I.L. and Rose, R.M. (1982) Changes in the bone-cement interface after total hip replacement. *Journal of Bone and Joint Surgery* **64-A**: 1188-1200.

Rahn, B.A. and Perren, S.M. (1970) Calcein blue as a fluorescent label in bone. *Experientia* **26**: 519.

Rahn, B.A. and Perren, S.M. (1971) Xylenol orange, a fluorochrome useful in polychrome sequential labelling of calcifying tissues. *Stain Technology* **46**: 125-129.

Rahn, B.A. (1977) Polychrome fluorescence labelling of bone formation, instrumental aspects and experimental use. *Zeiss Information* **22 (85)**: 36-39.

Reifsneider, K.L. (1990) Damage and damage mechanics. In: Reifsneider, K.L. (Ed.) *Fatigue of composite materials,* Elsevier: New York.

Reilly, G. (2000) Observations of microdamage around osteocyte lacunae in bone. *Journal of Biomechanics* **33:** 1131-1134.

Rice, J.C., Cowin, S.C. and Bowman, J.A. (1988) On the dependence of elasticity and strength of cancellous bone on apparent density. *Journal of Biomechanics* **21**: 155-168.

Riggs, B.L. and Melton, L.J.III (1995) The worldwide problem of osteoporosis: Insights afforded by epidemiology. *Bone* **17 Suppl.**: 505S-511S.

Robinovitch, S.N., Hayes, W.C. and McMahon, T.A. (1991) Prediction of femoral impact forces in falls on the hip. *Journal of Biomechanical Engineering* **113:** 366-374.

Ross, P.D., Davis, J.W., Epstein, R.S. and Wasnich R.D. (1993) Pre-existing fractures and bone mass predict vertebral fracture incidence in women. *Ann. Int. Med.* **114:** 919-923.

Rost, F.W.D. (1992) *Fluorescence microscopy, Volume I*, Cambridge: Cambridge University Press.

Rost, F.W.D. (1995) *Fluorescence microscopy, Volume II*, Cambridge: Cambridge University Press.

Ryan, C. (1998) Fatigue testing of bone, BAI Thesis, *University of Dublin.*

Sahni, M., Guenther, H.L., Fleisch, H., Collin, P. and Martin, T.J. (1993) Bisphosphonates act on rat bone resorption through the mediation of osteoblasts. *Journal of Clinical Investigation* **91**: 2004-2011.

Sato, M., Grasser, W., Endo, N., Akins, R., Simmons, H., Thompson, D.D., Golub, E. and Rodan, G.A. (1991) Bisphosphonate action. Alendronate localization in rat bone and effects on osteoclast ultrastructure. *Journal of Clinical Investigation* **88**: 2095-2105.

Schaffler, M.B., Radin, E.L. and Burr, D.B. (1989) Mechanical and morphological effects of strain rate on fatigue in compact bone. *Bone* **10**: 207-214.

Schaffler, M.B., Radin, E.L. and Burr, D.B. (1990) Long-term fatigue behaviour of compact bone at low strain magnitude and rate. *Bone* **11**: 321-326.

Schaffler, M.B., Choi, K. and Milgrom, C. (1994a) Microcracks and aging in human femoral compact bone. *Proceedings of the Orthopaedic Research Society* **19:** 190 (Abstract).

Schaffler, M.B., Pitchford, W., Choi, K. and Riddle, J.M. (1994b) Examination of compact bone microdamage using back-scattered electron microscopy. *Bone* **15**: 483-488.

Schaffler, M.B., Choi, K. and Milgrom, C. (1995) Aging and matrix microdamage accumulation in human compact bone. *Bone* **17**: 521-525.

Schenk, R.K., Olah, A.J. and Herrmann, W. (1984) Preparation of calcified tissues for light microscopy. In: Dickson, G.R. (Ed.) *Methods of calcified tissue preparation,* Elsevier: Oxford.

Schiller, A.L. (1994) Bone and Joints. In: Rubin, E. and Farber, J.L. (Eds.) *Pathology*, 2nd edn. Philadelphia: J.B. Lippincott.

Sherman, S. and Hadley, E.C. (1993) Aging and bone quality: an unexplored frontier. *Calcified Tissue International* **53 (Suppl 1)**: S1.

Small, H., Stevens, T.S. and Bauman, W.C. (1975) *Analytical Chemistry* **47**: 1801.

Stover, S.M., Johnson, B.J., Daft, B.M., Read, D.H., Anderson, M., Barr, B.C., Kinde, H., Moore, J., Stoltz, J. and Ardans, A.A. (1992) An association between complete and

incomplete stress fractues of the humerus in racehorses. *Equine Veterinary Journal* **24:** 260-263.

Stover, S.M., Martin, R.B., Pool, R.R., Taylor, K.T. and Harrington, T.M. (1993) *In vivo* labeling of microdamage in cortical bone tissue. *Proceedings of the Orthopaedic Research Society* **18**: 541(Abstract).

Suzuki, H.K. and Mathews, A. (1966) Two-color fluorescent labeling of mineralizing tissues with tetracycline and 2,4-bis[N, N'-di-(carbomethyl) aminomethyl] fluorescein. *Stain Technology* **41**: 57-60.

Taylor, D. and Prendergast, P.J. (1995) Damage accumulation in compact bone - a fracture mechanics approach to estimate damage and repair rates. In: *Advances in Bioengineering* BED- vol. 13, New York: American Society of Mechanical Engineers 337-338.

Taylor, D. and Prendergast, P.J. (1997) A model for fatigue crack propagation and remodelling in compact bone. *Journal of Engineering in Medicine (Proceedings, Institution of Mechanical Engineers Part H)* **211:** 369-375.

Taylor, D. (1997) Bone maintenance and remodelling: a control system based on fatigue damage. *Journal of Orthopaedic Research.* **15:** 601-606.

Taylor, D. (1998a) Fatigue of bone and bones: an analysis based on stressed volume. *Journal of Orthopaedic Research* **16:** 163-169.

Taylor, D. (1998b) Microcrack growth parameters for compact bone deduced from stiffness variations. *Journal of Biomechanics* **31**: 587-592.

Taylor, D. and Lee, T.C. (1998) Measuring the shape and size of microcracks in bone. *Journal of Biomechanics* **31**: 1177-1180.

Taylor, D. (1999a) Fatigue damage in bone: links to adaption. In: Pedersen, P. and Bendsoe, M.P.(Eds.) *Synthesis in BioSolid Mechanics,* Dortrecht: Kluwer Academic Publishers.

Taylor, D., O'Brien, F.J., Prina Mello, A., Ryan, C., O'Reilly, P. and Lee, T.C. (1999b) Compression data on bovine bone confirms that 'stressed volume' principle explains the variability of fatigue strength results. *Journal of Biomechanics* **32:** 1199-1203.

Thomson, B.M., Saklatvala, J. and Chambers, T.J. (1986) Osteoblasts mediate interleukin-1 stimulation of bone resorption by rat osteoclasts. *Journal of Experimental Medicine* **164**: 104-112.

Tschantz P, Rutishauser E. (1967) La surcharge mecanique de l'os vivant. Les deformations plastiques initiales et l'hypertrophie de l'adaptation. *Annales d'Anatomie Pathologique* **12:** 223-248.

Turner, C. (1993) Age, bone material properties and bone strength. *Calcified Tissue International* **53 Suppl 1**: S32-S33.

Van der Meulen, M.C.H. and Prendergast, P.J. (2000) Mechanics in skeletal development, adaptation and disease. *Transactions of the Royal Philosophical Society of London* **358:** 565-578.

Vashishth, D., Johnson, C., Clovis, N., Tanner, K.E. and Bonfield, W. (1994) Double staining technique for histological evaluation of microcracks in cortical bone. *Proceedings of the Second World Congress of Biomechanics* **I**: 44.(Abstract).

Vashishth, D., Norman, T.L., Nivargikar, S., Behiri, J.C. and Bonfield, W. (1995) Failure of longitudinal osteons under tensile and shear loads. *Proceedings of the Orthopaedic Research Society* **20**: 130(Abstract).

ashishth, D., Verborgt, O., Divine, G., Schaffler, M.B. and Fyhrie, D.P. (2000) Decline osteocyte lacunar density in human cortical bone is associated with accumulation of icrocracks with age. *Bone* **26:** 375-380.

erborgt, O., Gibson, G.J., Schaffler, M.B. (2000) Loss of osteocyte integrity in sociation with microdamage and bone remodeling after fatigue in vivo. *Journal of one and Mineral Reseaarch* **15:** 60-67.

illaneuva, A.R. and Lundin, K.D. (1989) A versatile new mineralized bone stain for multaneous assessment of tetracycline and osteoid seams. *Stain Technology* **64**: 129-38.

Vachtel, E.F. and Keaveny, T.M. (1995) The dependence of trabecular damage on pplied strain level for bovine trabecular bone. *Proceedings of the Orthopaedic Research ociety* **20**: 132(Abstract).

Volff, J. (1892) Das gesetz der transformation der knochen. Berlin: Hirchwald.

Vright, T.M. and Hayes, W.C. (1976) The fracture mechanics of fatigue crack ropagation in compact bone. *Journal of Biomedical Materials Research* 7: 637-648.

Zioupos, P. and Currey, J.D. (1994a) The extent of microcracking and the morphology of microcracks in damaged bone. *Journal of Materials Science* **29**: 978-986.

Zioupos, P., Currey, J.D. and Sedman, A.J. (1994b) An examination of the micromechanics of failure in bone and antler by acoustic emission tests and laser scanning confocal microscopy. *Medical Engineering and Physics* **16**: 203-212.

Zioupos, P., Wang, X.T. and Currey, J.D. (1996) Experimental and theoretical quantification of the development of damage in fatigue tests of bone and antler. *Journal of Biomechanics* **29**: 989-1002.

Appendix 2.1 CNC Program for waisting gauge length of test specimen

```
OPERATION LIST        POST:          FANUC-(HARRISON-LATHE)
-----------------------------------------------
OP                  1 DIAMETER    POCKET      TOOL                 7 HARRISON
          TOOL        TIP           RAD         1.9975,    DEPTH      OF
          PROFILE     TOOL          2MM         RAD
          Feed        Distance:           60.2 Time        for        OP
-----------------------------------------------
Total     Feed        Distance      .....................       60.2
Tool      Change      Time          .....................0m       05s
Total     Time        .....................1m        02s
-----------------------------------------------
Material:  Bone
-------------------------------  . 7 HARRISON  PROFILE    2MM        RAD)
START
'(7MMGUAGI 11/2/98)
'(OP                1 DIAMETER    POCKET      TOOL
'(TOOL     TIP        RAD           1.9975,     DEPTH      OF         CUT (0.1)
'(PROFILE  TOOL       2MM           RAD)
(PROGRAM   PRODUCED   -                    11 FEB          98)
:1101
Line Number
N10        G21        G97           G40         G99        M42
N20        G50        S400          M13
N30        G0         T0707         '           SELECT     TOOL                 7
N40        G50        (X...         Z...)
N50        G50        S400
N60        G96        S200          M03         G99
N70        G0         X200.         Z0.
N80        X20.559    Z0.
N90        X20.559    Z-12.082
N100       X6.371     Z-12.082
N110       G2         X6.171        Z-12.248    R3.562     F0.7
N120       G1         Z-22.752      F0.2
N130       G2         X6.371        Z-22.918    R3.562     F0.7
N140       G0         X6.725        Z-22.742
N150       X6.725     Z-12.248
N160       G1         X6.171        F0.1
N170       G2         X5.971        Z-12.438    R3.562     F0.2
N180       G1         Z-22.562
N190       G2         X6.171        Z-22.752    R3.562
N200       G0         X6.525        Z-22.575
N210       X6.525     Z-12.438
N220       G1         X5.971        F0.1
N230       G2         X5.771        Z-12.662    R3.562     F0.2
N240       G1         Z-22.338
N250       G2         X5.971        Z-22.562    R3.562
N260       G0         X6.325        Z-22.385
N270       X6.325     Z-12.662
N280       G1         X5.771        F0.1
N290       G2         X5.571        Z-12.942    R3.562     F0.2
N300       G1         Z-22.058
N310       G2         X5.771        Z-22.338    R3.562
N320       G0         X6.125        Z-22.161
N330       X6.125     Z-12.942
N340       G1         X5.571        F0.1

N350       G2         X5.371        Z-13.345    R3.562     F0.2
N360       G1         Z-21.655
N370       G2         X5.571        Z-22.058    R3.562
N380       G0         X5.925        Z-21.881
N390       X5.925     Z-13.345
N400       G1         X5.371        F0.1
N410       G2         X5.25         Z-14.       R3.562     F0.2
N420       G1         Z-21.
N430       G2         X5.371        Z-21.655    R3.562
N440       G0         X5.725        Z-21.478
N450       X20.559    Z-21.478
N460       X20.559    Z0.
N470       X200.      Z0.
N480       M09        '             CANCEL      TOOL                  7
N490       T0700
N500       M02
%
```

Appendix 2.2 Microsoft Turbo C Program used during fatigue tests

```
/* * * * * * * * * * * * * * * * * * * * * * * * * * * * * * * * * * * *   * * *
     Trinity College Dublin - Dept. of Mechanical Eng.-  July 1998

  Program that store in HDD max and min of any waveform between +/-1.5V
 * * * * * * * * * * * * * * * * * * * * * * * * * * * * * * * * * * * * * * * * */
#include <pc30at.h>
#include <stdio.h>
#include <dos.h>
#define NAV 15

float j;
int n;

void main(void);
float a2d();

void main(void) {


FILE *scandat;
float max,min,mean,def;
float def0,diff,k,l;
int i,d,t,m,dly;
int block;
unsigned seconds;
unsigned cnt=0;
char filename[20]; float temp[2000];
clrscr();
```

Appendix 2.2 Microsoft Turbo C Program -continued

```
initaddr(0x340);
printf("\n\n\n*************************************************************
*******");
printf("\n\t\t\t\tMINMAX.C");
printf("\n\t LOGGING PROG for PC30AT.      APM & PDN July/98 V0");
printf("\n Ch1.    Data saved to user filename.");
printf("\n BA0X340 BIP+/-1.5V  NAV=15 \n");
printf("\nProgram saves blocks of 5 sample sets at approx N seconds
intervals");
printf("\n*************************************************************
***\n\n\n");

printf("\nenter time between blocks [seconds]:"); scanf("%d",&seconds);

printf("\nEnter data filename and path : ");  scanf("%s",filename);
if(!(scandat=fopen(filename,"w")))  printf("\nerror opening file");
else printf("\nData file opened OK.        Please wait.....");



delay(1500);  printf("\n\n\n\n\tHit 'S' to START sampling.\n");
printf("\n\tHit any key to STOP sampling");
printf("\n\t\tor press pause key to PAUSE sampling.\n\n");
while(getch()!='s');

block=0; m=0;
chans[0] = 2; setadchans(1);    //select channel


while(!kbhit())
 {
    fprintf(scandat,"\n\nBlock:%d",block);
    printf("\nsampling Data.......");

    for(cnt=0;cnt<5;cnt++)
    {

     for(i=0;i<1000;i++)
      {
      temp[i]=(a2d());      //acquisition samples
      }

     max=-1.5;                  //initialization
     min=1.5;
     def=def0=1;

     for(i=1;i<1000;i++)        //1000
      {
         if(temp[i]>max) max=temp[i];        //function follow and forget
         else if (temp[i]<min) min=temp[i]; // max and min

      }


     max=((max*.2448)+.0047);
     min=((min*.2448)+.0047);            //
     def=(max-min);                     //def in mm
```

Appendix 2.2 Microsoft Turbo C Program -continued

```
    if((block==0)&(m==0))
     {
     def0=def;          //store first deformation
     m=1;
     }
     else diff=((def-def0)/def0);

    fprintf(scandat,"\n Max: %f Min: %f def: %f diff %f",max,min,def,diff);
                                          //max,min,def in mm

   }

  printf("\nTrend Max:%.3f mm  Min:%.3f mm def: %.3f mm diff:%.3f
mm",max,min,def,diff);
  printf("\nBlock No:%d is most recent to be saved",block);
  block++;

  for(t=0;t<seconds;t++)  delay(1000);


 }

printf("\n\aSAMPLING STOPPED    Closing file"); fclose(scandat);
delay(1500);
getch();
while(!kbhit());

return 0;
}



float a2d()   {                    //function acquisition and average
           j=0;                  // noise compensation
           for(n=0;n<NAV;n++)

           j=j+(calcvolts(BIP,1.5,adconv()));
           return(j/NAV);
           }

 /*  //*****************************************************************    */
```

Appendix 2.3 Failure history of specimens

Specimen	Stress Range [MPa}	No. of Cycles to Failure Nf
1	100	No Data
2	100	No Data
3	100	No Data
4	100	No Data
5	100	80000
6	100	7500
7	100	82000
8	100	6000
9	100	68000
10	100	140000
11	100	5500
12	100	38000
13	100	7000
14	100	1082
15	100	514
16	100	5425
17	100	82450
18	100	11150
19	100	27620
20	100	32000
21	100	85000
22	100	43000
23	100	11920
24	100	14540
25	100	12870
		Mean 36265
		SD 38521

Appendix 4.1 Failure history of specimens

Specimen	Stress Range [MPa}	No. of Cycles to Failure Nf
1	80	57500
2	80	95041
3	80	112056
4	80	62384
5	80	106112
6	80	111722
7	80	105659
8	80	78980
9	80	120002
10	80	84300
11	80	79320
12	80	69240
		Mean 90193
		SD 21119

Appendix 4.2 Longitudinal crack data from three agent tests
Total number of cracks includes preexisting cracks labelled with alizarin

Specimen	No. of Cracks Xylenol	No. of Cracks Calcein	No. of Cracks Propagating	No. of Cracks Total
1	No Data	No Data	No Data	No Data

Specimen	No. of Cracks Xylenol	No. of Cracks Calcein	No. of Cracks Propagating	No. of Cracks Total
2	No Data	No Data	No Data	No Data

Specimen	No. of Cracks Xylenol	No. of Cracks Calcein	No. of Cracks Propagating	No. of Cracks Total
3	15	33	0	48
	Average Length 87.6	Average Length 126.0	Ave Lgt Xyl	Average Length 114.0
	Crack Density (No./ mm^2) 0.094	Crack Density (No./ mm^2) 0.21	Ave Lgt Cal	Crack Density (No./ mm^2) 0.30
	Surface Density (μm crk. lgt/ mm^2) 8.231	Surface Density (μm crk. lgt/ mm^2) 26.061	Ave Lgt Total	Surface Density (μm crk. lgt/ mm^2) 34.293
		Ratio Cal: Xyl 2.2		

Specimen	No. of Cracks Xylenol	No. of Cracks Calcein	No. of Cracks Propagating	No. of Cracks Total
4	9	24	6	39
			Ave Lgt Xyl 143.55	
			Ave Lgt Cal 194.79	
	Average Length 202.3	Average Length 120.6	Ave Lgt Total 338.330	Average Length 159.2
	Crack Density (No./ mm^2) 0.032	Crack Density (No./ mm^2) 0.085	Crack Density (No./ mm^2) 0.021	Crack Density (No./ mm^2) 0.138
	Surface Density (μm crk. lgt/ mm^2) 6.467	Surface Density (μm crk. lgt/ mm^2) 10.276	Surface Density (μm crk. lgt/ mm^2) 7.209	Surface Density (μm crk. lgt/ mm^2) 24.977

Specimen	No. of Cracks Xylenol	No. of Cracks Calcein	No. of Cracks Propagating	No. of Cracks Total
5	3	18	0	22
			Ave Lgt Xyl	
			Ave Lgt Cal	
	Average Length 243.8	Average Length 142.4	Ave Lgt Total	Average Length 156.8
	Crack Density (No./ mm^2) 0.034	Crack Density (No./ mm^2) 0.205	Crack Density (No./ mm^2) 0	Crack Density (No./ mm^2) 0.251
	Surface Density (μm crk. lgt/ mm^2) 8.345	Surface Density (μm crk. lgt/ mm^2) 29.240	Surface Density (μm crk. lgt/ mm^2) 0.000	Surface Density (μm crk. lgt/ mm^2) 60.754

Specimen	No. of Cracks Xylenol	No. of Cracks Calcein	No. of Cracks Propagating	No. of Cracks Total
6	18	39	3	60
			Ave Lgt Xyl 120.25	
			Ave Lgt Cal 95.21	
	Average Length 98.2	Average Length 179.5	Ave Lgt Total 215.460	Average Length 156.9
	Crack Density (No./ mm^2) 0.078	Crack Density (No./ mm^2) 0.169	Crack Density (No./ mm^2) 0.013	Crack Density (No./ mm^2) 0.259
	Surface Density (μm crk. lgt/ mm^2) 7.654	Surface Density (μm crk. lgt/ mm^2) 30.316	Surface Density (μm crk. lgt/ mm^2) 2.799	Surface Density (μm crk. lgt/ mm^2) 40.769

Specimen	No. of Cracks Xylenol	No. of Cracks Calcein	No. of Cracks Propagating	No. of Cracks Total
7	6	24	6	39
			Ave Lgt Xyl 155.83	
			Ave Lgt Cal 134.39	
	Average Length 114.7	Average Length 96.2	Ave Lgt Total 290.212	Average Length 117.2
	Crack Density (No./ mm^2) 0.039	Crack Density (No./ mm^2) 0.157	Crack Density (No./ mm^2) 0.04	Crack Density (No./ mm^2) 0.258
	Surface Density (μm crk. lgt/ mm^2) 4.554	Surface Density (μm crk. lgt/ mm^2) 15.286	Surface Density (μm crk. lgt/ mm^2) 11.533	Surface Density (μm crk. lgt/ mm^2) 31.762

Specimen	No. of Cracks Xylenol	No. of Cracks Calcein	No. of Cracks Propagating	No. of Cracks Total
8	12	33	6	51
			Ave Lgt Xyl 72.05	
			Ave Lgt Cal 115.36	
	Average Length 150.2	Average Length 188.8	Ave Lgt Total 187.410	Average Length 179.1
	Crack Density (No./ mm^2) 0.066	Crack Density (No./ mm^2) 0.182	Crack Density (No./ mm^2) 0.033	Crack Density (No./ mm^2) 0.282
	Surface Density (μm crk. lgt/ mm^2) 9.984	Surface Density (μm crk. lgt/ mm^2) 34.506	Surface Density (μm crk. lgt/ mm^2) 6.227	Surface Density (μm crk. lgt/ mm^2) 50.717

Specimen	No. of Cracks Xylenol	No. of Cracks Calcein	No. of Cracks Propagating	No. of Cracks Total
9	24	63	6	93
			Ave Lgt Xyl 214.68	
			Ave Lgt Cal 401.21	
	Average Length 203.8	Average Length 343.2	Ave Lgt Total 615.89	Average Length 315.1
	Crack Density (No./ mm^2) 0.256	Crack Density (No./ mm^2) 0.673	Crack Density (No./ mm^2) 0.064	Crack Density (No./ mm^2) 0.99
	Surface Density (μm crk. lgt/ mm^2) 52.227	Surface Density (μm crk. lgt/ mm^2) 230.948	Surface Density (μm crk. lgt/ mm^2) 39.467	Surface Density (μm crk. lgt/ mm^2) 322.642

Specimen	No. of Cracks Xylenol	No. of Cracks Calcein	No. of Cracks Propagating	No. of Cracks Total
10	21	21	3	45
			Ave Lgt Xyl 155.64	
			Ave Lgt Cal 298.44	
	Average Length 146.9	Average Length 326.3	Ave Lgt Total 454.080	Average Length 251.1
	Crack Density (No./ mm^2) 0.218	Crack Density (No./ mm^2) 0.218	Crack Density (No./ mm^2) 0.031	Crack Density (No./ mm^2) 0.468
	Surface Density (μm crk. lgt/ mm^2) 32.076	Surface Density (μm crk. lgt/ mm^2) 71.271	Surface Density (μm crk. lgt/ mm^2) 28.336	Surface Density (μm crk. lgt/ mm^2) 117.515
		Ratio Cal: Xyl 1.00		

Specimen	No. of Cracks Xylenol	No. of Cracks Calcein	No. of Cracks Propagating	No. of Cracks Total
11	6	27	0	33
			Ave Lgt Xyl 0.00	
			Ave Lgt Cal 0.00	
	Average Length 182.8	Average Length 273.0	Ave Lgt Total 0.000	Average Length 235.2
	Crack Density (No./ mm^2) 0.018	Crack Density (No./ mm^2) 0.08	Crack Density (No./ mm^2) 0.000	Crack Density (No./ mm^2) 0.098
	Surface Density (μm crk. lgt/ mm^2) 3.264	Surface Density (μm crk. lgt/ mm^2) 21.930	Surface Density (μm crk. lgt/ mm^2) 0.000	Surface Density (μm crk. lgt/ mm^2) 25.194

Specimen	No. of Cracks Xylenol	No. of Cracks Calcein	No. of Cracks Propagating	No. of Cracks Total
12	21	42	6	69
			Ave Lgt Xyl 164.20	
			Ave Lgt Cal 235.53	
	Average Length 320.6	Average Length 468.3	Ave Lgt Total 399.73	Average Length 418.2
	Crack Density (No./ mm^2) 0.19	Crack Density (No./ mm^2) 0.38	Crack Density (No./ mm^2) 0.054	Crack Density (No./ mm^2) 0.62
	Surface Density (μm crk. lgt/ mm^2) 60.918	Surface Density (μm crk. lgt/ mm^2) 177.968	Surface Density (μm crk. lgt/ mm^2) 21.701	Surface Density (μm crk. lgt/ mm^2) 264.495

Appendix 4.3 Transverse crack data from three agent tests
Total number of cracks includes preexisting cracks labelled with alizarin

Specimen	No. of Cracks Xylenol	No. of Cracks Calcein	No. of Cracks Propagating (X-C)	No. of Cracks Total
3	15	33	3	51
	No. Osteonal 3	No. Osteonal 6	Ave Lgt Xyl 120.25	
	No. Interstitial 12	No. Interstitial 27	Ave Lgt Cal 95.21	
	Average Length 71.8	Average Length 63.6	Ave Lgt Total 215.460	Average Length 66.2
	Crack Density (No./ mm^2) 0.119	Crack Density (No./ mm^2) 0.262	Crack Density (No./ mm^2) 0	Crack Density (No./ mm^2) 0.406
	Surface Density (μm crk. lgt/ mm^2) 8.567	Surface Density (μm crk. lgt/ mm^2) 16.716	Surface Density (μm crk. lgt/ mm^2) 5.145	Surface Density (μm crk. lgt/ mm^2) 30.428

Specimen	No. of Cracks Xylenol	No. of Cracks Calcein	No. of Cracks Propagating	No. of Cracks Total
4	27	33	1	62
	No. Osteo 0	No. Osteo 6	Ave Lgt Xyl 317.01	
	No. Inter 27	No. Inter 27	Ave Lgt Cal 132.25	
	Average Length 78.6	Average Length 112.6	Ave Lgt Total 449.257	Average Length 103.5
	Crack Density (No./ mm^2) 0.300	Crack Density (No./ mm^2) 0.37	Crack Density (No./ mm^2) 0.011	Crack Density (No./ mm^2) 0.689
	Surface Density (μm crk. lgt/ mm^2) 22.077	Surface Density (μm crk. lgt/ mm^2) 41.291	Surface Density (μm crk. lgt/ mm^2) 14.975	Surface Density (μm crk. lgt/ mm^2) 78.444

Specimen	No. of Cracks Xylenol	No. of Cracks Calcein	No. of Cracks Propagating	No. of Cracks Total
5	9	24	0	33
	No. Osteo 0	No. Osteo 3	Ave Lgt Xyl	
	No. Inter 9	No. Inter 21	Ave Lgt Cal	
	Average Length 62.3	Average Length 55.5	Ave Lgt Total	Average Length 57.3
	Crack Density (No./ mm^2) 0.116	Crack Density (No./ mm^2) 0.31	Crack Density (No./ mm^2) 0	Crack Density (No./ mm^2) 0.426
	Surface Density (μm crk. lgt/ mm^2) 7.241	Surface Density (μm crk. lgt/ mm^2) 17.202	Surface Density (μm crk. lgt/ mm^2) 0.000	Surface Density (μm crk. lgt/ mm^2) 24.443

Specimen	No. of Cracks Xylenol	No. of Cracks Calcein	No. of Cracks Propagating	No. of Cracks Total
6	6	15	0	21
	No. Osteo 0	No. Osteo 0	Ave Lgt Xyl	
	No. Inter 6	No. Inter 15	Ave Lgt Cal	
	Average Length 66.6	Average Length 87.6	Ave Lgt Total	Average Length 83.8
	Crack Density (No./ mm^2) 0.043	Crack Density (No./ mm^2) 0.107	Crack Density (No./ mm^2) 0	Crack Density (No./ mm^2) 0.15
	Surface Density (μm crk. lgt/ mm^2) 2.855	Surface Density (μm crk. lgt/ mm^2) 9.383	Surface Density (μm crk. lgt/ mm^2) 0.000	Surface Density (μm crk. lgt/ mm^2) 14.376

Specimen	No. of Cracks Xylenol	No. of Cracks Calcein	No. of Cracks Propagating	No. of Cracks Total
7	15	33	0	48
	No. Osteo 0	No. Osteo 15	Ave Lgt Xyl	
	No. Inter 15	No. Inter 18	Ave Lgt Cal	
	Average Length 81.7	Average Length 88.8	Ave Lgt Total	Average Length 87.9
	Crack Density (No./ mm^2) 0.188	Crack Density (No./ mm^2) 0.414	Crack Density (No./ mm^2) 0	Crack Density (No./ mm^2) 0.6
	Surface Density (μm crk. lgt/ mm^2) 14.307	Surface Density (μm crk. lgt/ mm^2) 36.770	Surface Density (μm crk. lgt/ mm^2) 0.000	Surface Density (μm crk. lgt/ mm^2) 54.983

Specimen	No. of Cracks Xylenol	No. of Cracks Calcein	No. of Cracks Propagating	No. of Cracks Total
8	9	18	0	27
	No. Osteo 0	No. Osteo 6	Ave Lgt Xyl	
	No. Inter 9	No. Inter 12	Ave Lgt Cal	
	Average Length 69.5	Average Length 77.8	Ave Lgt Total	Average Length 74.6
	Crack Density (No./ mm^2) 0.141	Crack Density (No./ mm^2) 0.282	Crack Density (No./ mm^2) 0	Crack Density (No./ mm^2) 0.405
	Surface Density (μm crk. lgt/ mm^2) 9.816	Surface Density (μm crk. lgt/ mm^2) 21.979	Surface Density (μm crk. lgt/ mm^2) 0.000	Surface Density (μm crk. lgt/ mm^2) 35.092

Specimen	No. of Cracks Xylenol	No. of Cracks Calcein	No. of Cracks Propagating	No. of Cracks Total
9	9	30	3	43
	No. Osteo 3	No. Osteo 12	Ave Lgt Xyl 84.01	
	No. Inter 6	No. Inter 18	Ave Lgt Cal 112.58	
	Average Length 90.6	Average Length 120.5	Ave Lgt Total 196.590	Average Length 116.1
	Crack Density (No./ mm^2) 0.205	Crack Density (No./ mm^2) 0.683	Crack Density (No./ mm^2) 0.068	Crack Density (No./ mm^2) 0.979
	Surface Density (μm crk. lgt/ mm^2) 18.565	Surface Density (μm crk. lgt/ mm^2) 82.296	Surface Density (μm crk. lgt/ mm^2) 13.428	Surface Density (μm crk. lgt/ mm^2) 120.408

Specimen	No. of Cracks Xylenol	No. of Cracks Calcein	No. of Cracks Propagating	No. of Cracks Total
10	24	36	3	64
	No. Osteo 6	No. Osteo 0	Ave Lgt Xyl 92.82	
	No. Inter 18	No. Inter 36	Ave Lgt Cal 51.90	
	Average Length 136.1	Average Length 197.2	Ave Lgt Total 144.715	Average Length 178.6
	Crack Density (No./ mm^2) 0.678	Crack Density (No./ mm^2) 1.017	Crack Density (No./ mm^2) 0.084	Crack Density (No./ mm^2) 1.808
	Surface Density (μm crk. lgt/ mm^2) 92.240	Surface Density (μm crk. lgt/ mm^2) 200.554	Surface Density (μm crk. lgt/ mm^2) 12.264	Surface Density (μm crk. lgt/ mm^2) 318.792

Specimen	No. of Cracks Xylenol	No. of Cracks Calcein	No. of Cracks Propagating	No. of Cracks Total
11	9	30	0	41
	No. Osteo 0	No. Osteo 6	Ave Lgt Xyl 0.00	
	No. Inter 9	No. Inter 24	Ave Lgt Cal 0.00	
	Average Length 117.2	Average Length 118.9	Ave Lgt Total 0.000	Average Length 107.7
	Crack Density (No./ mm^2) 0.063	Crack Density (No./ mm^2) 0.21	Crack Density (No./ mm^2) 0.0000	Crack Density (No./ mm^2) 0.28
	Surface Density (μm crk. lgt/ mm^2) 7.383	Surface Density (μm crk. lgt/ mm^2) 24.984	Surface Density (μm crk. lgt/ mm^2) 0.000	Surface Density (μm crk. lgt/ mm^2) 33.115

Specimen	No. of Cracks Xylenol	No. of Cracks Calcein	No. of Cracks Propagating	No. of Cracks Total
12	21	33	4	60
	No. Osteo 0	No. Osteo 15	Ave Lgt Xyl 141.23	
	No. Inter 21	No. Inter 18	Ave Lgt Cal 123.98	
	Average Length 141.6	Average Length 188.4	Ave Lgt Total 265.206	Average Length 170.5
	Crack Density (No./ mm^2) 0.38	Crack Density (No./ mm^2) 0.59	Crack Density (No./ mm^2) 0.072	Crack Density (No./ mm^2) 1.08
	Surface Density (μm crk. lgt/ mm^2) 53.740	Surface Density (μm crk. lgt/ mm^2) 112.379	Surface Density (μm crk. lgt/ mm^2) 57.528	Surface Density (μm crk. lgt/ mm^2) 187.075

Appendix 4.4 Longitudinal crack data from four agent tests
Total number of cracks includes preexisting cracks labelled with alizarin

Specimen	No. of Cracks First 10000 Cycles	No. of Cracks 10-50000 Cycles	No Cracks 50000-Failure	No. of Cracks Propagating	No. of Cracks Total
13	15	6	21	0	42
	Average Length 248.6	Average Length 297.0	Average Length 300.4	Ave Lgt Total 0.000	Average Length 282.0
	Crack Density (No./ mm^2) 0.081	Crack Density (No./ mm^2) 0.033	Crack Density (No./ mm^2) 0.115	Crack Density (No./ mm^2) 0.000	Crack Density (No./ mm^2) 0.23
	Surface Density (μm crk. lgt/ mm^2) 20.545	Surface Density (μm crk. lgt/ mm^2) 4.909	Surface Density (μm crk. lgt/ mm^2) 34.760	Surface Density (μm crk. lgt/ mm^2) 0.000	Surface Density (μm crk. lgt/ mm^2) 60.215

Specimen	No. of Cracks First 10000	No. of Cracks 10-50000	No Cracks 50000-Fail	No. of Cracks Propagating	No. of Cracks Total
14	15	6	33	6	61
	Average Length 311.5	Average Length 275.0	Average Length 196.0	Ave Lgt Total 188.000	Average Length 260.8
	Crack Density (No./ mm^2) 0.144	Crack Density (No./ mm^2) 0.057	Crack Density (No./ mm^2) 0.32	Crack Density (No./ mm^2) 0.057	Crack Density (No./ mm^2) 0.59
	Surface Density (μm crk. lgt/ mm^2) 35.877	Surface Density (μm crk. lgt/ mm^2) 7.918	Surface Density (μm crk. lgt/ mm^2) 62.079	Surface Density (μm crk. lgt/ mm^2) 5.413	Surface Density (μm crk. lgt/ mm^2) 105.874

Specimen	No. of Cracks First 10000	No. of Cracks 10-50000	No Cracks 50000-Fail	No. of Cracks Propagating	No. of Cracks Total
15	14	4	18	3	39
	Average Length 266.0	Average Length 198.0	Average Length 349.2	Ave Lgt Total 0.000	Average Length 293.9
	Crack Density (No./ mm^2) 0.093	Crack Density (No./ mm^2) 0.026	Crack Density (No./ mm^2) 0.119	Crack Density (No./ mm^2) 0.006	Crack Density (No./ mm^2) 0.26
	Surface Density (μm crk. lgt/ mm^2) 26.478	Surface Density (μm crk. lgt/ mm^2) 7.884	Surface Density (μm crk. lgt/ mm^2) 41.708	Surface Density (μm crk. lgt/ mm^2) 0.000	Surface Density (μm crk. lgt/ mm^2) 76.070

Appendix 4.5 Transverse crack data from four agent tests
Total number of cracks includes preexisting cracks labelled with alizarin

Specimen	No. of Cracks First 10000	No. of Cracks 10-50000	No. of Cracks 50000-Fail	No. of Cracks Propagating	No. of Cracks Total
13	15	6	45	0	66
	No. Osteonal 3	No. Osteonal 0	No. Osteonal 18		
	No. Interstitial 12	No. Interstitial 6	No. Interstitial 27		
	Average Length 117.2	Average Length 102.0	Average Length 135.1	Ave Lgt Total 0.000	Average Length 104.3
	Crack Density (No./ mm^2) 0.101	Crack Density (No./ mm^2) 0.041	Crack Density (No./ mm^2) 0.305	Crack Density (No./ mm^2) 0.0000	Crack Density (No./ mm^2) 0.446
	Surface Density (μm crk. lgt/ mm^2) 11.925	Surface Density (μm crk. lgt/ mm^2) 4.151	Surface Density (μm crk. lgt/ mm^2) 41.229	Surface Density (μm crk. lgt/ mm^2) 0.000	Surface Density (μm crk. lgt/ mm^2) 16.077

Specimen	No. of Cracks First 10000	No. of Cracks 10-50000	No. of Cracks 50000-Fail	No. of Cracks Propagating	No. of Cracks Total
14	15	6	18	0	42
	No. Osteo 3	No. Osteo 0	No. Osteo 6		
	No. Inter 12	No. Inter 6	No. Inter 12		
	Average Length 119.0	Average Length 100.0	Average Length 84.2	Ave Lgt Total 0.000	Average Length 91.7
	Crack Density (No./ mm^2) 0.144	Crack Density (No./ mm^2) 0.057	Crack Density (No./ mm^2) 0.172	Crack Density (No./ mm^2) 0.0000	Crack Density (No./ mm^2) 0.4
	Surface Density (μm crk. lgt/ mm^2) 17.132	Surface Density (μm crk. lgt/ mm^2) 5.759	Surface Density (μm crk. lgt/ mm^2) 14.541	Surface Density (μm crk. lgt/ mm^2) 0.000	Surface Density (μm crk. lgt/ mm^2) 23.917
Specimen	No. of Cracks First 10000	No. of Cracks 10-50000	No. of Cracks 50000-Fail	No. of Cracks Propagating	No. of Cracks Total
15	21	0	30	3	57
	No. Osteo 3	No. Osteo 0	No. Osteo 0	Ave Lgt Xyl 63.00	
	No. Inter 18	No. Inter 0	No. Inter 30	Ave Lgt Cal 123.00	
	Average Length 61.4	Average Length 0.0	Average Length 143.6	Ave Lgt Total 186.000	Average Length 74.6
	Crack Density (No./ mm^2) 0.138	Crack Density (No./ mm^2) 0.000	Crack Density (No./ mm^2) 0.197	Crack Density (No./ mm^2) 0.019	Crack Density (No./ mm^2) 0.375
	Surface Density (μm crk. lgt/ mm^2) 9.907	Surface Density (μm crk. lgt/ mm^2) 0.000	Surface Density (μm crk. lgt/ mm^2) 28.34	Surface Density (μm crk. lgt/ mm^2) 3.671	Surface Density (μm crk. lgt/ mm^2) 10.61

Appendix 4.5 Unpaired t-test: 3 Agent Data

Transverse Sections

CRACK TYPE	STAGE 2	STAGE 3	STAGE 3	PROPAGATING	PROPAGATING	PREEXIST.
Num. Density (No./mm2)	0.203	0.386	0.386	0.049	0.049	0.040
S.D.	0.193	0.287	0.287	0.084	0.084	0.035
Variance	0.037	0.082	0.082	0.007	0.007	0.001
sample	30.000	30.000	30.000	30.000	30.000	30.000
N value	58.000		58.000		58.000	58.000
Pooled standard error	0.063		0.055		0.017	
tvalue	2.898		6.172		0.539	
tcritical	2.009		2.009		2.009	

	STAGE 2	STAGE 3	STAGE 3	PROPAGATING	PROPAGATING	PREEXIST.
Surface Density (_m /mm2)	21.500	49.700	49.700	9.400	9.400	3.400
S.D.	27.600	61.600	61.600	17.700	17.700	3.100
Variance	761.760	3794.560	3794.560	313.290	313.290	9.610
sample	30.000	30.000	30.000	30.000	30.000	30.000
N value	58.000		58.000		58.000	
Pooled standard error	12.324		11.702		3.281	
tvalue	2.288		3.444		1.829	
tcritical	2.009		2.009		2.009	

Crack Length	96.5	115.6	115.6	263.9	263.9	61.6
SD	61.8	84.4	84.4	117.2	117.2	38.78
Variance	3819.240	7123.360	7123.360	13735.840	13735.840	1503.888
sample	144	285	285	30	30	24
N Value	427		313		52	
Pooled standard error	7.178		21.974		22.815	
tvalue	2.661		6.749		8.867	
tcritical	1.984		1.984		2.009	

Longitudinal

CRACK TYPE	STAGE 2	STAGE 3	STAGE 3	PROPAGATING	PROPAGATING	PREEXIST.
Num. Density (No./mm2)	0.103	0.236	0.236	0.032	0.032	0.021
S.D.	0.087	0.174	0.174	0.023	0.023	0.024
Variance	0.008	0.030	0.030	0.001	0.001	0.001
sample	30.000		30.000	30.000	30.000	30.000
N value	56.000		58.000		58.000	58.000
Pooled standard error	0.036		0.032		0.006	
tvalue	3.745		6.366		1.812	
tcritical	2.009		2.009		2.009	

CRACK TYPE	STAGE 2	STAGE 3	STAGE 3	PROPAGATING	PROPAGATING	PREEXIST.
Surface Density (_m /mm2)	19.4	64.8	64.8	14.8	14.8	1.5
S.D.	21.3	76.4	76.4	13.7	13.7	1.7
Variance	453.690	5836.960	5836.960	187.690	187.690	2.890
n	30.000	30.000	30.000	30.000	30.000	30.000
N value	58.000		58.000		58.000	58.000
Pooled standard error	14.481		14.171		2.520	
tvalue	3.135		3.528		5.277	
tcritical	2.009		2.009		2.009	

CRACK TYPE	STAGE 2	STAGE 3	STAGE 3	PROPAGATING	PROPAGATING	PREEXIST.
Crack Length	177.2	249	249	357.3	357.3	50.26
SD	108.8	181.1	181.1	148.25	148.25	58.41
Variance	11837.44000	32797.210	32797.210	21978.063	21978.063	3411.7281
sample	111	261	261	35	36	30
N Value	370		295		64	
Pooled standard error	15.242		27.132		26.911	
tvalue	4.711		3.992		11.409	
tcritical	1.984		1.984		2.179	

Appendix 4.6 Unpaired t-test: 4 Agent Data

Transverse Sections

CRACK TYPE	STAGE 1	STAGE 2	STAGE 2	STAGE 3	STAGE 3	PROPAGATING	PROPAGATING	PREEXIST.
Num. Density (No./mm2)	0.128	0.033	0.033	0.225	0.225	0.007	0.007	0.023
S.D.	0.023	0.012	0.012	0.07	0.07	0.011	0.011	0.005
Variance	0.00053	0.00014	0.00014	0.00490	0.00490	0.00012	0.00012	0.00003
sample	9	9	9		9	9	9	9
N value	16		16		16		16	
Pooled standard error	0.009		0.024		0.024		0.004	
tvalue	10.986		8.110		9.230		3.973	
tcritical	2.12		2.12		2.12		2.12	

CRACK TYPE	STAGE 1	STAGE 2	STAGE 2	STAGE 3	STAGE 3	PROPAGATING	PROPAGATING	PREEXIST.
Surface Density (_m /mm2)	12.98	4.95	4.95	28.03	28.03	1.87	1.224	1.87
S.D.	3.728	1.137	1.137	13.35	13.35	0.394	2.119	0.394
Variance	13.89798	1.29277	1.29277	178.22250	178.22250	0.15524	4.49016	0.15524
sample size	9	9	9	9	9	9	9	9
N value	16		16		16		16	
Pooled standard error	1.299		4.466		4.506		0.718	
tvalue	6.181		5.168		5.949		0.899	
tcritical	2.12		2.12		2.12		2.12	

CRACK TYPE	STAGE 1	STAGE 2	STAGE 2	STAGE 3	STAGE 3	PROPAGATING	PROPAGATING	PREEXIST.
Crack Length	99	101	101	128	128	123	123	83
SD	43.8	16.1	16.1	60.9	60.9	22	22	23
Variance	1918.44000	259.21000	259.21000	3708.81000	3708.81000	484.00000	484.00000	529.00000
sample	51	12	12	99	99	3	3	9
N Value	61		109		100		10	
Pooled standard error	7.695		7.685		14.100		14.836	
tvalue	0.260		3.513		0.355		2.696	
tcritical	2.009		1.984		1.984		2.228	

Longitudinal Sections

CRACK TYPE	STAGE 1	STAGE 2	STAGE 2	STAGE 3	STAGE 3	PROPAGATING	PROPAGATING	PREEXIST.
Num. Density (No./mm2)	0.109	0.043	0.043	0.184	0.184	0.021	0.021	0.023
S.D.	0.032	0.013	0.013	0.115	0.115	0.031	0.031	0.005
Variance	0.00102	0.00017	0.00017	0.01323	0.01323	0.00096	0.00096	0.00003
sample	9	9	9	9	9	9	9	9
N value	16		16		16		16	16
Pooled standard error	0.012		0.039		0.040		0.010	
tvalue	5.733		3.655		4.106		0.191	
tcritical	2.12		2.12		2.12		2.12	

CRACK TYPE	STAGE 1	STAGE 2	STAGE 2	STAGE 3	STAGE 3	PROPAGATING	PROPAGATING	PREEXIST.
Surface Density (_m /mm2)	27.63	5.9	6.9	46.18	46.18	1.8	1.8	0.5
S.D.	7.73	1.72	1.72	14.19	14.19	3.12	3.12	0
Variance	59.753	2.958	2.958	201.356	201.356	9.734	9.734	0.000
n	30.000	30.000	30.000	30.000	30.000	30.000	30.000	30.000
N value	58.000		58.000		58.000		58.000	
Pooled standard error	1.446		2.610		2.653		0.570	
tvalue	14.338		15.052		16.731		2.282	
tcritical	2.009		2.009		2.009		2.009	

CRACK TYPE	STAGE 1	STAGE 2	STAGE 2	STAGE 3	STAGE 3	PROPAGATING	PROPAGATING	PREEXIST.
Crack Length	272.8	242	242	264.8	264.8	243	243	56
SD	67.2	65.8	65.8	165.8	165.8	77.8	77.8	0
Variance	4515.840	4329.640	4329.640	27489.640	27489.640	6052.840	6052.840	0.000
sample	45	18	18	72	72	9	9	12
N Value	61		88		79		19	
Pooled standard error	18.463		24.947		32.471		25.933	
tvalue	1.568		0.914		0.671		7.211	
tcritical	2.009		1.984		1.984		2.228	

Appendix 4.7 Unpaired t-tests: 3 agent v 4 agent tests

3 Agent Tests

Transverse Sections

CRACK TYPE	STAGE 2	STAGE 3	PROPAGATING	PREEXIST.
Num. Density (No./mm2)	0.203	0.386	0.049	0.040
S.D.	0.193	0.287	0.084	0.036
Variance	0.037	0.082	0.007	0.001
sample	10.000	10.000	10.000	10.000

4 Agent Tests

Transverse Sections

CRACK TYPE	STAGE 1	STAGE 2	STAGE 3	PROPAGATING	PREEXIST.
Num. Density (No./mm2)	0.128	0.033	0.225	0.007	0.023
S.D.	0.023	0.012	0.07	0.011	0.005
Variance	0.00053	0.00014	0.00490	0.00012	0.00003
sample	3	3	3	3	3
N value		11.000	11.000	11.000	11.000
Pooled standard error		0.061	0.099	0.027	0.012
tvalue		2.768	1.621	1.538	1.447
tvalue		2.201	2.201	2.201	2.201

3 Agent Tests

Longitudinal Sections

CRACK TYPE	STAGE 2	STAGE 3	PROPAGATING	PREEXIST.
Surface Density (μm /mm2)	0.103	0.236	0.032	0.021
S.D.	0.087	0.174	0.023	0.024
Variance	0.008	0.030	0.001	0.001
sample	10.000	10.000	10.000	10.000

4 Agent Tests

Longitudinal Sections

CRACK TYPE	STAGE 1	STAGE 2	STAGE 3	PROPAGATING	PREEXIST.
Surface Density (μm /mm2)	0.109	0.043	0.184	0.021	0.023
S.D.	0.032	0.013	0.115	0.031	0.005
Variance	0.00102	0.00017	0.01323	0.00096	0.00003
sample	3	3	3	3	3
N value		11.000	11.000	11.000	11.000
Pooled standard error		0.029	0.086	0.019	0.008
tvalue		2.104	0.603	0.569	0.246
tcritical		2.201	2.201	2.201	2.201

3 Agent Tests

Transverse Sections

CRACK TYPE		STAGE 2	STAGE 3	PROPAGATING	PREEXIST.
Surface Density (µm /mm2)		21.500	49.700	9.400	3.400
S.D.		27.600	61.600	17.700	3.100
Variance		761.76	3794.56	313.29	9.61
sample		10.000	10.000	10.000	10.000

4 Agent Tests

Transverse Sections

CRACK TYPE	STAGE 1	STAGE 2	STAGE 3	PROPAGATING	PREEXIST.
Surface Density (µm /mm2)	12.98	4.95	28.03	1.224	1.87
S.D.	3.728	1.137	13.35	2.119	0.394
Variance	13.89798	1.29277	178.22250	4.49016	0.15524
sample size	3	3	3	3	3
N value		11.000	11.000	11.000	11.000
Pooled standard error		8.753	20.949	5.729	1.006
tvalue		2.588	1.602	2.876	1.222
tvalue		2.201	2.201	2.201	2.201

3 Agent Tests

Longitudinal Sections

CRACK TYPE		STAGE 2	STAGE 3	PROPAGATING	PREEXIST.
Surface Density (µm /mm2)		19.4	64.8	14.8	1.5
S.D.		21.3	76.4	13.7	1.7
Variance		453.690	5836.960	187.690	2.890
sample		10.000	10.000	10.000	10.000

4 Agent Tests

Longitudinal Sections

CRACK TYPE	STAGE 1	STAGE 2	STAGE 3	PROPAGATING	PREEXIST.
Surface Density (µm /mm2)	27.63	6.9	46.18	1.8	0.5
S.D.	7.73	1.72	14.19	3.12	0
Variance	59.753	2.958	201.356	9.734	0.000
sample	3	3	3	3	3
N value		11.000	11.000	11.000	11.000
Pooled standard error		6.808	25.511	4.692	0.538
tvalue		1.836	0.730	2.771	1.860
tcritical		2.201	2.201	2.201	2.201

Appendix 4.8 Unpaired t-tests: In vivo v preexisting microcracks

In Vivo v Preexisting Cracks

CRACK TYPE	In Vivo	Preexisting
Num. Density (No./mm2)	0.014	0.04
S.D.	0.005	0.036
Variance	0.00003	0.00130
sample	3.000	10.000
N value	11.000	
Pooled standard error	0.012	
tvalue	2.214	
tcritical	2.201	

CRACK TYPE	In Vivo	Preexisting
Num. Density (No./mm2)	0.005	0.021
S.D.	0.01	0.024
Variance	0.00010	0.00058
sample	3.000	10.000
N value	11.000	
Pooled standard error	0.010	
tvalue	1.678	
tcritical	2.201	

Appendix 4.9 Unpaired t-tests: Transverse v dongitudinal data

CRACK TYPE	Transverse	Longitudinal
Num. Density (No./mm2)	0.749	0.374
S.D.	0.533	0.264
Variance	0.28409	0.06970
sample	9	30
N value	58	
Pooled standard error	0.184	
tvalue	2.037	
tcritical	2.201	

CRACK TYPE	Transverse	Longitudinal
Surface Density µm /mm2)	81.56	97.31
S.D.	96.53	107.77
Variance	9318	11614
n	30	30
N value	58	
Pooled standard error	26.415	
tvalue	0.596	
tcritical	2.364	

Appendix 5.1 History of cadavers from which ribs were harvested

Cadaver Number	Gender	Age at Death	Cause of Death
1	M	80	renal failure
2	F	81	pneumonia
3	F	81	aspiration pneumonia
4	M	92	bronchopneumonia
5	M	79	carcinoma of stomach
6	F	82	cardiac arrest
7	F	69	ovarian carcinoma
8	M	87	prostate cancer
9	F	88	respiratory infection

Appendix 5.2 Crack data from fuchsin stained rib sections

Specimen	Area (mm^2)	No. of Cracks	Crack Density (No./ mm^2)
1	100.77	8	0.0793

Average Length
483.5
SD
284.9

Specimen	Area (mm^2)	No. of Cracks	Crack Density (No./ mm^2)
2	120.6	11	0.09121

Average Length
436.0
SD
188.0

Specimen	Area (mm^2)	No. of Cracks	Crack Density (No./ mm^2)
3	104.21	8	0.07677

Average Length
400.5
SD
163.8

Specimen	Area (mm^2)	No. of Cracks	Crack Density (No./ mm^2)
4	81.22	24	0.2955

Average Length
391.1
SD
274.2

Specimen	Area (mm^2)	No. of Cracks	Crack Density (No./ mm^2)
5	116.59	8	0.0686

Average Length
245.9
SD
174.3

Specimen	Area (mm^2)	No. of Cracks	Crack Density (No./ mm^2)
6	77.83	3	0.0385

Average Length
358.8
SD
162.1

Specimen	Area (mm^2)	No. of Cracks	Crack Density (No./ mm^2)
7	88.29	4	0.045

Average Length
285.4
SD
197.0

Specimen	Area (mm^2)	No. of Cracks	Crack Density (No./ mm^2)
8	64.71	19	0.293

Average Length
324.2
SD
141.3

Specimen	Area (mm^2)	No. of Cracks	Crack Density (No./ mm^2)
9	72.13	7	0.097

Average Length
364.81
SD
190.4